DESIGN AND ANALYSIS OF M-ARY MODULATION DRIVEN FREE SPACE OPTICAL TRANSCEIVER USING COHERENT DETECTION AND DSP ALGORITHMS

Thesis

Submitted in partial fulfillment of the requirements for the degree of

MASTER OF TECHNOLOGY

in

ELECTRONICS AND COMMUNICATION ENGINEERING

(WIRELESS COMMUNICATION)

by

SAHIL NAZIR POTTOO

Registration No. 1818693

Supervisor: Dr. Rakesh Goyal

Co-Supervisor: Dr. Amit Gupta

DEPARTMENT OF ELECTRONICS AND COMMUNICATION ENGINEERING
I. K. GUJRAL PUNJAB TECHNICAL UNIVERSITY, KAPURTHALA

May 2020

CERTIFICATE

I hereby certify that the work which is being presented in the thesis entitled "Design and Analysis of M-ary Modulation driven Free Space Optical Transceiver using Coherent Detection and DSP Algorithms" in partial fulfillment of the requirements for the award of the degree of Master of Technology in Electronics and Communication Engineering (Wireless Communication) submitted in the Department of Electronics and Communication Engineering at the I. K. Gujral Punjab Technical University, Kapurthala is an authentic record of my own work carried out under the supervision of Dr. Rakesh Goyal and Dr. Amit Gupta, Assistant Professors, Department of Electronics and Communication Engineering. The research work presented in this thesis has not been submitted by me in any other University/Institute for the award of any other degree.

Signature of the Student

This is to certify that the above statement made by the candidate is correct to the best of our knowledge.

Signature of the Supervisor   Signature of the Co-Supervisor

The M.Tech. Online Viva-Voice Examination of Sahil Nazir Pottoo has been held on 29-May-2020 and accepted.

Signature of External Examiner   Signature of H.O.D.

Signature of the Supervisor   Signature of the Co-Supervisor

ACKNOWLEDGEMENT

ABSTRACT

In this work, we propose the design and analysis of polarization division multiplexed M-ary modulation-based free-space optical (FSO) transceiver using balanced homodyne detection (BHD) and digital signal processing (DSP) at the receiver end. We have employed DP-QPSK, DP-16-QAM, and DP-256-QAM optical modulation techniques to gain greater spectral efficiency and data rates. A series of high-level digital impairment compensation algorithms have been implemented strategically between BHD and signal retrieval stages to mitigate amplitude and phase noise and compensate for the free-space loss. The proposed design exhibits a 3 dB greater receiver sensitivity using BHD compared to heterodyne detection. The system performance has been numerically evaluated with regard to bit error rate, error vector magnitude, laser linewidth requirements, optical signal-to-noise ratio tolerance, receiver sensitivity, launched optical power, beam divergence, and constellation diagrams. We have achieved successful transmission of 120, 400, and 720 Gbps data-bearing optical signals through 2.65, 2, and 1.31 km transmission distances for the respective proposed systems. Additionally, the performance comparison between all the proposed system designs has been carried out. Furthermore, a 100G-based or beyond single optical carrier communication system is favored by the telecommunications community since it reduces the cost and complexity of the transceiver system. Also, the optical IQM and DSP unit can be fabricated into electronic-photonic integrated circuits (EPICs) that can emerge as an attractive solution for future optical systems, since it can reduce the production cost, pushing the boundaries of optoelectronic devices and modules. The outcomes of this research demonstrate direct practical relevance, and could therefore form the basis for the development of high-speed and long-haul future optical networks.

TABLE OF CONTENTS

LIST OF FIGURES

LIST OF TABLES

LIST OF SYMBOLS

P_{RX}	Received Optical Power
P_{TX}	Transmitted Optical Power
η_{RX}	Receiver Optics Efficiency
g_{TX}	Transmitter Gain
g_{RX}	Receiver Gain
L_{TX}	Transmitter Pointing Loss Factor
L_{RX}	Receiver Pointing Loss Factor
λ	Wavelength
R	Transmission Range
D_{TX}	Transmitter Telescope Diameter
D_{RX}	Receiver Telescope Diameter
θ_{TX}	Transmitter Azimuth Pointing Error Angle
θ_{RX}	Receiver Azimuth Pointing Error Angle
P_{e0} / P_{e1}	Symbol Probability for Bit 0/1
K / L	Number of Samples for Bit 0/1
b_0 / b_1	Average Values
W	Threshold Value
α	Atmospheric Attenuation
θ	Beam Divergence Angle
E_l	System Loss
L_{ch}	Channel Loss
a_s	Signal Amplitude
t_1	Pulse Position
t_c	Duty Cycle
T	Bit Period
δ_1	MZM Insertion Loss
$\sqrt{P_s P_{lo}}$	Branch Current Magnitude
e_s	Polarization Coefficient of Transmitted Optical Signal
e_{lo}	Polarization Coefficient of Local Oscillator
$\beta(\omega_s)$	Propagation Constant

$\Delta \emptyset(t)$	Phase Change
i_{sh}	Shot Noise Photocurrent
c_n^2	Index Refraction Coefficient
P_s	Signal Power
P_n	Noise Power
ω	Angular Frequency
j	Imaginary Number
c	Speed of Light
D	Dispersion Coefficient
λ_o	Reference Wavelength
ϕ_b	Carrier Phase Angle
ρ	Correlation Co-efficient
ω_n	Nyquist Frequency
p	Dispersion Order
μ	Step Size Parameter

LIST OF ACRONYMS

ADC	Analog to Digital Converter
AE	Adaptive Equalizer
AI	Artificial Intelligence
ANN	Artificial Neural Network
AO	Adaptive Optics
APD	Avalanche Photodiode
ASE	Amplified Spontaneous Emission
AWGN	Additive White Gaussian Noise
BER	Bit Error Rate
BHD	Balanced Homodyne Detection
BPF	Bandpass Filter
BPS	Blind Phase Search
BPSK	Binary Phase Shift Keying
BTB	Back to Back
BTS	Base Transceiver Station
CC	Cloud Computing
CD	Chromatic Dispersion
CMA-RD	Constant Modulus Algorithm-Radius Directed
CPE	Carrier Phase Estimation
CSI	Channel State Information
CSRZ	Carrier Suppressed Return to Zero
DAC	Digital to Analog Converter
DBP	Digital Back Propagation
DC	Direct Current
DD	Direct Detection
DP	Dual Polarization
DSF	Digital Square Filter
DSP	Digital Signal Processing
DWDM	Dense Wavelength Division Multiplexing
EDFA	Erbium Doped Fiber Amplifier
EMI	Electromagnetic Interference

EVM	Error Vector Magnitude
FEC	Forward Error Correction
FOE	Frequency Offset Estimation
FSO	Free Space Optics
GSOP	Gram Schmidt Orthogonalization Procedure
HAP	High Altitude Platform
HDR	High Data Rate
HDTV	High Definition Television
IC	Integrated Circuit
ICI	Inter Channel Interference
IM	Intensity Modulation
IoT	Internet of Things
IQM	Inphase and Quadrature Modulator
IR	Infrared
ISI	Inter Symbol Interference
ITU	International Telecommunication Union
LAN	Local Area Network
LED	Light Emitting Diode
LO	Local Oscillator
LoS	Line of Sight
LPF	Low Pass Filter
MAN	Metropolitan Area Network
MIMO	Multiple Input Multiple Output
MISO	Multiple Input Single Output
MTBF	Mean Time Between Failures
M2M	Machine to Machine
MZM	Mach Zehnder Modulator
NL	Nonlinear
NRZ	Non Return to Zero
OFC	Optical Fiber Communication
OOFDM	Optical Orthogonal Frequency Division Multiplexing
OOK	On Off Keying
OSNR	Optical Signal to Noise Ratio

OWC	Optical Wireless Communication
PBC	Polarization Beam Combiner
PBS	Polarization Beam Splitter
PD	Photodiode
PDM	Polarization Division Multiplexing
PLL	Phase Locked Loop
PMD	Polarization Mode Dispersion
PolSK	Polarization Shift Keying
PON	Passive Optical Network
PRBS	Pseudo Random Bit Sequence
PSK	Phase Shift Keying
PSTN	Public Switched Telephone Network
QAM	Quadrature Amplitude Modulation
QI	Quadrature Imbalance
QoS	Quality of Service
QPSK	Quadrature Phase Shift Keying
RF	Radio Frequency
RMS	Root Mean Square
ROV	Remotely Operated Vehicle
RZ	Return to Zero
SE	Spectral Efficiency
SISO	Single Input Single Output
SPM	Self-Phase Modulation
UAV	Unmanned Aerial Vehicle
UV	Ultraviolet
VLC	Visible Light Communication
VV	Viterbi Viterbi
WDM	Wavelength Division Multiplexing
WLAN	Wireless Local Area Network
WPAN	Wireless Personal Area Network

RESEARCH DISSEMINATION

Peer-Reviewed Articles:

S. N. Pottoo, R. Goyal and A. Gupta, "Development of 32-GBaud DP-QPSK Free Space Optical Transceiver using Homodyne Detection and Advanced Digital Signal Processing for Future Optical Networks," *Optical and Quantum Electronics*, vol. 52, no. 11, pp. 1-17, 2020. DOI: 10.1007/s11082-020-02623-y

S. N. Pottoo, R. Goyal and A. Gupta, "Design and Investigation of Free Space Optical System for Diverse Atmospheric Transmission Windows," *Journal of Optical Communications*, 2020. DOI: 10.1515/joc-2020-0023

Peer-Reviewed Conference Paper:

S. N. Pottoo, R. Goyal and A. Gupta, "Performance Investigation of Optical Communication System using FSO and OWC Channel," *2020 Indo – Taiwan 2nd IEEE International Conference on Computing, Analytics and Networks (Indo–Taiwan ICAN)*, Rajpura, Punjab, India, 2020, pp. 176-180. DOI: 10.1109/ Indo-TaiwanICAN48429.2020.9181322

CHAPTER 1: INTRODUCTION

1.1 Overview of free-space optical communication

Free space optical (FSO) communication is a lightwave communication technology that operates in the near-infrared (IR) region of the electromagnetic spectrum (about 700 to 1675 nm) and uses an atmospheric channel as the transmission medium for both inter-satellite and terrestrial communication. FSO is a direct line-of-sight (LoS) wireless communication technology that offers high data rate (HDR) communication link, low bit error rate (BER), unlicensed bandwidth, low power operation, ease of deployment, and last-mile access. FSO communication systems have long been used in inter-satellite communication due to the vast optical bandwidth of laser sources. Henceforth, FSO communication systems can be exploited for wideband communication to fulfill the bandwidth requirements of 5G and the rising number of internet of thing (IoT) devices. Laser communication has the rewards of high fidelity and strong anti-interference operation, but the right choice of optical transmission window becomes important for skin and eye safety concerns [1]. The combination of adaptive optics (AO) and optical numerical simulations can be utilized to monitor the performance of a vast number of FSO applications ranging from novel unmanned aerial vehicles (UAVs) based FSO transmission system to lightwave based remotely operated vehicles (ROVs) for underwater FSO communication link to any terrestrial FSO communication network [2]. FSO is a viable alternative to traditional radio frequency (RF) based wireless data transmission technologies since it uses optical beams as information carrier signals which have unregulated spectrum and are abundantly available to provide high-speed data links with secure information transmission [3]. Light-based options promise to pick up where RF technology leaves off. Growing data demands have led to the consideration of using IR, visible, and ultraviolet (UV) light to provide point-to-point communication through the air, space, and water. Laser optical communication systems offer a much narrower and more focused beam than traditional RF solutions that leads to increased signal intensity at the receiver [4]. Figure 1.1 shows a typical scenario of a fiber/free-space communication system where any electrical information source that could be voice, music, video or data is fed to an encoder and the modulated optical signal is sent over free space channel

(backend system connected over fiber) and demodulated by the photodetector (PD) at the receiver and converted back to the original data.
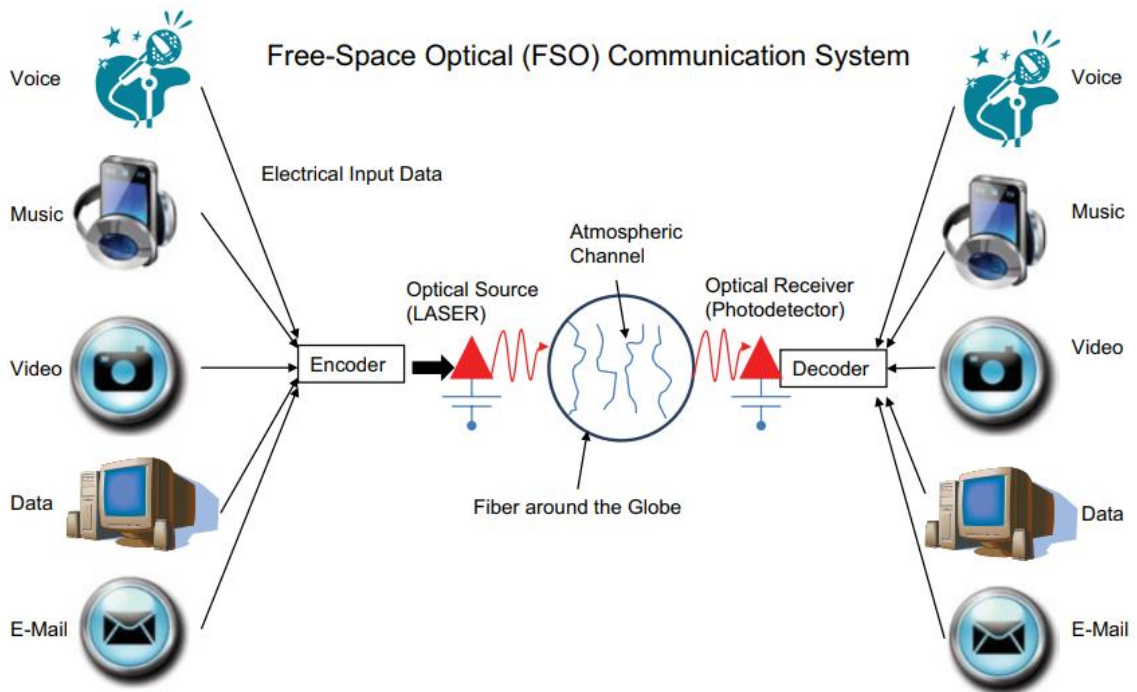
Fig. 1.1 A typical scenario of fiber/free space single-channel communication system [5].

Terrestrial FSO has now been established to be a worthwhile alternative in overcoming the scarcity of available bandwidth and high transmission rate requisite of end-user at a reasonable cost [6]. Thus, today FSO is a promising technology that can meet the requirements of cloud computing (CC), IoT, multiple-input multiple-output (MIMO) systems, big data, artificial intelligence (AI), and 5G network by offering vast license-free bandwidth, ultra-high-speed data rates up to 1 Tbps, last-mile access, economical and easy installation, high immunity to electromagnetic interference (EMI) and jamming. FSO has the potential to provide fast short to medium distance point to point communications [7]. FSO networks are much dependent on the perfect alignment of the transmitter and receiver. Depending on the deployment scenario and application, FSO communication systems are suitable for terrestrial and space-based communication. In the case of terrestrial communication, FSO systems are usually set up for last-mile access, enterprise connectivity, and fiber backup. For space-based communication, FSO systems are applied for inter-satellite communication, human spaceflight, data broadcasting satellites and

2

satellite and ground station communications. The next generation of high speed FSO communication systems will utilize seamless connection of free-space and optical fiber links operating at 1550 nm. By directly coupling the received beam into an optical fiber, the FSO communication system signal throughput is greatly enhanced. Seamlessly coupling a free-space beam to optical fiber bandwidth and protocol transparent communication link is achieved.

1.2 Need of free-space optical communication

FSO technology is useful where optical fiber cable cannot be implemented [8]. FSO communication uses light to transmit data through the atmosphere instead of fiber [9]. Light travels through air faster than glass, so FSO is communication at the speed of light in the atmosphere. This technology is useful where laying fiber optic cables is impractical. Communication is possible when there is direct LoS between source and destination as depicted in Fig. 1.2. Light can be focused by using light-emitting diodes (LEDs) and laser
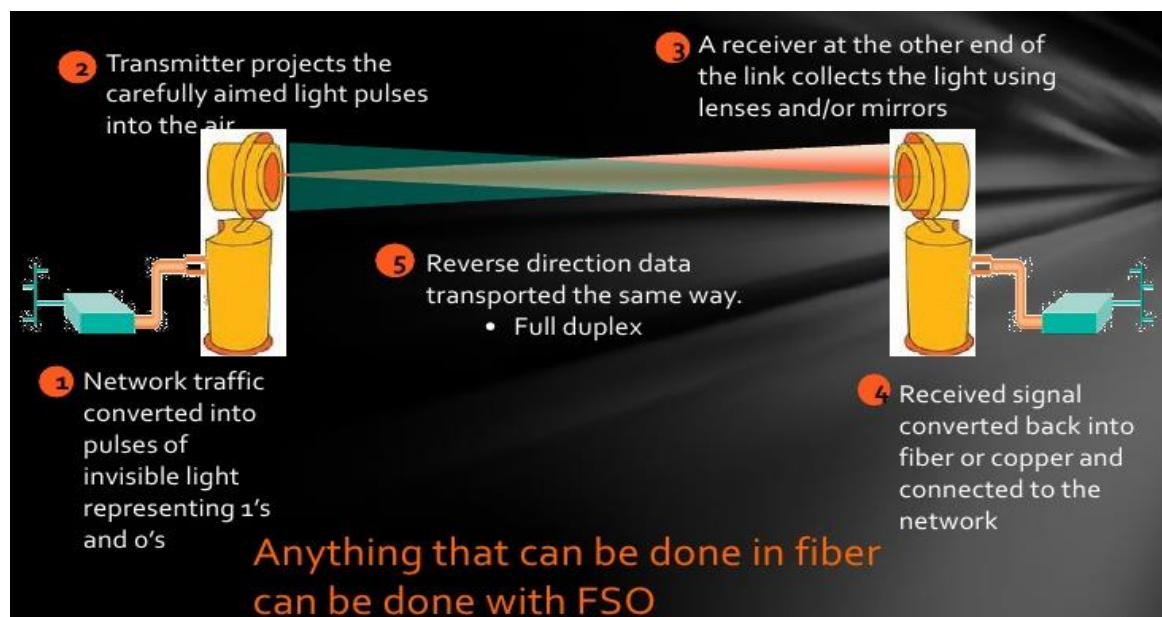
Fig. 1.2 Working scheme of FSO transmission system [10].

diodes [11]. FSO technology allows optical connectivity between two points without the need for fiber cable and spectrum license [12]. Optical fiber systems are time-consuming and are expensive to install and operate. FSO link can be used in the situation where optical fiber cable is under construction or as a disaster recovery by providing an active secondary

path to keep the network running until the primary path is restored [13]. Nowadays, the demand for broadband capacity is increasing exponentially due to the popularity of CC, big-data analysis, and 4K/8K video broadcast. To provide a cost-effective and high capacity last-mile access system to end-users, the FSO network would be a promising system for high-speed data traffic and spectrum scarcity [14]. FSO systems can also be used as a prime alternate system to RF wireless systems and the RF wireless services. Services like native space network, local area network (LAN)-to-LAN communication, disaster recovery, high definition TV (HDTV), biomedical imaging and videography transmission, metropolitan area network (MAN), cellular networks, and wireless on-demand videos can be explored with FSO system [15]. In addition to terrestrial communication, FSO also has a significant role in space applications [16]. In telecommunication, satellite communication uses an artificial satellite to provide communication links between various points on earth [17]. In past decades, FSO has attracted attention for various applications such as satellite to satellite cross-links, up and downlinks between space platforms [13]. The coverage area of the satellite-based system is large as compared to terrestrial-based wireless communication system. FSO communication systems (in space and terrestrial regions) have been evolved in counter to a growing need of high speed and bug-free information transmission and reception systems [18]. The last-mile need of FSO system are such as, communication involving deep-space link establishment, terrestrial stations links, UAVs, high altitude platforms (HAPs), inter-satellite communications, airliner, nomadic communication systems used in integrated systems of military and civilian context, fiber back up and enterprise connectivity to provide network security and overcome geographic restrictions.

1.3 Characteristics of free-space optical communication

FSO communication has progressively attracted attention in the past decade for many applications for providing high bandwidth wireless communication links. The basic characteristics of FSO technology are as following:

(i)   The inherent high carrier frequency in the range 20-375 THz enables FSO to provide HDR links.

(ii)   The optical carrier frequency which includes IR, UV, and visible light frequencies is greater than RF. The usable carrier frequency range in the case of RF is

comparatively lower by a factor of 10^5 [13]. Therefore, wireless optical communication guarantees an increase in information capacity.

(iii)   First/last mile access in areas hit by natural disasters. FSO link can act as an immediate recovery link.

(iv)   It takes less than 30 minutes to install the FSO link at normal locations.

(v)   Low power usage per transmitted bit.

(vi)   FSO offers dense spatial reuse.

(vii)   It is a secure system because of LoS operation and no security up-gradation is needed.

(viii)   The mean time between failure (MTBF) should be less than 10 years.

(ix)   The transmitted power is only concentrated in a narrow area. Thus providing FSO link with suitable spatial isolation from its potential interferers. The tight spatial confinement also allows the laser beam from the optical source to operate independently and makes the data interception by the unauthenticated user difficult.

(x)   As the information in FSO is not spread out in space but kept in a narrow beam of light, so, FSO is highly secured. LoS technology also makes FSO a secure and high-speed communication.

(xi)   Due to the congestion of the RF spectrum, the interference from adjacent carriers is a major problem faced by wireless RF communication. FSO systems take advantage of using the near IR portion of the electromagnetic spectrum which is not regulated by the International Telecommunications Union (ITU) thus solving the issue of spectrum scarcity and increasing the frequency reuse.

1.4 Advantages and disadvantages of free-space optical communication

FSO systems are used for HDR communication between two fixed points over distances up to several kilometers. FSO communication system offers several advantages over the RF system as well as certain disadvantages. FSO systems have attracted attention as an efficient solution for the last mile problem [19] to bridge the gap between the end-user and the fiber optic infrastructure already in place.

The advantages are listed as follows:

(i)   License-free communication or protocol transparency.

(ii)   Backhaul for expensive optical fiber communication (OFC).

(iii)   Quick and easy deployment.

(iv)   High-speed transmission.

(v)   No electromagnetic interference (EMI).

(vi)   Low power prerequisite due to low path loss.

(vii)   Low bit error rate (BER).

(viii)   High security.

(ix)   Low maintenance.

(x)   No Fresnel zone necessary.

(xi)   Absence of side lobes.

(xii)   Green communication.

(xiii)   Reduced multipath distortion.

(xiv)   Larger rejection of ambient background light.

(xv)   Improved link budget.

(xvi)   Last-mile access.

(xvii)   Easily expandable and reduces the size of network segments.

The disadvantages are listed as follows:

(i)   The main hindrance in the FSO communication is its high sensitivity towards geometrical and atmospheric effects which is the reason FSO being short-range communication.

(ii)   Links are highly susceptible to blocking (or shadowing), and therefore, they cannot provide mobility in a typical indoor environment.

(iii)   Reduced flexibility as it does not support point-to-multipoint broadcast links.

(iv)   Tight alignment between transmitter and receiver is required making it less convenient for certain applications.

1.5 Applications of free-space optical communication

In comparison to RF counterparts, the FSO link has a very high optical bandwidth available, allowing much higher bit rates. Terrestrial FSO products with transmission rates of 10 Gb/s are already in the market and the speeds of recent experimental FSO systems are competing with optical fiber [20]. Telecom carriers have already made substantial investments to augment the capacity of their fiber backbones [21]. To fully utilize the existing capacity, and therefore to generate revenue, this expansion in the backbone of the

networks should be accompanied by a comparable growth at the network edge where end users get access to the system. FSO systems are also appealing for a wide range of applications as shown in Fig. 1.3 and some of which are elaborated as follows:
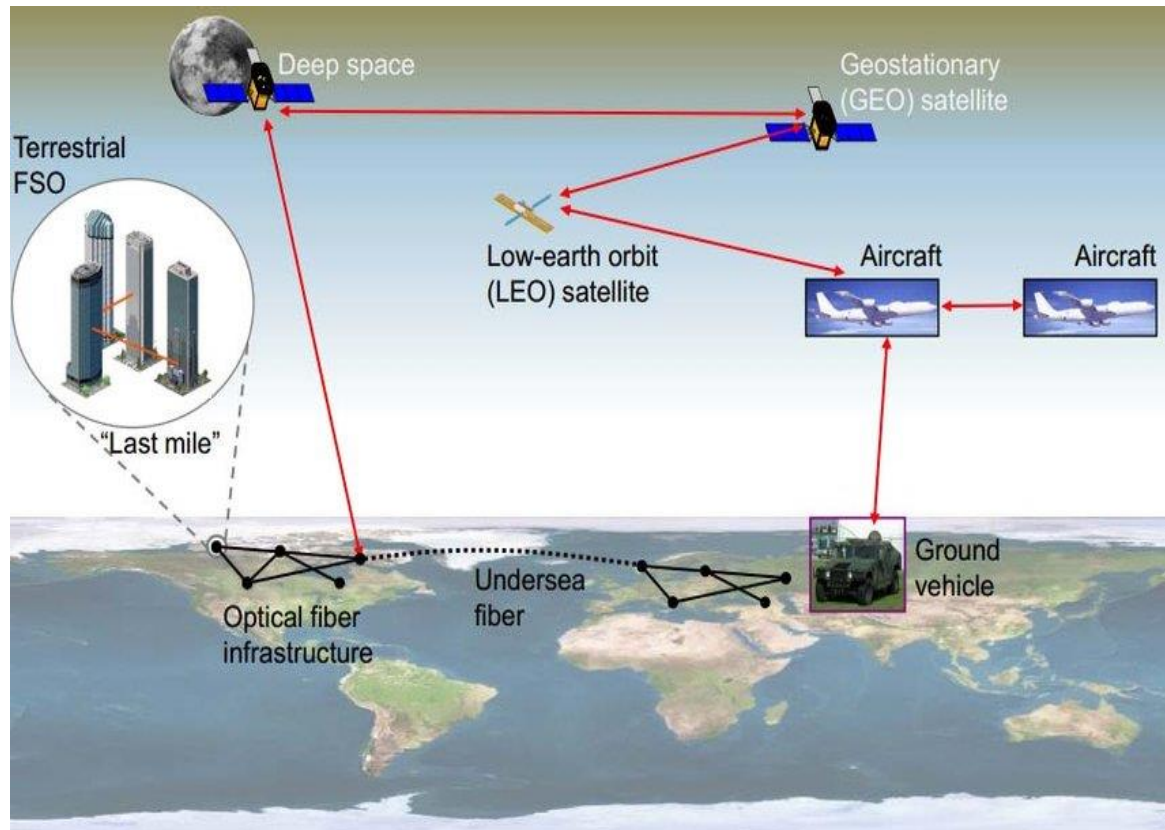
Fig. 1.3 Terrestrial and inter-satellite applications of FSO [22].

(i) **Enterprise connectivity:** FSO systems are easily installable. This feature makes it applicable for interconnecting LAN segments to connect two buildings. FSO systems can bridge multiple buildings in corporate and campus networks supporting ultra-high speeds without the cost of dedicated fiber-optic connections. FSO can be used in many optical links, such as building to building, ship to ship, aircraft to the ground, and satellite-to-ground.

(ii) **Video surveillance and monitoring:** Surveillance cameras are widely deployed in commercial, law enforcement, public safety, and military applications. Wireless video is convenient and easy to deploy, but conventional wireless technologies fail to deliver high throughput requirements for video streaming. FSO technology presents a powerful alternative to support high-quality video transmission.

(iii) **Back-haul for cellular systems:** Wireline connections and microwave links are typically deployed between the base stations and the mobile switching center in a cellular system. The growing number of bandwidth-intensive mobile phone services now requires the deployment of technologies such as FSO which allow much higher throughput.

(iv) **Redundant link and disaster recovery:** Natural disasters, terrorist attacks, and emergencies require flexible and innovative responses. Temporary FSO links can be readily deployed within hours in such disaster situations in which local infrastructure could be damaged or unreliable.

(v) **Security:** Today's cryptosystems can offer only computational security within the limitations of conventional computing power and the realization of quantum computers would, for example, make electronic money instantly worthless. Based on the firm laws of physics, quantum cryptography provides a radically different solution for encryption and promises unconditional security. Quantum cryptography systems are typically considered in conjunction with fiber optic infrastructure. FSO links provide a versatile alternative in cases where the fiber optic deployment is costly and/or infeasible.

(vi) **Broadcasting:** In broadcasting of live events such as sports and ceremonies or television reporting from remote areas and war zones, signals from the camera (or several cameras) need to be sent to the broadcasting vehicle which is connected to a central office through a satellite uplink. The required high-quality transmission between the cameras and the vehicle can be provided by an FSO link.

(vii) **The backbone for IoT:** The integration of FSO links with IoT and machine-to-machine (M2M) transmission links can provide high-speed large-capacity networks to realize global IoT.

(viii) **Fiber backup:** FSO can provide a backup link in case of failure of transmission through the fiber link.

(ix) **Military access:** As FSO is a secure and undetectable system, it can connect large areas safely with minimal planning and deployment time.

(x) **Backhaul:** FSO can help carry the traffic of cellular telephone from the base transceiver system (BTS) back to the public switched telephone network (PSTN) with high speed.

1.6 Challenges and issues in free-space optical communication

Free space optical communication uses light to transmit data through the atmosphere. But along its transmission path, various issues come into the picture. The primary challenges being whether attenuation loss [23], geometric loss, misalignment error, background noise, atmospheric turbulence [24], and scintillation [25]. Geometrical losses arise due to beam divergence between the transmitter and the receiver while atmospheric phenomena like fog, haze, snow, rain, and turbulence cause attenuation of the optical signal [26] and hence additional losses and this undoubtedly poses a great challenge to the FSO system designers. Furthermore, the Pointing error effect which occurs due to the misalignment between the transmitter and the receiver positions causes misalignment error [27]. Hence, despite many advantages, the performance of the FSO communication system is influenced by unpredictable atmospheric conditions as depicted in Fig. 1.4.
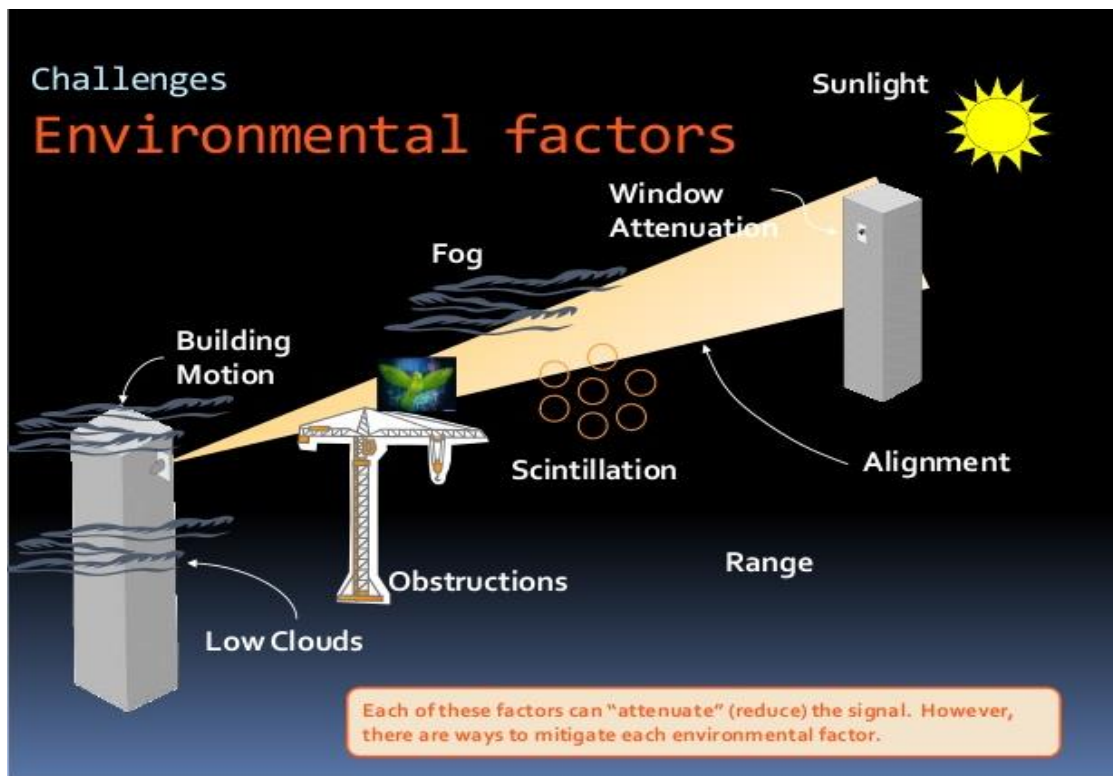
Fig. 1.4 Challenges and issues surrounding FSO [28].

The primary factors that deteriorate the FSO link performance are absorption, scattering, and turbulence. Out of these, atmospheric turbulence [29] is a major challenge that may lead to serious degradation in the link performance and make the communication

link infeasible [30]. Geometric loss arises due to the optical beam divergence due to propagation, laser beam diffusion, and the receiver aperture size while misalignment error or Pointing error are caused by wind, earthquake, and building vibrations [31]. FSO communication systems are affected by different weather attenuation losses due to haze, dust, fog, rain, smoke, and snow. Also, background noise comes into play due to exposure of the receiver to direct or in-direct sunlight or artificial lights. Background noise reduces the optical signal-to-noise ratio (OSNR) and can be eliminated through a bandpass filter (BPS) before photo-detection. Atmospheric turbulence causes a phase shift of the propagating optical signals resulting in distortions [32]. Turbulence is caused by temperature variation in the atmosphere which results in random fluctuation in the refractive index of air. The change in temperature, moisture, and pressure produces variations in the air refractive index. Because of the turbulence effect, the beam gets defocused, producing intensity fluctuation and spreading of the transmitted beam in the atmosphere [33]. The average power received at the FSO receiver also decreased by the effect of turbulence. The scintillation phenomenon is the most notable one for FSO system performance deterioration. Light traveling through scintillation will experience intensity fluctuations, even over relatively short propagation paths. The fluctuation in amplitude and phase of the optical signal propagating in free space is called scintillation. Scintillation is caused due to atmospheric turbulence. Also, scintillation is the result of constructive and destructive interference between the rays of the optical beams. Scattering of light is considered as the dispersion of energy that makes the signal divert from its original target. Geometrical scattering is the result of snow and raindrops that are made of larger molecules. Light scattering can drastically impact the performance of the FSO systems. The particles or atmospheric molecules that the light encounters during the propagation to its destination cause scattering. Several scattering regimes exist, depending on the characteristic size of the particles. While designing an FSO link, the designer has to ensure that the chosen operating wavelength has to be eye and skin safe. This means that the laser should not pose any kind of danger to the people who might encounter the communication beam but light above 1400 nm is absorbed by the cornea.

CHAPTER 2: LITERATURE SURVEY AND OUTLINE

2.1 Introduction

A lot of research work has been already done and is underway in the field of FSO. But, the developments made till now could not exploit the full potential of FSO. Researchers have been working over the feasibility of FSO systems for long-range communication and turbulent channel. From time to time, research work has been going on to overcome the challenges in the FSO link and to enhance potential system capacity, spectral efficiency (SE), and transmission distance. To achieve these objectives, different higher-order modulation techniques, coding schemes, channel models, homodyne and heterodyne coherent detection, and digital signal processing (DSP) techniques can be found in the literature. Based on the gaps found in the latest literature, research objectives and methodology have been laid down. Then, follows the thesis organization.

2.2 Higher-order modulation formats for higher spectral efficiency and better linearity

Higher-order quadrature amplitude modulation (QAM) driven FSO communication systems provide high data rates but at the cost of noise margin [34]. However, recently it has been shown that employing diversity techniques in coherent FSO communication systems improves receiver OSNR significantly [35][36]. The OSNR requirement of an optical wireless network is acute since it reduces the working budget and supplements the data transmission rate [37][38]. Sacchierit et al. [39] analyzed dense wavelength division multiplexing (DWDM) based FSO system. Kikuchi et al.[40] reported that at peak signal power, receiver sensitivity of QPSK modulation technique is 6 dB higher compared to the IM scheme since symbol distance on the I/Q plane is twice it. Wang et al.[41] demonstrated a 5 GBaud QPSK modulation driven mid-infrared (MIR) communication system using wavelength conversion technique over 10 m FSO link. All amplitude and phase information was retained due to the utilization of coherent detection and DSP at a power penalty of 2.73 dB compared with back to back (B-2-B) system. Singh et al.[42] proposed the development of an FSO link with thirty-two Nyquist wavelength division multiplexing (WDM) channels each carrying 200 Gb/s DP-QPSK data under the impact of diverse

atmospheric conditions. The results revealed that the tendency to transport high-speed data over each channel for longer distances was attributed to the use of DSP techniques for suppression of phase disparity within the transmitted symbols and local oscillator (LO) signal. Feng et al.[43] showed the feasibility of a coherent full-duplex QPSK-FSO communication system for high-speed and long range operation realizing a data rate of 40 Gbit/s for 1 km at received power of −16.5 dBm and power penalty of 2.6 dB. In DWDM, the signals from various sources are combined and transmitted over different wavelengths. Fusion of DWDM with the FSO results in high data rates up to 40 Gb/s with increased capacity and range. Chaman-Motlagh et al. [44] studied the performance of atmospheric effects on the FSO link with multiple receivers. Various environmental factors like reflection, absorption, scintillation, Doppler shift result in signal degradation and hence attenuation. With the employment of multiple receivers, it was observed that the OSNR decreases after a particular link range. Mohan et al. [45] worked upon the FSO system using intensity modulation/direct detection (IM/DD) with on-off keying (OOK) for the log-normal channel. Here, they have considered aperture averaging and spatial diversity techniques to overcome turbulence in the log-normal channel and concluded that spatial diversity gave better SNR and BER values. Jiao et al. [46] studied quadrature amplitude multiplexing (QAM) based FSO system with spatial diversity in the turbulent atmosphere and BER and outage probability were derived. It was shown that the system gave better results than the single input single output (SISO) system. Prabu et al. [47] studied polarization shift keying (POLSK) and coherent OWC based FSO system in a turbulent channel for various modulation techniques like on-off keying (OOK), POLSK, and coherent OWC to evaluate average spectral efficiency (ASE), they concluded that ASE decreases with growth in turbulence. Dayal et al. [48] studied a wavelength division multiplexing (WDM) based FSO system with optical amplifiers. FSO is a short-range communication system owing to atmospheric factors like rain, snow, haze, and clouds which deteriorate the system performance over long-distance [49]. M-ary QAM modulation technique allows multiple bits to be transmitted simultaneously by mapping them into one symbol [50]. The advantages of single-carrier M-ary QAM include simplicity, easy wavelength allocation, more compactness, low power dissipation, and it can be implemented in real-time [51]. Optical M-ary QAM signal can be generated by modulating a single narrow linewidth cavity laser using a single or multiple in-phase and

quadrature modulator (IQM) [52]. Rakesh et al. [53] showed that multimedia transmission over WDM/TDM passive optical network (PON) with 128 optical network units (ONUs) is possible up to a range of 28 km with different modulation techniques but the most appropriate data format being non-return-to-zero (NRZ) rectangular. Ali et al. [54] designed and experimentally established a 10 Gb/s OWC system for data center networks up to a 3 m distance with an acceptable BER of 10^{-9} that permits flexibility in transceiver design with increased capacity and low power usage. Israr et al. [55] showed that MIMO is a promising choice for FSO communication. They analyzed the 4×4 MIMO FSO system under various modulation formats and observed the effect of varying distance, transmitted optical power, and attenuation on system performance and established that return-to-zero (RZ) is well-matched for the MIMO FSO system. A quadrature phase-shift keying (QPSK) modulator is used to modulate a narrowband optical laser in quadrature phases using multilevel electrical signals from high-speed digital to analog converter (DAC) and driving amplifiers [56]. Immadi et al. [32] worked upon the effect of adverse attenuation due to scintillation, haze, fog, snow and rain on the performance of FSO communication system under various attenuation models like CARBONNEA, JAPAN, SAMIR and SURIZA. Their observation regarding the variation of received optical power, received electrical power and quality factor with rain intensity revealed that the received optical power and Q-factor were highest for SURIZA model and lowest for SAMIR model both at low and high rain intensities.

2.3 Optical coherent detection

Coherent optical transmission refers to optical communication systems that apply higher-order modulation format at the transmitter side and coherent detection using a local oscillator (LO) and digital signal processing (DSP) at the receiver side. Coherent optical transmission is the key to achieve high data rates that are required for next-generation optical networks [57]. It provides high SE and long transmission distance [58]. Using higher-order modulation formats such as M-ary QAM and QPSK would allow better utilization of bandwidth, hence greater SE [59]. The rebirth of coherent optical transmission started with the development of a coherent optical system based on optical differential quadrature phase-shift keying (DQPSK) [60]. This scheme increased the bit rate by 4-fold compared to IM/DD systems, achieving 40 Gb/s at 20 Gbaud per WDM

channel. Between 2005 and 2010, the research efforts focused on applying DSP techniques and polarization division multiplexing (PDM) to further increase the data rate of coherent optical systems to 100 Gb/s [61]. The first coherent optical system that was based on orthogonal PDM and QPSK became commercially available [62]. The system provides 100 Gb/s at 25 Gbaud and applies DSP extensively for bit coding, laser source nonlinearity compensation, fiber non-linearity precompensation, pulse shaping, carrier phase, and frequency estimation, as well as chromatic dispersion (CD) and polarization mode dispersion (PMD) compensation [63]. The 100 Gb/s PDM-QPSK coherent optical system by far has been the highest data rate optical system available in the market. Currently, coherent optical communication systems with data rates beyond 100 Gb/s per optical channel are under investigation [64]. The goal is to achieve 400 Gb/s per WDM channel using higher-order QAM modulation formats such as 16-QAM and 64-QAM [65]. The coherent optical transmission allows higher network flexibility by supporting different baud rates and modulation formats per single optical carrier leading to increment in spectral efficiency and reduction of the cost per bit of transmitted information. The Internet traffic demand has been growing at a rate of 25% per year owing to the emergence of HDR solutions including high definition 3D TV, video conferencing, online gaming, CC, and big data. Commercially available coherent optical systems are based on PDM and 4-QAM or PDM-QPSK [66]. However, optical QAM transmitters based on multiple QPSK modulators that are driven by binary electrical signals appears to be the most promising as they eliminate the need for high speed DAC and driving amplifiers associated with single QPSK modulator that is driven by multilevel electrical signals [67]. In coherent receivers, there are two approaches of homodyne and heterodyne signal detection [68]. Homodyne detection permits a better detection sensitivity but requires an accurate optical phase-locked loop (PLL), which is very expensive to realize. Due to this reason, heterodyne detection has been more widely considered in the literature. Coherent detection provides spectral shaping functionality that enables the usage of flexible grid systems and allows the rejection of interference from adjacent channels. This increases the spectral efficiency by placing the optical carriers closer to one another within the transmission band. By virtue of DSP capability, coherent optical systems allow an increase of receiver sensitivity by 15 dB to 20 dB and therefore increasing the transmission distance [69].

2.4 Digital signal processing for the compensation of linear and nonlinear impairments

The digital signal at the output of ADC is further processed using DSP circuits for noise removal and data recovery. DSP refers to various techniques for improving the reliability and accuracy of coherent optical communication links through the removal of channel impairments, such as CD, self-phase modulation (SPM), and PMD as well as laser phase and frequency noise [70]. The use of DSP in conjunction with coherent detection allows the preservation of full information of the incoming signal, which in return increases receiver sensitivity [71]. To achieve a transmission capacity closer to the Shannon limit, high-speed DSP algorithms are employed to estimate and correct the signal impairments in the electrical domain [72]. DSP compensates for transmission impairments such as CD and PMD, which in return eliminates the need for DC modules and allows robust performance [73]. The signal at the output of the ADC is fed to the CD compensation block which focuses on eliminating the CD in the digital domain using multiple techniques such as digital square filter (DSF), static time-domain finite impulse response filter, and frequency domain equalizers [74]. By employing DSP techniques including the constant modulus algorithm (CMA), it was possible to mitigate the multipath effect in a 400G fiber/wireless hybrid system combined with polarization division multiplexing (PDM) and multiple-input multiple-output (MIMO) communication [37]. The PMD is also removed in the digital domain using adaptive filters such as the least mean square and CMA filters. Carrier phase estimation (CPE) algorithms track and remove the phase noise using different methods such as normalized least means square estimator, differential phase estimation, and the Viterbi-Viterbi (VV) estimators [75]. The decision circuit with the appropriate threshold levels is used to recover the bits. The bits are decoded and converted to a serial bit stream at the output. Although it is still difficult to establish a high speed and long haul FSO link owing to challenges put forth by climate and physical installation, but coherent detection along with advanced digital modulation techniques and digital signal processing (DSP) algorithms have considerably assisted to resolve the trouble [76]. At the receiver, the signals are converted to electrical signals utilizing heterodyne or homodyne detection. The received signal errors are compensated using DSP techniques. Coherent receivers enjoy the high sensitivity associated with homodyne detection but with the added benefit of advanced DSP that offers the possibility to compensate for linear impairments

such as CD and PMD [77]. In that respect, the remarkable tolerance of coherent receivers against optical noise, CD, as well as PMD have been reported [78]. All these features highlight the potential of joint implementation of coherent detection and DSP to develop high bit rate solutions that meet the system requirements.

2.5 Gaps and motivation

(i)   The IM/DD-based wireless optical communication systems do not meet the requirements of next-generation optical networks.

(ii) The range of wavelengths between 400 to 1400 nm can cause potential eye hazards or even skin damage. However, the light below 400 nm and above 1400 nm is absorbed by the cornea and does not reach the retina.

(iii) Amplitude and phase imbalances within the in-phase (I) and quadrature (Q) signals can result due to laser phase jitter and atmospheric attenuation at several points along the transmission path.

(iv) Employment of FSO communication in indoor environments has been done mainly by using diffuse optics. Such proposals have been challenged due to the limited power of a single source that is being diffused in all directions.

(v)   Linear and nonlinear distortions such as CD, PMD, SPM, cross-phase modulation (XPM), cross-polarization modulation (XPolM), and four-wave mixing (FWM) limit the spectral efficiency in optical communication.

2.6 Research objectives

(i)   To design a free-space optical transceiver system for different advanced digital modulation techniques – QPSK, 16-QAM, 256-QAM for higher optical spectral efficiency and data rates.

(ii) To implement balanced homodyne detection and several high-level digital signal processing algorithms at receiver for digital compensation of signal impairments.

(iii) To analyze the performance of all proposed systems with respect to BER, EVM, OSNR, transmission distance, launched optical power, received optical power, laser linewidth, beam divergence, and carry out the performance comparison between all the proposed systems with various M-ary modulation formats.

2.7 Research methodology

To achieve all the mentioned objectives, the design of all the proposed systems, optimization of link parameters, and test was carried out in OptiSystem V. 16 simulation design suite. The obtained values of the performance parameters were recorded and plotted using MATLAB R2018b.

2.8 Thesis organization

This thesis comprises a total of eight chapters together with this introductory chapter. Chapter 2 discusses the literature review regarding the FSO communication with a prime focus upon the latest research developments made in areas of optical advanced modulation formats, coherent optical transmission, and DSP techniques which allows for the identification of gaps, henceforth formulating the research objectives and research methodology respectively. Chapter 3 deals with the analysis of a two-channel wireless optical communication system. Chapter 4 presents the analysis of the FSO communication system under three different optical windows: 850 nm, 1310 nm, and 1550 nm. Chapter 5 deals with the design and analysis of DP-QPSK based FSO transceiver system with the application of coherent detection and DSP algorithms for maximum reach. Chapter 6 presents the design and performance analysis of the DP-16-QAM terrestrial FSO transceiver system using homodyne detection and DSP at the receiver for the high-speed digital data link. Chapter 7 deals with the design and analysis of DP-256-QAM based FSO transceiver with coherent detection and DSP algorithms for ultra-high-speed and 5G applications. The system performance is measured concerning BER, EVM, OSNR, beam divergence, transmission distance, launched and received optical power respectively. To finish, conclusions and recommendations are presented in Chapter 8, which is followed by a comprehensive list of references.

CHAPTER 3: DESIGN OF TWO-CHANNEL WIRELESS OPTICAL COMMUNICATION SYSTEM

3.1 Introduction

FSO is also known as fiber-less optics is a subset of optical wireless communication (OWC). The former uses a guided laser beam in the near-infrared (IR) region to transmit data at high speed but the latter uses infrared, ultraviolet (UV), or unguided visible light to carry an optical signal. Terrestrial FSO has now been established to be a worthwhile alternative in overcoming the scarcity of available bandwidth and high transmission rate requisite of end-user at a reasonable cost [79]. Thus, today optical wireless communication is a promising technology that can meet the requirements of cloud computing (CC), internet of things (IoT), multiple-input multiple-output (MIMO) systems, big data, artificial intelligence (AI), and 5G network by offering vast license-free bandwidth, high-speed data rates up to 100 Gbps, last-mile access, economical and easy installation, high immunity to electromagnetic interference (EMI) and jamming [80]. The main hindrance in the FSO communication is its high sensitivity towards geometrical and atmospheric effects which is the reason FSO being short-range communication [81]. Geometrical losses arise due to beam divergence between the transmitter and the receiver while atmospheric phenomena like fog, haze, snow, rain, and turbulence cause attenuation of an optical signal and hence additional losses [23]. Furthermore, the Pointing error effect which occurs due to the misalignment between the transmitter and the receiver positions causes misalignment error [27]. In this chapter, two optical communication systems, one with an FSO channel (channel A) and another with an OWC channel (channel B) have been proposed and analyzed. The performance evaluation has been done based on quality factor (Q-factor) and bit error rate (BER) variation concerning link distance for different varying link parameters. Geometrical losses due to the divergence of the beam have been countered by aperture averaging in which the transmitter aperture diameter (5 cm) is kept small and the receiver aperture diameter (20 cm) is kept large. Beam divergence is taken from 2 to 5 mrad. An operating wavelength of 1310 nm is taken with attenuation varying from 0.32 dB/km to 4 dB/km. Similarly, additional losses are taken from 5 dB to 10 dB and the data rate is set at 1.5 Gb/s.

3.2 Proposed system

Wireless optical communication system consists of three main components: a transmitter, a channel (FSO/OWC), and a receiver. The block diagram of the proposed system is shown in Fig. 3.1. The transmitter unit holds a pseudo-random bit sequence generator (PRBS), a line encoder (NRZ), a continuous wave (CW) laser, and a Mach-Zehnder modulator (MZM). The PRBS generates a pseudo-noise sequence which is represented in NRZ format by the line encoder. This NRZ electrical output is fed at one input port of MZM while another input port is fed with a laser beam (optical source). The modulator superimposes the NRZ signal onto the high-frequency optical carrier signal and generates an optical signal output at its output port. This modulated optical signal is propagated along a wireless channel, here, in this case, an FSO link (channel A) and an OWC link (channel B).
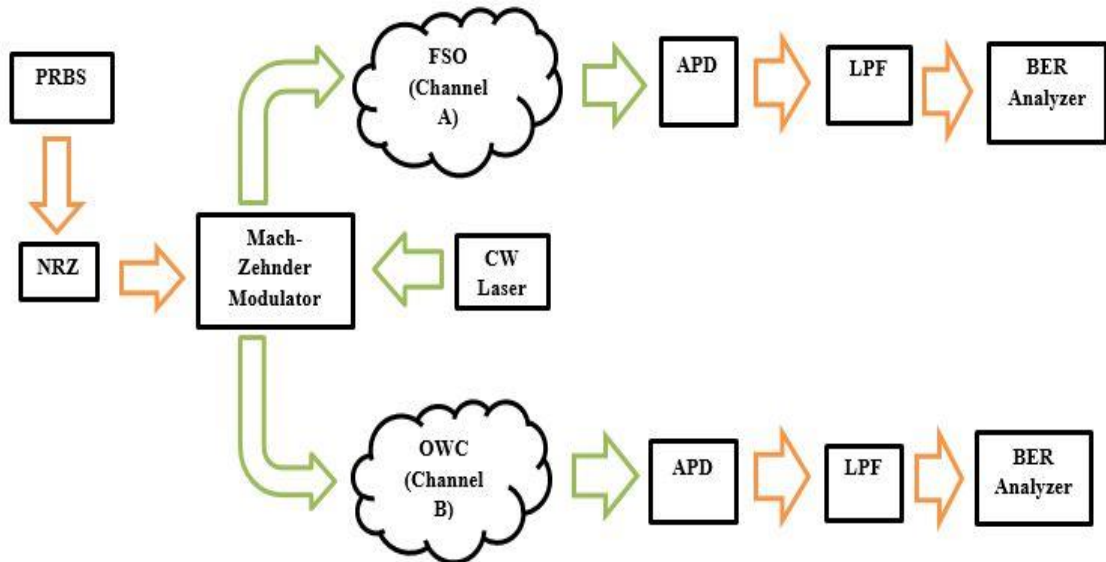
Fig. 3.1 Design schematic of the two-channel wireless optical communication system.

The receiver end sub-system contains an avalanche photodiode (APD), a low pass filter (LPF), and a BER analyzer. An APD (optical detector) converts the received optical signal back to its electrical output. Then, an LPF blocks any high-frequency signal (noise) and the output is fed to a BER analyzer that lets the user analyze and demonstrate the BER and Q-factor of the signal under consideration [82]. The reduction of the laser power rests on two main factors: attenuation and geometrical loss [83][84]. Attenuation is the degradation of signal strength due to atmospheric impediments while geometric loss arises owing to beam spreading between the transmitter and the receiver.

Table 3.1 Simulation parameters considered in the proposed design.

Parameter	Value
Launched optical power	10 dBm
Data rate	1.5 Gbps
Transmitter optics efficiency	1
Receiver optics efficiency	1
Beam divergence	2 - 5 mrad
Atmospheric attenuation	0.32 - 4 dB/km
Wavelength	1310 nm
Range	100-1000 m (channel A),
	10-100 km (channel B)
Additional loss	5 -10 dB

In wireless systems, the power received at the receiving antenna is given by the equation [85]

$$P_{RX} = P_{TX} \eta_{TX} \eta_{RX} g_{TX} g_{RX} L_{TX} L_{RX} (\lambda/4\pi R)^2 \qquad (3.1)$$

where P_{RX} is the received power, P_{TX} is the transmitted power, η_{TX} is the transmitter optics efficiency, η_{RX} is the receiver optics efficiency, g_{TX} is the transmitter gain, g_{RX} is the receiver gain, L_{TX} is transmitter pointing loss factor, L_{RX} is the receiver pointing loss factor, λ is the wavelength, R is the distance between transmitter and receiver [86]. All the parameter values taken in the simulation model have been listed in Table 1. The transmitter gain can be written as [85]

$$g_{TX} = (\pi D_{TX}/\lambda)^2 \qquad (3.2)$$

where D_{TX} is transmitter telescope diameter. The receiver gain can be written as

$$g_{RX} = (\pi D_{RX}/\lambda)^2 \qquad (3.3)$$

where D_{RX} is the receiver telescope diameter. Pointing error arises from the off-balance between the transmitter and the receiver [87]. Beam divergence, the aperture diameter of

the transmitting and receiving antenna, and jitter alteration impact the pointing error effect. The influence of pointing error on the performance of FSO and OWC systems is taken into account by pointing loss factor which is given by [88]

$$L_{TX} = e^{(-g_{TX}\theta_{TX}^2)} \tag{3.4}$$

and

$$L_{RX} = e^{(-g_{RX}\theta_{RX}^2)} \tag{3.5}$$

where θ_{TX} and θ_{RX} are transmitter and receiver azimuth pointing error angle. In the simulation model, we have taken transmitter pointing error and receiver pointing error as 0 μrad.

3.3 Results and analysis

The design and performance analysis of the proposed model has been done in OptiSystem V. 16. At times the values of BER have come out to be largely due to the limitations of the simulation platform but 10^{-9} has been taken as the minimum acceptable BER for each observation.

3.3.1 Performance analysis of FSO link system

Figure 3.2 shows the eye diagrams took for range from 100 to 1000 m with varying simulation parameters for the FSO channel. By carefully examining the eye diagrams, we could get the values of Q-factor, minimum BER, and eye height. Their values have been listed in Table 3.2.

| (a) | (b) | (c) |

(d)   (e)   (f)

(g)   (h)   (i)

(j)
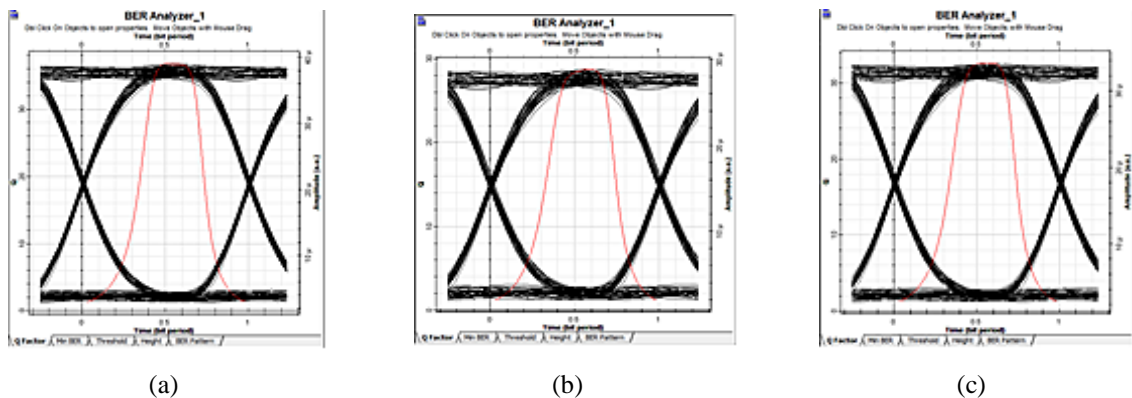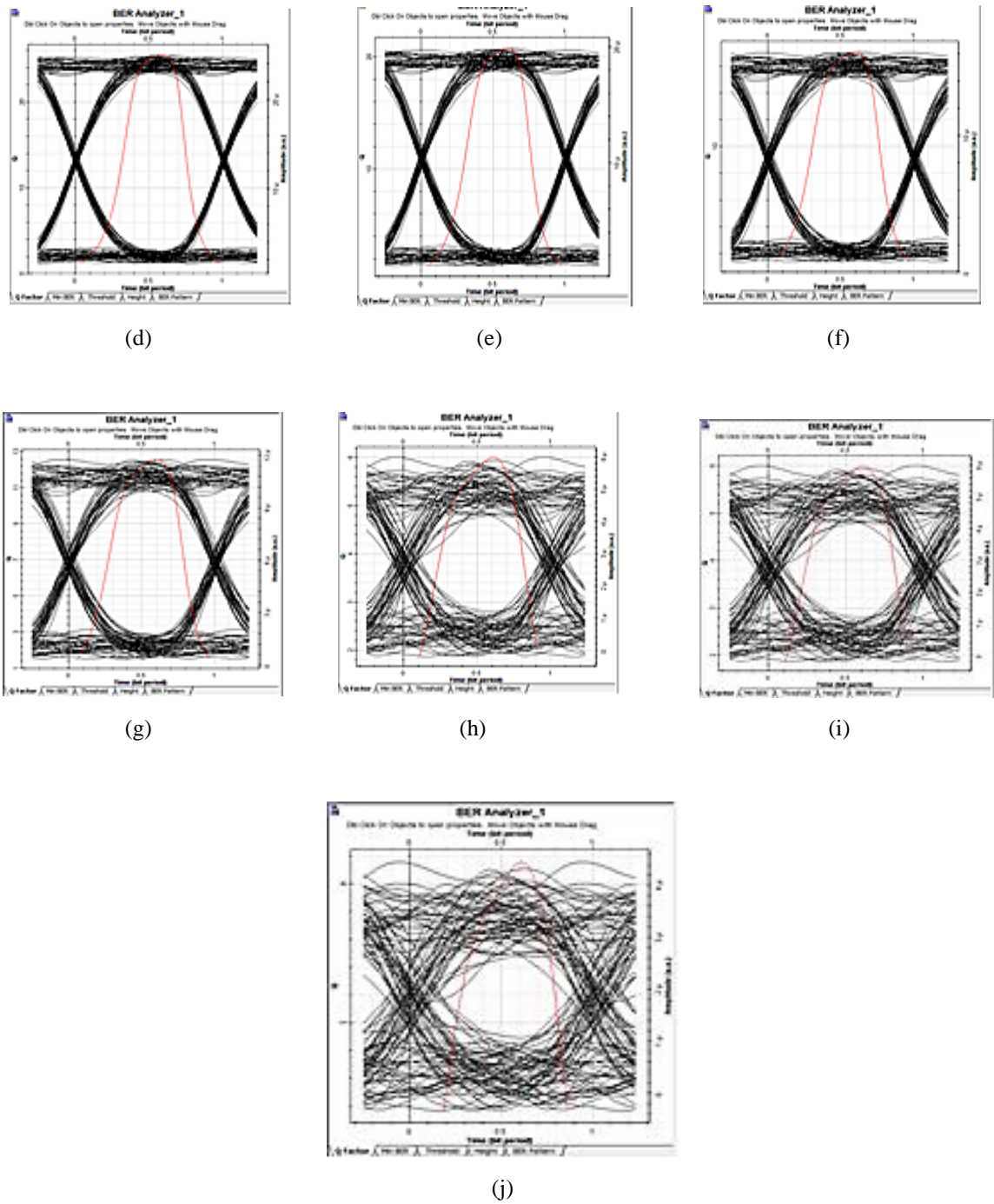
Fig. 3.2 Eye diagrams for FSO link at transmission distances of (a) 100 m, (b) 200 m, (c) 300 m, (d) 400 m, (e) 500 m, (f) 600 m, (g) 700 m, (h) 800 m, (i) 900 m and (j) 1000 m.

On observing the eye diagrams and Table 3.2, it can be concluded that the FSO channel gives optimal performance up to 800 m but afterwards, both the Q-factor and BER performance deteriorates due to atmospheric effects and losses.

Table 3.2 Values of performance parameters obtained for FSO channel.

Range (m)	Q-factor	BER	Eye height (a.u.)
100	36.78	10^{-296}	10^{-5}
200	32.60	10^{-233}	10^{-5}
300	28.74	10^{-182}	10^{-5}
400	25.43	10^{-143}	10^{-5}
500	20.72	10^{-95}	10^{-5}
600	17.07	10^{-65}	10^{-5}
700	12.56	10^{-36}	10^{-6}
800	8.34	10^{-18}	10^{-6}
900	6.00	10^{-6}	10^{-6}
1000	4.12	10^{-5}	10^{-7}
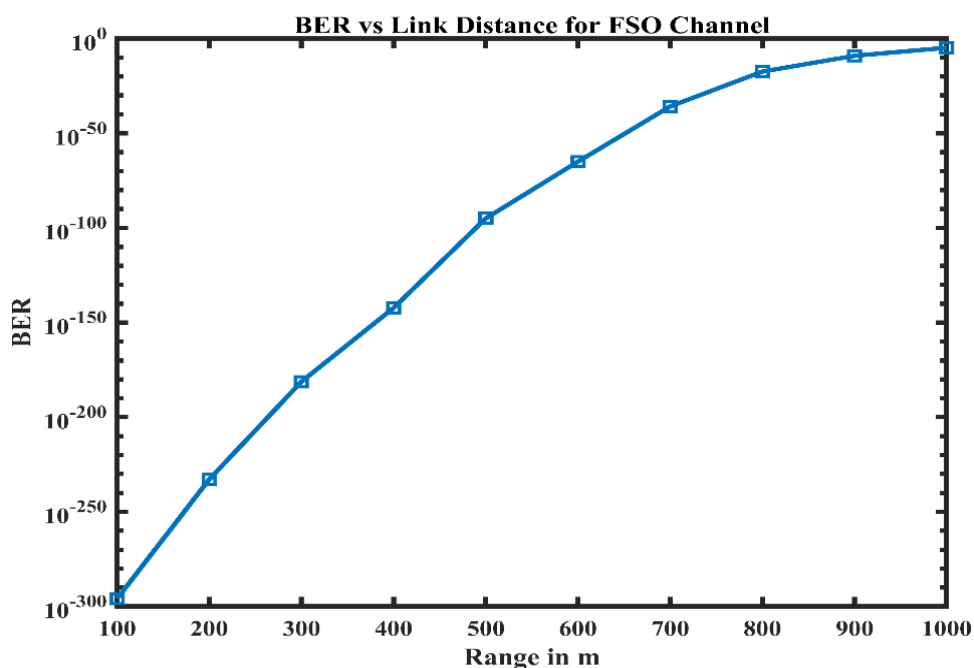
Fig. 3.3 Variation of BER with link range for FSO channel.

Figures 3.3 and 3.4 bring out the variation of BER and Q-factor with link distance for the FSO system respectively. As can be seen from the results, BER increases with an increase in transmission distance, and Q-factor decreases with increasing transmission range. Thus, the FSO link is suitable for short-range communication systems only.
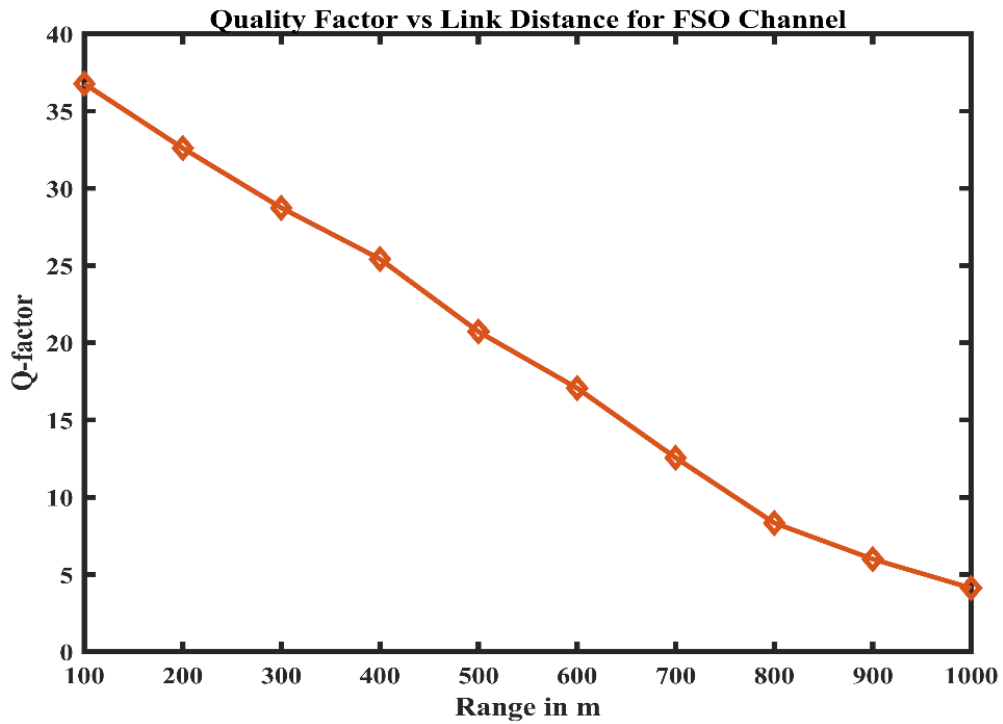
Fig. 3.4 Variation of Q-factor with link range for FSO channel.

3.3.2 Performance analysis of OWC link system

Figure 3.5 shows the eye diagrams obtained at a specific link range from 10 km to 100 km for the OWC channel with various simulation parameters. Also, the relation of BER and Q-factor with respect to link distance is depicted in Figures 3.6 and 3.7 respectively. By carefully examining the eye diagrams, we could get the values of Q-factor, minimum BER, and eye height. Their values have been listed in Table 3.3.


| (a) | (b) | (c) |

(d)   (e)   (f)

(g)   (h)   (i)

(j)
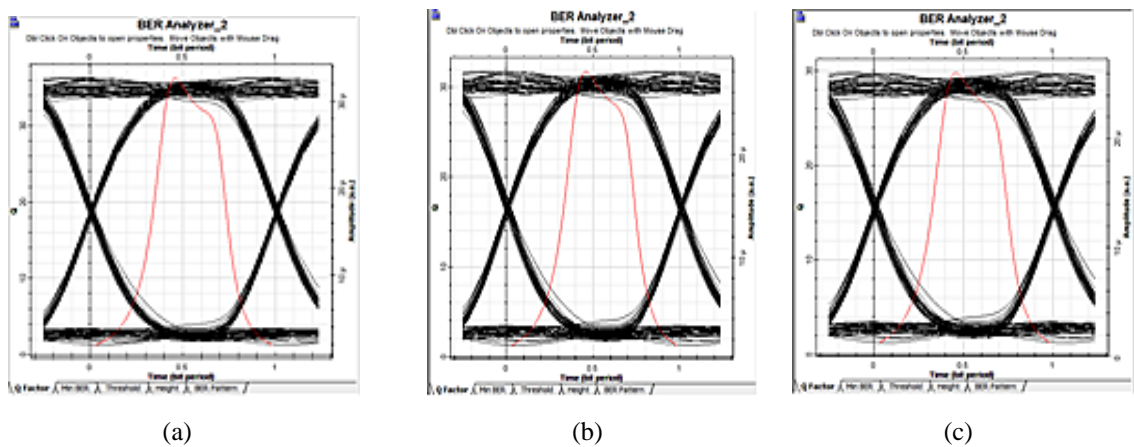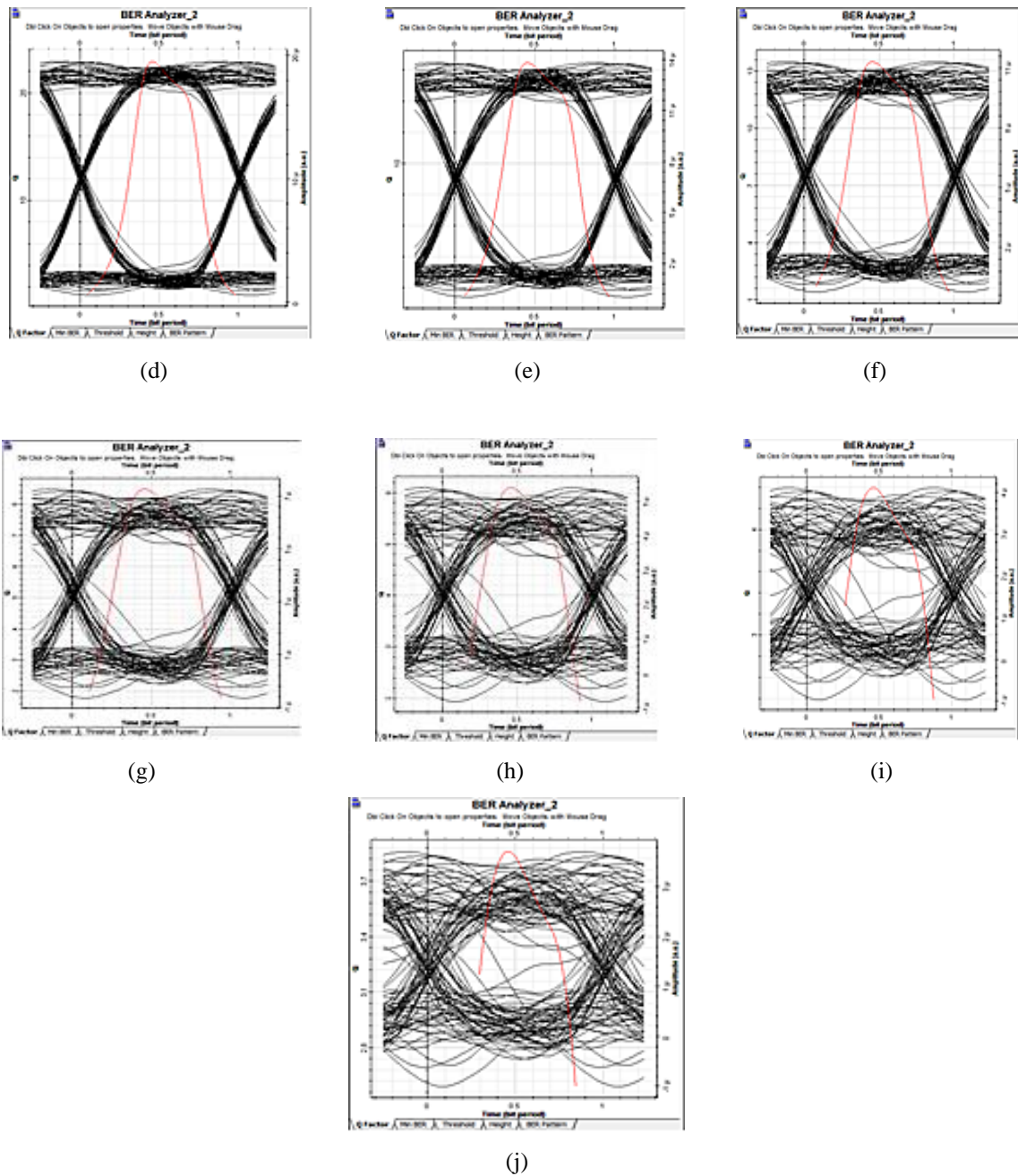
Fig. 3.5 Eye diagrams for OWC link at a transmission distance of (a) 10 km, (b) 20 km, (c) 30 km, (d) 40 km, (e) 50 km, (f) 60 km, (g) 70 km, (h) 80 km, (i) 90 km, and (j) 100 km.

On observing the eye diagrams and Table 3.3, it can be concluded that the OWC channel gives optimal performance up to 80 km supporting a data rate of 1.5 Gbps but then both the Q-factor and BER performance deteriorates as revealed in Fig. 3.6 and Fig. 3.7 respectively. Henceforth, with the results obtained it can be verified that the OWC channel supports long-range communication with reliable system performance.

Table 3.3 Values of performance parameters obtained for OWC channel.

Range (km)	Q-factor	BER	Eye height (a.u.)
10	36.26	10^{-288}	10^{-5}
20	31.73	10^{-221}	10^{-5}
30	29.76	10^{-195}	10^{-5}
40	22.90	10^{-116}	10^{-5}
50	16.46	10^{-61}	10^{-6}
60	13.43	10^{-42}	10^{-6}
70	8.48	10^{-17}	10^{-6}
80	6.09	10^{-10}	10^{-6}
90	4.39	10^{-6}	10^{-7}
100	3.02	10^{-5}	10^{-7}
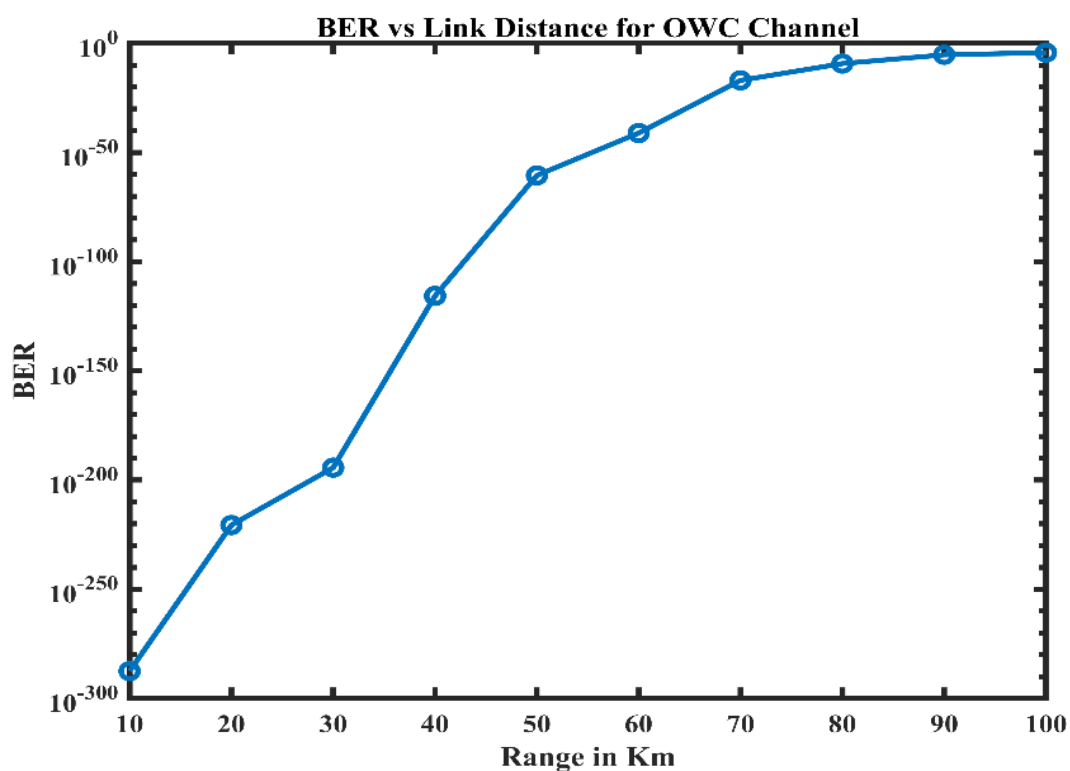
Fig. 3.6 Variation of BER with link range for OWC channel.
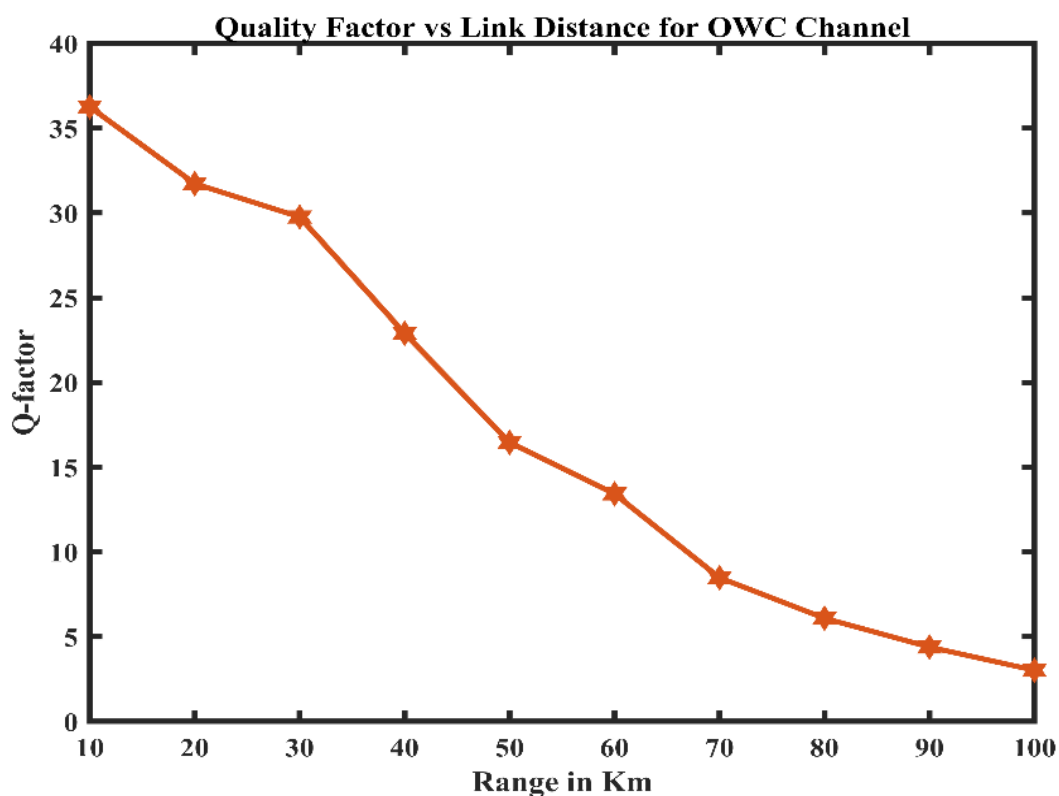
Fig. 3.7 Variation of Q-factor with link range for OWC channel.

3.4 Concluding remarks

The OWC and FSO link performances are investigated by taking Q-factor and BER as performance metrics. It is realized that the operating wavelength of 1310 nm provides the optimum performance for both FSO and OWC channels for a specific range. Various system parameters are varied and simulated to examine their effect on the Q-factor and BER performance of both the links. As per the results analyzed from the eye diagrams using Q-factor and BER, the FSO channel is capable of data transmission at a data rate of 1.5 Gb/s up to a link distance of 800 m while the OWC channel can attain the same data rate up to 80 km. The system performance degrades with an increase in the range due to high attenuation and additional losses. The system can be further investigated for different wavelengths at different atmospheric conditions with and without optical amplifiers in the future course of work.

CHAPTER 4: STUDY OF FREE SPACE OPTICAL COMMUNICATION SYSTEM UNDER VARIOUS OPTICAL WINDOWS

4.1 Introduction

Free space optics is a light-wave communication technology that operates in the near-IR region of the electromagnetic spectrum (about 700 to 1675 nm) and uses an atmospheric channel as the transmission medium for both inter-satellite and terrestrial networks. The major challenge in the FSO system is its short-range operation due to its vulnerability to atmospheric attenuation induced by rain, fog, snow, haze, and additional losses which come into play due to misalignment and scintillation. These shortcomings lead to laser phase jitter, signal attenuation, and beam wandering which degrade the quality of service (QoS) in FSO [89]. Due to the random distribution of turbulence cells called eddies, the reliability of the FSO system is difficult to boost [90]. To overcome this uncertainty, the design of a homogenous optical filter based on an artificial neural network (ANN) model for all three optical windows has been implemented in the literature to predict the optical specifications through machine learning [91]. Although it is still difficult to establish a high speed and long haul FSO link owing to challenges put forth by climate and physical installation, but coherent detection along with advanced digital modulation techniques and digital signal processing (DSP) algorithms have considerably assisted to resolve the trouble. In a strong turbulent scenario, atmospheric attenuation could grow up to 100 dB/km or beyond with a steep rise in additional losses also. Nevertheless, wavelength and frequency play an important role in the operation of the FSO system; the amount of optical power received, beam divergence, scattering losses, attenuation, and link range are all wavelength-dependent. Therefore, if we want to aim at long-range FSO communication systems, we need to choose the operating wavelength wisely. This is significant because free space optics is a practical alternative to radiofrequency (RF) technology and hence knowing how it responds with each optical window becomes important for a seamless communication system. The most frequently used wavelengths for FSO are 850 nm, 1310 nm, and 1550 nm [92]. All these atmospheric transmission windows have their pros and cons; 850 nm and 1310 nm laser diodes deliver economical operation but offer short-range

connectivity [93] while 1550 nm laser diode is preferred for eye safety reasons and long-distance communication but are quite expensive. In this chapter, the FSO system with 2000 m link range has been designed and investigated for three atmospheric transmission windows - 850 nm, 1310 nm, and 1550 nm to record and contrast their performance and integrity both realistically and mathematically by way of BER, Q-factor and optical power as performance parameters. The analysis put forth in this work demonstrates the fitness of FSO systems for diverse optical windows under different operating conditions. To achieve our objectives, each time we modeled our system for a different set of wavelengths, we recorded the measurements for performance metrics with respect to link parameters and analyzed them both graphically and mathematically.

4.2 System design

The proposed FSO system comprises a transmitter unit, the FSO channel, a receiver unit, and visualizer components as shown in Fig. 4.1. The FSO communication system under consideration is analyzed for the behavior of performance metrics with varying link parameters for various optical windows. The transmitter side involves a pseudo-random bit sequence generator (PRBS) that generates a pseudo-noise (PN) sequence of 1's and 0's which is fed to an NRZ pulse generator that produces an electrical signal. The laser emits
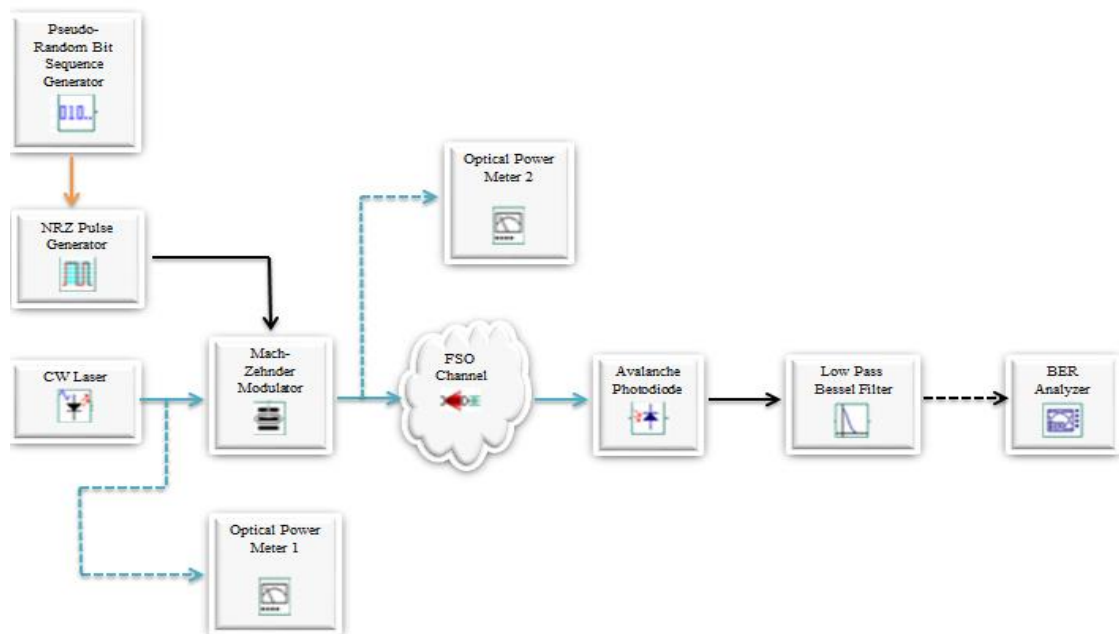

Fig. 4.1 Proposed FSO communication system design.

a continuous wave optical signal; here for three different optical transmission windows - 850 nm, 1310 nm, and 1550nm that corresponds to frequencies of 352.7 THz, 228.9 THz, and 193.4 THz. Both the outputs of the NRZ line encoder and CW laser are fed to input terminals of the Mach-Zehnder modulator (MZM) where the low-frequency signal is superimposed over the high-frequency signal and transmitted over the FSO channel. Along its way, the optical signal is affected by atmospheric impediments like scintillation, haze, fog, and rain [94]. However, in our analysis, we have considered overall fair weather conditions. The receiver side consists of an avalanche photodiode (APD) that transforms the received optical signal into its electrical counterpart. A low pass filter (LPF) filters out any surplus frequency components. This signal is then fed to the BER analyzer which displays the minimum BER of input electrical signal, its Q-factor, eye height, threshold value, and BER pattern. The eye diagrams for each measurement are drawn and observed for BER performance and Q-factor. Besides, two optical power meters have been used as visualizer components to record the values of transmitted optical power and received optical power used for system analysis. The intensity-modulated/direction detection (IM/DD) based OOK digital modulation scheme is preferred due to its simplicity and efficiency for short link range FSO systems. Laser communication regarding 1550 nm is considered safe power for human eye safety, as such nowadays optoelectronic devices, use 1550 nm laser diodes abundantly for high-speed FSO link. Table 4.1 lists all the link parameters and their values used in system design and analysis. Laser power is set at 8 dBm and data rate at 2.5 Gbps for all three wavelengths. FSO channel component mimics the effects of atmospheric channel thus atmospheric attenuation, additional losses, and geometrical losses have been considered in the system analysis. An attenuation of 2.5 dB/km, 0.4 dB/km and 0.2 dB/km is taken for 850 nm, 1310 nm and 1550 nm wavelengths separately [95]. An additional loss of 10 dB has been taken to consider the pointing error effect and scintillation. To counter geometrical losses due to beam spreading, transmitter aperture diameter and receiver aperture diameter have been held at 5 cm and 15 cm, a greater receiver aperture diameter neutralizes the effect of beam spreading and scintillation, this is called aperture averaging.

Table 4.1 Link parameters.

Parameter	Value
Bit rate (Gb/s)	2.5
Frequency (nm)	850; 1310; 1550
Attenuation (dB/km)	2.5; 0.4; 0.2
Linewidth (MHz)	0.1
Extinction ratio (dB)	30
Range (m)	2000
Power (dBm)	8
Transmitter aperture diameter (cm)	5
Receiver aperture diameter (cm)	15
Beam divergence (mrad)	4
Additional losses (dB)	10
Responsivity (A/W)	1
Dark current (nA)	10
Frequency spacing (THz)	0.1
Sequence length	128

4.3 Results and analysis

This segment presents various simulation results with their mathematical explanation to analyze the performance of the FSO system for each optical window under a given set of link parameters. The values of link parameters in the FSO system design for each optical window have been chosen to keep in mind the practical consequences so that our results match real-time system analysis. Figure 4.2 shows the variation of BER with the link range for the operating wavelengths of 850 nm, 1310 nm, and 1550 nm. As can be seen from the figure, BER performance degrades with an increase in link distance. For 850 nm wavelength, BER decreases from 10^{-18} at a distance of 200 m to 10^{-1} at 2000 m. For 1310 nm wavelength, BER decreases from 10^{-29} at a distance of 200 m to 10^{-3} at 2000 m. And for 1550 nm wavelength, BER decreases from 10^{-34} at a distance of 200 m to 10^{-7} at 2000 m. Eye diagrams in the figure show the point of minimum acceptable BER that is of the value of 10^{-9} corresponding to the value of the Q-factor of 6.
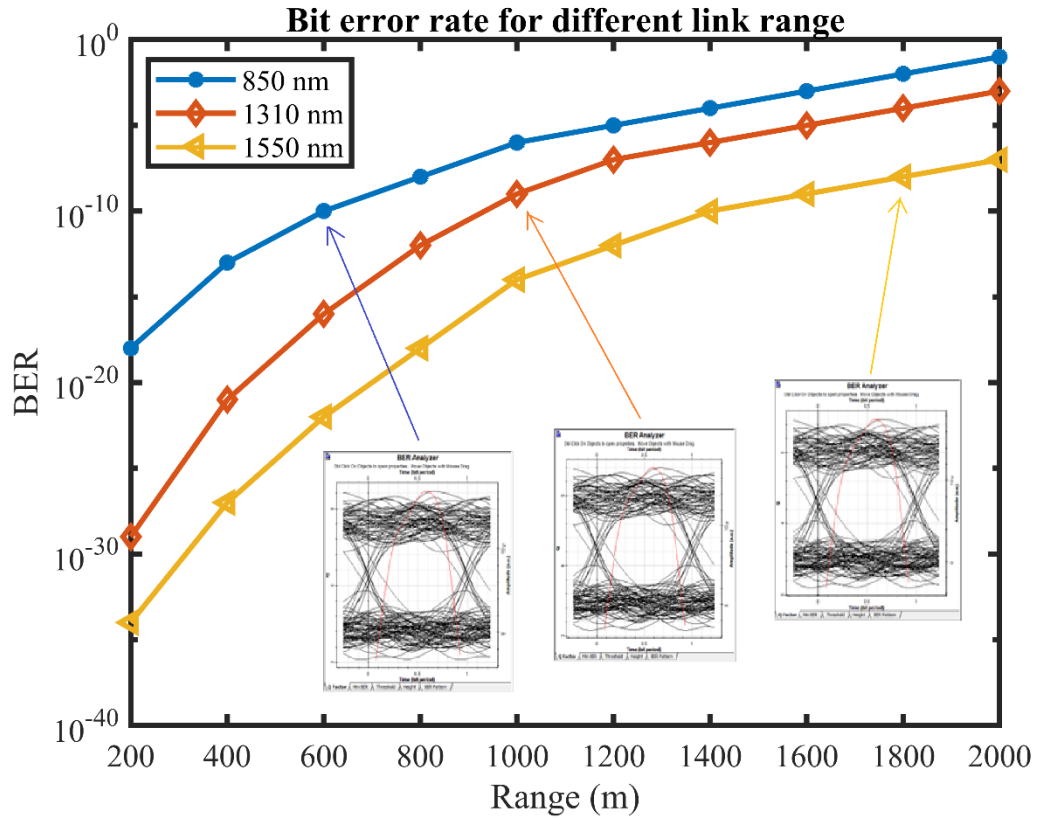
Fig. 4.2 Variation of BER with range.

In our analysis, a BER value of 10^{-9} was achieved for 850 nm, 1310 nm, and 1550 nm at a link distance of 600 m , 1000 m, and 1800 m respectively. This suggests the fact that the 1550 nm optical window is suitable for long-range FSO communication. Considering Gaussian noise with σ_0 and σ_1 as standard deviations, the BER is given by [96]

$$P_e = \frac{K}{L+K} P_{e0} + \frac{L}{L+K} P_{e1} \tag{4.1}$$

where, P_{e0} and P_{e1} are the symbol probabilities, K, and L are the number of samples for bit '0' and '1'. Likewise, P_{e0} and P_{e1} are given by

$$P_{e0} = \frac{1}{2} erfc \left(\frac{W - b_0}{\sqrt{2}\sigma_0}\right) \tag{4.2}$$

$$P_{e1} = \frac{1}{2} erfc \left(\frac{b_1 - W}{\sqrt{2}\sigma_1}\right) \tag{4.3}$$

where, b_0 and b_1 are average values and W is the threshold value.

Received optical power for different link range
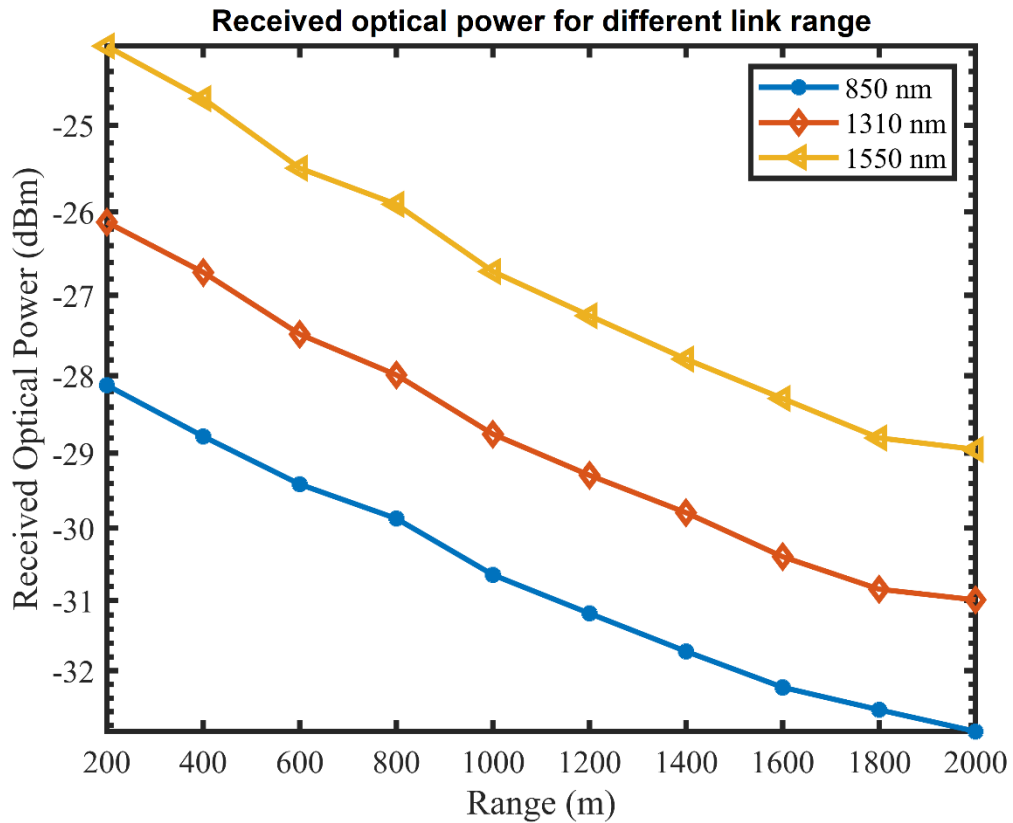
Fig. 4.3 Variation of received optical power with range.

Figure 4.3 portrays the variability of received optical power with link range concerning different wavelengths. It is observed that the received optical power decreases with an increase in the link range (inverse square law). At a 200 m distance, the optical power received for wavelengths - 850 nm, 1310 nm, and 1550 nm is -28 dBm, - 26 dBm, and -24 dBm. Similarly, at a 2000 m distance, the received optical power is -33 dBm, - 30.9 dBm, and -28.8 dBm respectively. The received optical power is given by [97]

$$P_{rxd} = P_{txd} \frac{D_{rxd}{}^2}{(D_{txd} + \theta R)^2} 10^{-\alpha R/10} \qquad (4.4)$$

where, D_{rxd} and D_{txd} are the receiver and transmitter aperture diameter, θ is beam divergence, R is link range and α is atmospheric attenuation.

Figure 4.4 depicts the variation of BER with respect to transmitted optical power for 850 nm, 1310 nm, and 1550 nm set of wavelengths. Looking at the figure, it is seen that BER performance improves with the increase in transmitted laser power. At a transmitter
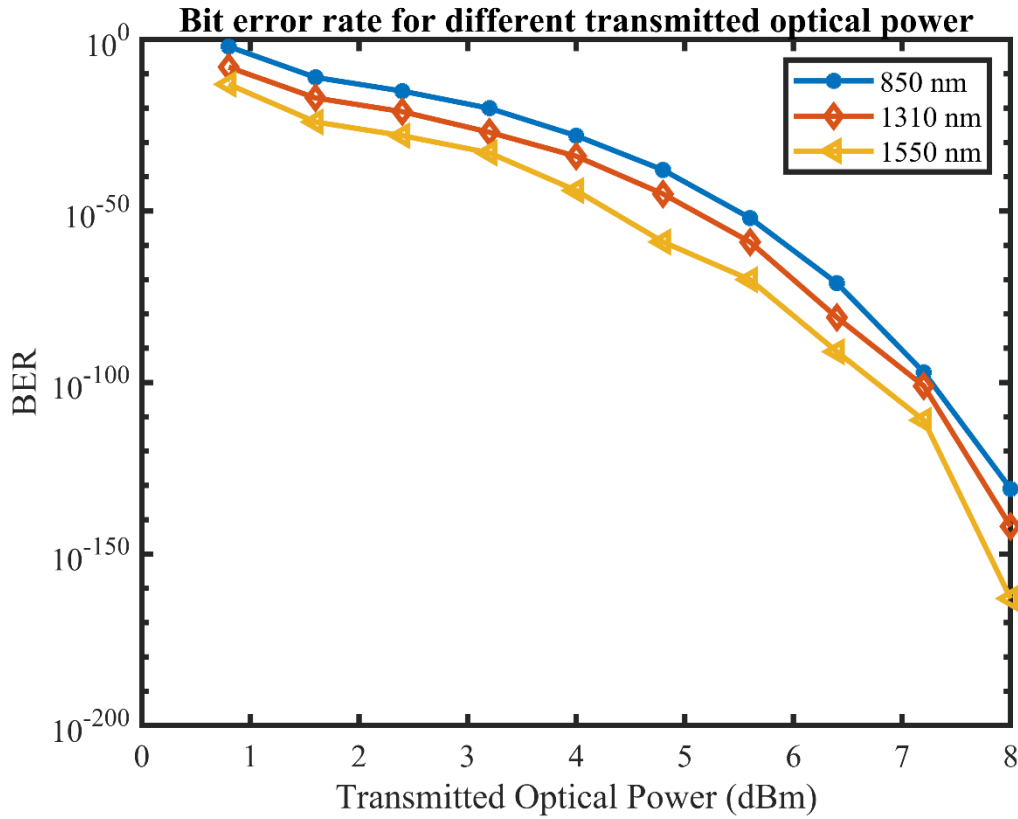
Fig. 4.4 Variation of BER with transmitted optical power.

power of 1 dBm, BER for wavelengths of 850 nm, 1310 nm, and 1550 nm is 10^{-2}, 10^{-10} and 10^{-15}. In the same way, at 8 dBm power, BER is 10^{-131}, 10^{-142} and 10^{-181} for the optical windows under consideration. The dependence of optical power on wavelength can be studied from the equation given by [97]

$$\frac{P_{rxd}}{P_{txd}} = (\pi/\lambda)^4 \, D_{txd}{}^2 D_{rxd}{}^2 L_{ch} E_l \tag{4.5}$$

or

$$\frac{P_{rxd}}{P_{txd}} = G_{txd} G_{rxd} L_{ch} E_l \tag{4.6}$$

since,

$$G_{txd} = (\frac{\pi D_{txd}}{\lambda})^2 \text{ and } G_{rxd} = (\frac{\pi D_{rxd}}{\lambda})^2 \tag{4.7}$$

where, G_{txd} and G_{rxd} are transmitter and receiver gain, E_l is system loss and L_{ch} is channel loss. The above equations show that the transmitted optical power and received optical

power follow a typical λ^{-4} dependency, so as wavelength increases, power decreases by a factor of 4. Gain and channel loss are also wavelength-dependent.
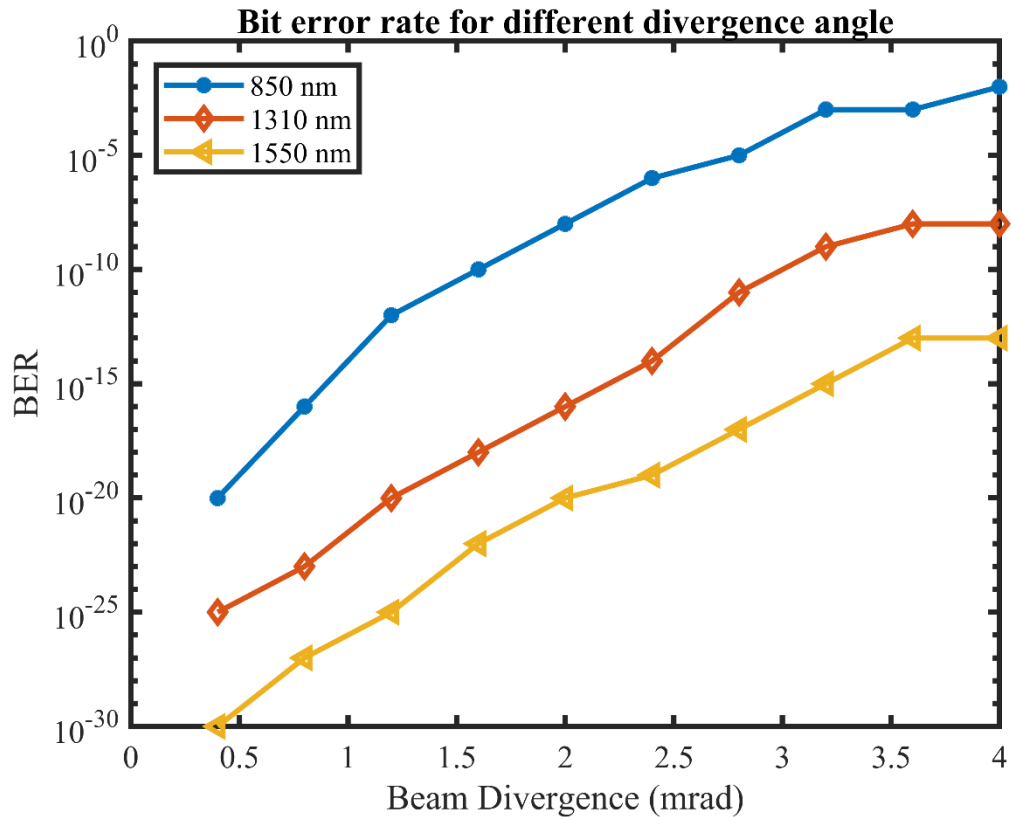
Fig. 4.5 Variation of BER with beam divergence.

Figure 4.5 illustrates the variation of BER with beam divergence. It can be seen that as the value of beam divergence increases, BER performance degrades noticeably. At a beam divergence of 0.45 mrad, BER is $10^{-20}, 10^{-25}$ and 10^{-30} at 850 nm, 1310 nm, and 1550 nm. Likewise, at beam divergence of 4 mrad, BER is $10^{-2}, 10^{-8}$ and 10^{-13}. A minimum acceptable BER of 10^{-9} for 850 nm and 1310 nm optical window is obtained at a beam divergence of 1.7 mrad and 3 mrad. 1550 nm wavelength still manages to give a BER of 10^{-13} at 4 mrad. Hence, the beam spreading effect is less in the 1550 nm window in comparison with other optical windows. Thus, the smaller the angle of beam divergence (θ), the lesser is the BER and vice-versa. Beam divergence is directly proportional to the operating wavelength.

Figure 4.6 displays the variation of Q-factor with range. From the figure, it is clear that the value of the Q-factor decreases significantly with increasing link distance. At a 200 m distance, a Q-factor of 21, 31, and 40 is obtained at 850 nm, 1310 nm, and 1550 nm. Also,
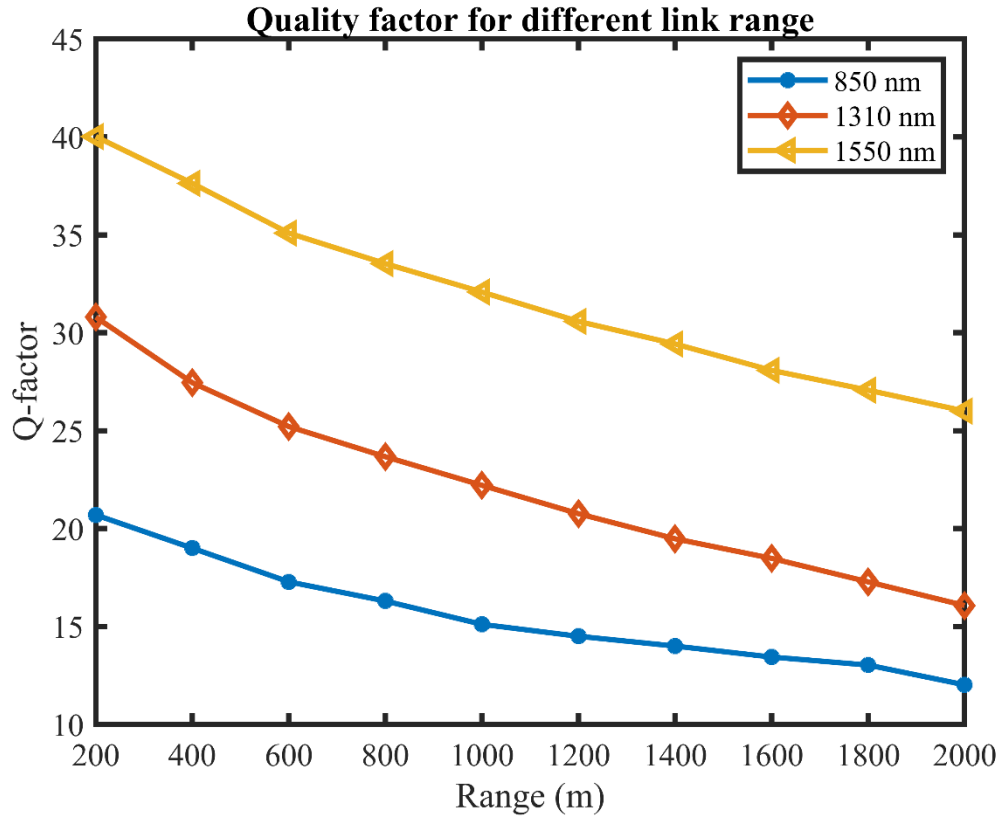
Fig. 4.6 Variation of the Q-factor with range.

at 2000 m, a Q-factor of 12, 16, and 26 is obtained for respective wavelengths. Hence, the 1550 nm window gives a high value of Q-factor even at a distance of 2000 m. Q-factor is one of the important performance metrics for FSO communication. Sometimes, it is difficult to analyze the system performance with BER as the performance metric. On the other hand, performance analysis with respect to Q-factor is fast and easy, but the results are not as much accurate as in the case of BER. Q-factor is the impression of overall link steadfastness and quality of service (QoS) and a minimum acceptable value of 6 is necessary for a reliable network. Q-factor can be calculated from the BER using the equation given by [91]

$$BER = \frac{exp\,(-Q^2/2)}{Q\sqrt{2\pi}} \tag{8}$$

4.4 Concluding remarks

The FSO communication system performance for different atmospheric transmission windows (850 nm, 1310 nm, and 1550 nm) is investigated taking BER, Q-factor, and received optical power as performance parameters. The link parameters such as range,

beam divergence, and transmitted optical power are varied from 200-2000 m, 0.4-4 mrad, and 1-8 dBm respectively, and simulated to analyze the variation pattern concerning performance metrics for each optical window. The analysis is carried out both graphically and mathematically to help us better understand the suitability of a certain optical window under a given set of parameters. All in all, we found that the 1550 nm wavelength presented better results in terms of high BER performance even up to 1800 m, superior Q-factor, and fifty times more eye-safe laser power operation. Expanding the work further, the FSO system at 1550 nm can be analyzed for a long-range multiple-input multiple-output (MIMO) system with EDFA and smart antenna technology.

CHAPTER 5: DESIGN OF 32 GBAUD DP-QPSK COHERENT FREE SPACE OPTICAL TRANSCEIVER WITH DIGITAL SIGNAL PROCESSING AT THE RECEIVER

5.1 Introduction

FSO communication link provides high-speed data transmission rate within LoS range for indoor as well as outdoor applications. The trend towards higher SE and the transition to advanced coherent modulation formats [98] pose stringent requirements in terms of inter symbol interference (ISI), spectrum compactness, and inter-channel interference (ICI) [99]. It is considered that optical coherent quadrature phase-shift keying (QPSK) based FSO systems can now form the basis for future generation optical wireless networks [100]. The proposed system in this chapter achieves 128 Gb/s of data rate with dual-polarization QPSK (DP-QPSK) modulation scheme and DSP techniques at the receiver for 1550 nm wavelength which is compatible with the existing optical backbone network. The system performance has been numerically evaluated with regard to bit error rate (BER $\leq 2 \times 10^{-3}$, i.e. FEC limit), error vector magnitude (EVM), and constellation diagram.

5.2 Proposed system

The setup of the proposed single-channel coherent FSO communication system shown in Fig. 5.1 consists of a transmitter section, a free space/atmospheric channel, and a receiver section. The input signal of sequence length $2^{17}-1$ is generated by a pseudo-random bit sequence (PRBS) generator. The PRBS generator is used to produce bits that could represent actual data transmitted in a practical scenario [101]. A CW laser source is bisected using a polarization beam splitter (PBS). Each half is QPSK-modulated by its own LiNbO dual-parallel Mach-Zehnder modulator (MMZ) and forms one of the two polarization channels [105]. The two polarization channels are multiplexed with a polarization beam combiner (PBC) to generate a DP-QPSK transmit signal. The 32 GBaud optical square DP-QPSK modulated signal is transmitted through the FSO channel. The coherent receiver involves a LO, polarization beam splitters (PBS), and an array of

balanced detectors (BD) which extract the I/Q electrical signals [102] [103]. The DSP element executes several signal processing techniques to recover the incoming transmission symbols. Lastly, the original signal is recovered after the symbols pass through the decision and decoding circuitry.

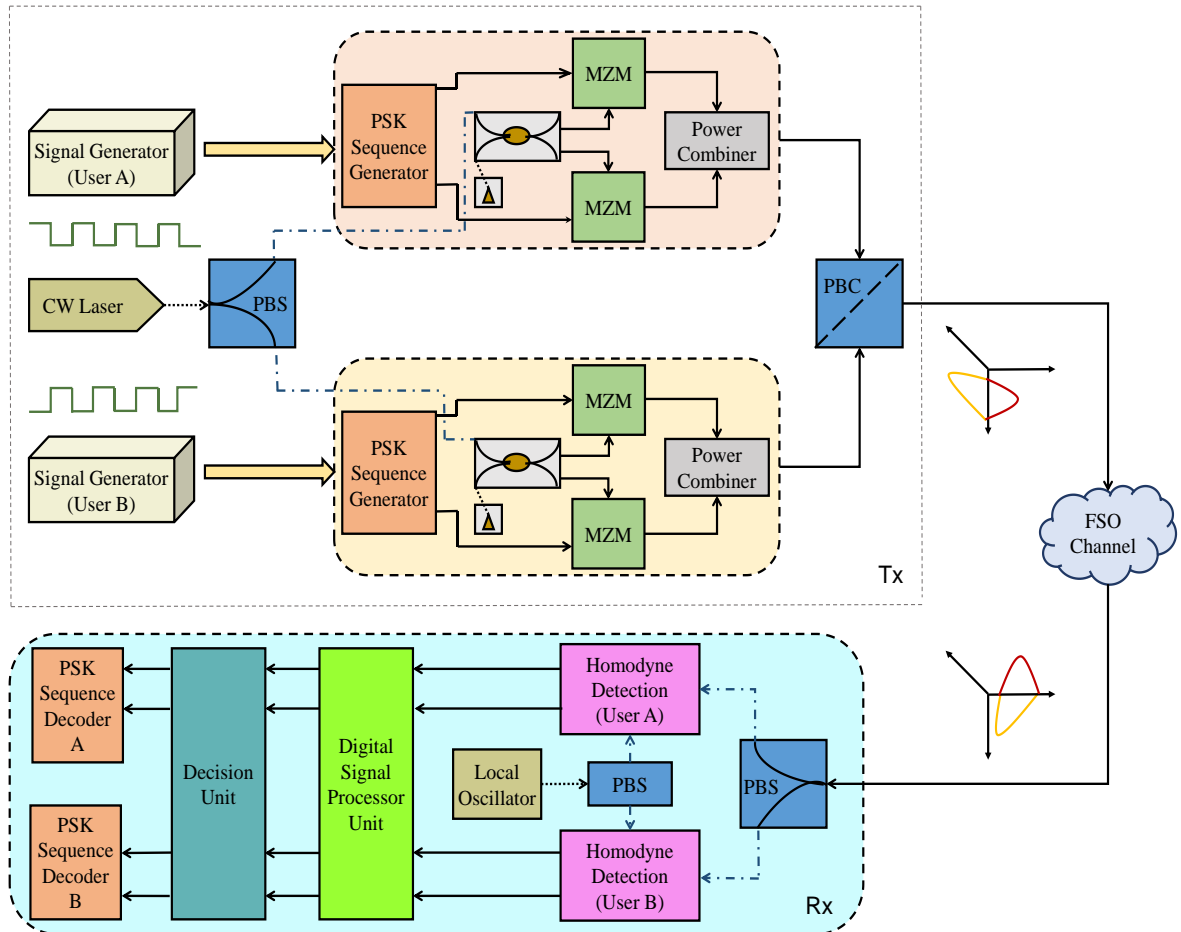**Fig. 5.1** The structure of the proposed DP-QPSK based FSO system with homodyne detection and digital signal processor unit.

A comprehensive internal structure design of the optical DP-QPSK transmitter can be found in Fig. 5.2. The continuous wave (CW) laser beam instantaneous electric field can be computed by the following Eq. [104]

$$E_l(t) = \sqrt{P(l)}\, e^{j(\omega_l t + \phi_l)} . \hat{e}, \tag{5.1}$$

where laser power is denoted by $P(l)$, angular frequency is given by $\omega_l = 2\pi f_l$, initial phase is defined by ϕ_l, and signal polarization is represented by $\hat{e}$. The equation for laser phase noise can be written as

$$f(\Delta\phi) = \frac{1}{2\pi\sqrt{\Delta f \Delta t}} e^{-\left(\frac{\Delta\phi^2}{4\pi\Delta f \Delta t}\right)} \tag{5.2}$$

where the phase difference is denoted by $\Delta\phi$ and time discretization is depicted by Δt. The phase change among two consecutive moments is specified by the Gaussian random variable of mean zero and variance $2\pi\sqrt{\Delta f}$ (Δf is laser linewidth). Using a linear polarization-based PBS (device angle $45°$) the lightwave is split into X- and Y- orthogonal polarization components which are then guided to each branch of the I/Q based modulator sections. Next, a cross-coupler (coupling coefficient 0.5) directs the optical carrier into separate I/Q branches of the modulator with bit rates R/2. Two equivalent M-ary symbol series are generated from the input binary signal by PSK sequence generators and directed towards M-ary pulse generators. This bit series is mapped into M symbols in a way there is a single bit alteration among any two adjacent symbols. This bit mapping is called Gray coding. Figure 5.2 depicts QPSK Gray-coded symbol constellations. Gray coding is essential to reduce bit error rate (BER) in the course of symbol recovery. This assures lesser modulation bandwidth and therefore greater SE of the proposed system and minor slips in the baseband signal.

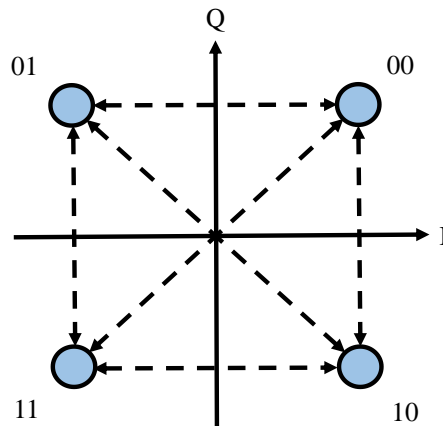
Fig. 5.2 Gray-coded QPSK symbol constellation. Q = quadrature-phase channel; I = in-phase channel.
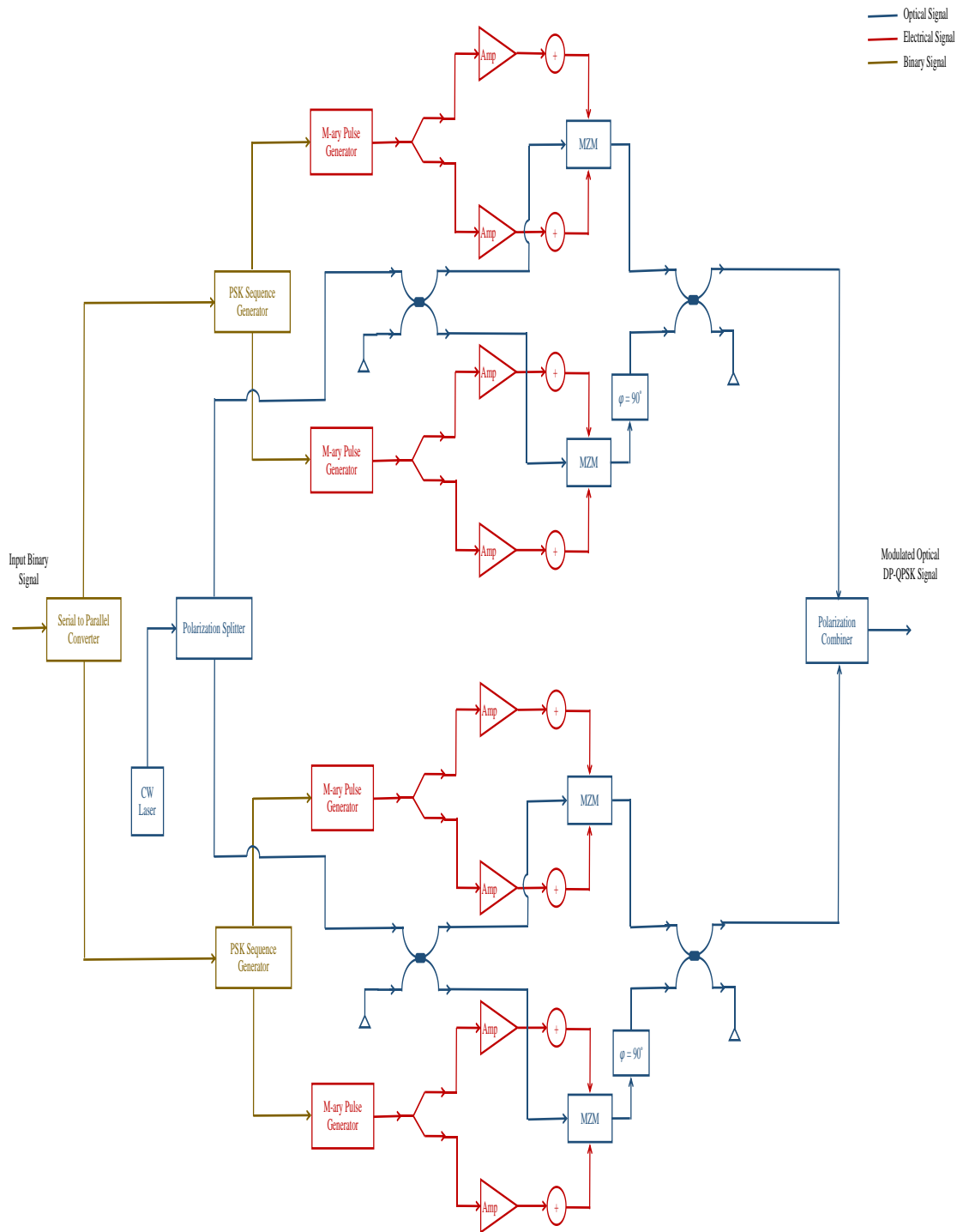
Fig. 5.3 Internal structure of optical DP-QPSK transmitter.

The multi-level signal output from M-ary pulse generators can be expressed as

$$V_o(t) = \begin{cases} b, \ 0 \le t < t_1 \\ ah(t) + b, \ t_1 \le t < t_1 + w \\ b, \ t_1 + w \le t < T \end{cases} \tag{5.3}$$

where b denotes parameter bias, t_1 gives pulse position, a depicts gain, w represents pulse duration, T indicates bit duration, and $h(t)$ is expressed as

$$h(t) = \left[\frac{sin\left(\frac{\pi t}{T}\right)cos\left(\frac{\delta \pi t}{T}\right)}{\frac{\pi t}{T}\left\{1 - \left(\frac{2\delta t}{T}\right)^2\right\}} \right] \tag{5.4}$$

where the roll-off factor is denoted by δ. These multi-level samples are directed towards dual-drive LiNbO₃ Mach-Zehnder modulators (MZM). At the peak point of operation, each modulator has a 30 dB extinction ratio, 3 V switching bias voltage, and 0 V bias voltages (V1 and V2). In each quadrature-phase branch of both the I/Q based modulators, a phase shift of $90°$ is appended to generate modulated optical QPSK signal. Then, the X- and Y-polarization elements are pooled using a PBC to generate a 32 GBaud DP-QPSK information signal at the transmitter output. This information signal is transported over the FSO channel and can be computed by the following Eq.

$$P_{rx} = P_{tx} \left[\frac{D_{rx}^2}{(D_{tx} + \theta d)^2} \right] 10^{-\alpha d/10} \tag{5.5}$$

where received and transmitted optical power are represented by P_{rx} and P_{tx} respectively. The receiver and transmitter telescope antenna diameter are denoted by D_{rx} and D_{tx}. The angle of beam divergence is depicted by θ. The free space propagation distance is denoted by d, and specific atmospheric attenuation constant is represented by α.

The internal layout of the optical coherent DP-QPSK receiver is illustrated in Fig. 5.4. It comprises LO, the PBS which extracts the distinct polarization signals, 90-degree optical hybrids which convert the phase information into the corresponding optical intensities, and BD for the conversion of the received optical intensities into I/Q electrical signals. These

I/Q currents for corresponding X- and Y-polarizations can be described as Eqs. 6 and 7
respectively.

$$
\begin{aligned}
I_{I(X/Y)}(t) = \; & 2\gamma_1\sqrt{P_l P_{lo}}\; e_l e_{lo} e^{-2\alpha d} \left\{ I(t-\tau)\cos\left(-\beta(\omega_l)d - \Delta\,\phi(t)\right)\right. \\
& \left. + Q\,(t-\tau)\sin(-\beta(\omega_l)\,d - \Delta\,\phi(t))\right\} + i_{shI}
\end{aligned}
$$

(5.6)

$$
\begin{aligned}
I_{Q(X/Y)}(t) = \; & 2\gamma_1\sqrt{P_l P_{lo}}\; e_l e_{lo} e^{-2\alpha d} \left\{ Q(t-\tau)\sin\left(-\beta(\omega_l)d - \Delta\,\phi(t)\right)\right. \\
& \left. - I\,(t-\tau)\cos(-\beta(\omega_l)\,d - \Delta\,\phi(t))\right\} + i_{shQ}
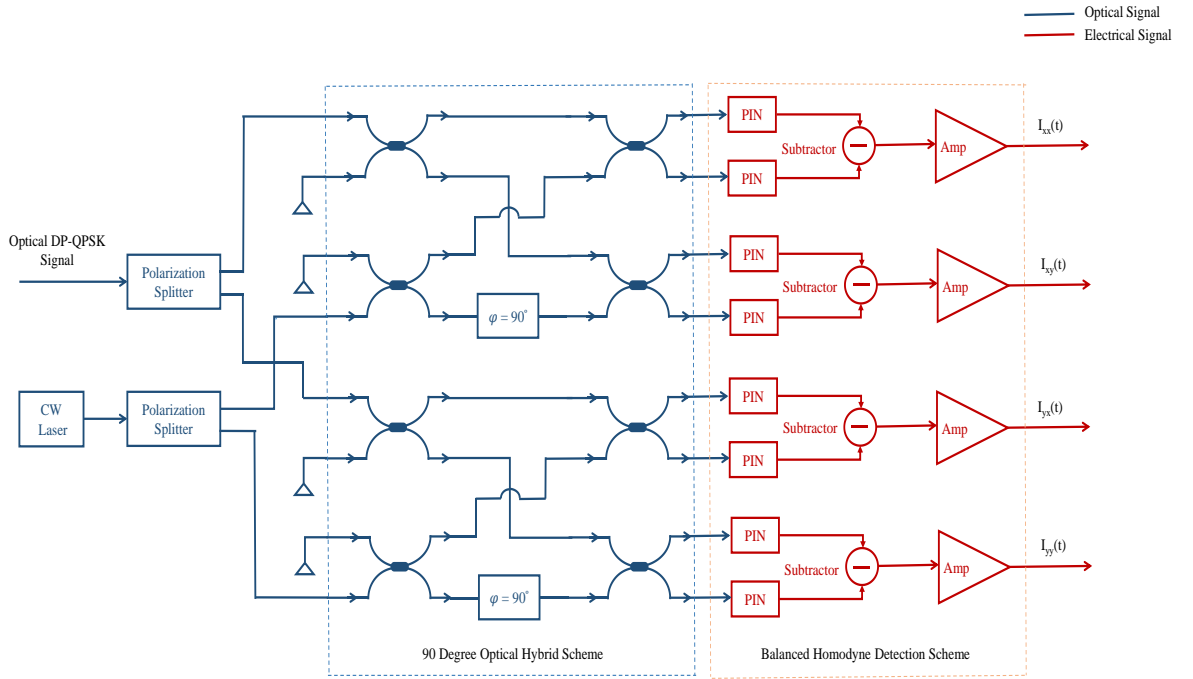\end{aligned}
$$

(5.7)

Fig. 5.4 Schematic diagram of the optical coherent DP-QPSK receiver.

where $\sqrt{P_l P_{lo}}$ represents the branch current magnitude, e_l and e_{lo} denote polarization
components of incoming optical beam and LO signal, $\Delta\,\phi(t)$ gives phase variation and i_{sh}
is the photocurrent generated by shot noise.

43

5.3 Results and analysis

The overall system performance is evaluated by observing the evolution of constellation diagrams after passing through each of the DSP algorithms and in terms of the impact of link length, launched optical power, laser linewidth, OSNR, and beam divergence over BER and EVM (%) under fair climatic conditions (i.e., $\alpha = 0.25$ dB/km for 1550 nm channel wavelength) with low turbulence level (i.e., atmospheric index refraction structure $C_n^2 = 5\times10^{-15}$ m$^{-2/3}$). Thus, the presence of different meteorological conditions like rain, snow, haze, and fog has been ignored. Also, unwanted obstructions like tall structures, trees, and birds are presumed not present. Table 1 summarizes different parameters and their values considered in the simulation design of the proposed FSO communication system.

The internal schematic of the DSP module shown in Fig. 5.5 integrated into our proposed design works by employing a sequence of several high-level digital algorithms,

Table 5.1 Design parameters used in the proposed system.

Parameters	Value
Bit rate	128 Gb/s
Launched laser power	18 dBm
Center frequency	193.414 THz
Atmospheric attenuation	0.25 dB/km
Baud rate	32 GBaud
Laser linewidth	0.1 MHz
Beam divergence	0.25 mrad
Geometrical loss	Yes
Transmitter antenna aperture diameter	5 cm
Receiver antenna aperture diameter	20 cm
Photodetector responsivity	1 A/W
Photodetector dark current	10 nA
Receiver loss	1 dB
Sequence length	65536

which are (1) low pass Bessel filter, (2) resampling, (3) quadrature imbalance (QI) compensation, (4) adaptive equalizer (AE), (5) frequency offset estimation (FOE), and (6) carrier phase estimation (CPE). All the estimation and equalization algorithms have been executed in the frequency domain which potentially provides the least complexity for the pol-mux optical coherent systems. Implementation of these algorithms not only resulted in successful mitigation of intensity and phase imbalances but also effective compensation of free space loss which is the principal factor behind the degradation of the optical signal strength. The space loss in the FSO communication system can be computed by the following Eq.

$$L_s = \left(\frac{\lambda}{4\pi d}\right)^2 \qquad (5.8)$$

where L_s is space loss factor and λ is the operating wavelength.

A comprehensive and comparative phase-wise analysis of the DSP unit is provided in conjunction with the constellation diagrams presented in Fig. 5.6 as follows. Figure 5.6a shows overlying and indistinguishable constellation points obtained from the demodulated X- and Y-component electrical signals soon after BHD. This fuzzy pattern is due to various transmission impairments like atmospheric attenuation, delay distortion, and noise. While passing through the first-stage DSP, a 3rd order low pass Bessel filter (optimal bandwidth: $0.75 \times$ symbol rate) removes the narrow-band noise. The signal constellation obtained after low pass filtering is illustrated in Fig. 5.6b. Then happens the resampling of the preceding sampled signal at a degree of 2 samples/symbol. Also, to adjust the current sampled signal to the new sampling rate cubic interpolation is employed. Figure 5.6c show the constellation diagram obtained after resampling. This is followed by QI compensation which is employed to mitigate the effects of amplitude and phase disparities between the I/Q electrical signals of DP-QPSK that originate from disproportionate bias voltage for the MZM, photodiode responsivity imbalance, misalignment of the PBS or PBC, and inadequacies in the 90-degree optical hybrid. This non-orthogonalization is corrected employing the Gram-Schmidt orthogonalization procedure (GSOP). Consider two non-orthogonal constituents of the input signal represented by $I_{NO}(t)$ and $Q_{NO}(t)$ respectively,
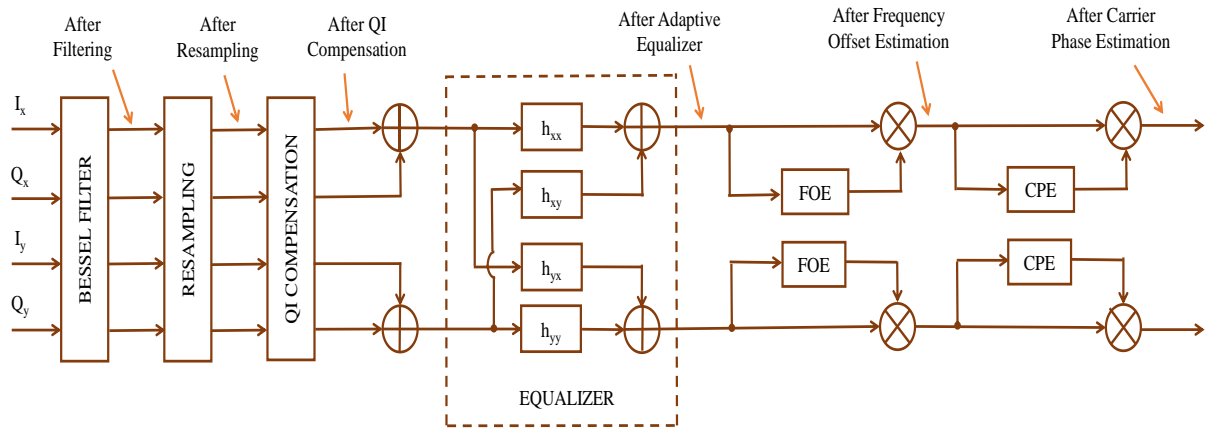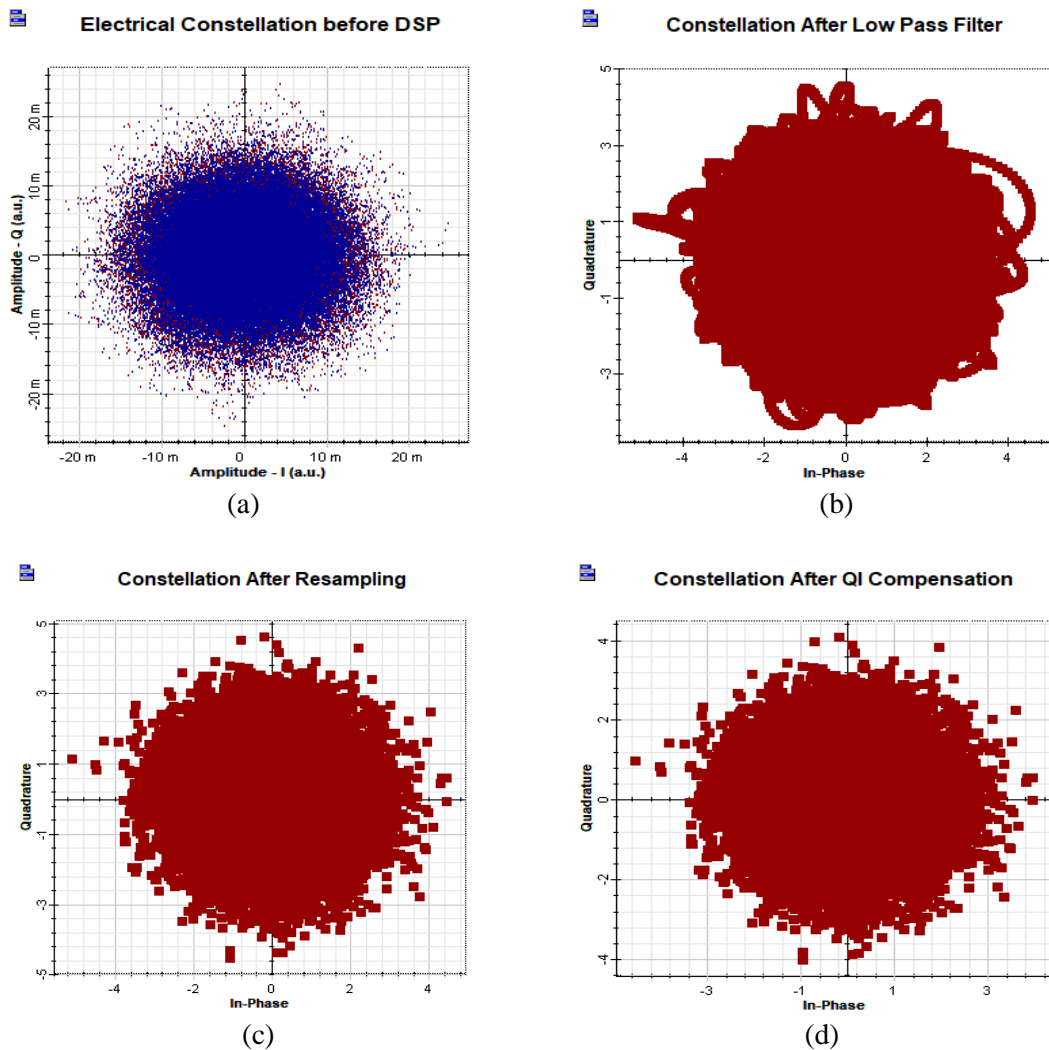
45

Fig. 5.5 The flowchart of the high-level DSP scheme for the proposed FSO link.

(a)

(b)

(c)

(d)

(e)

(f)

(g)
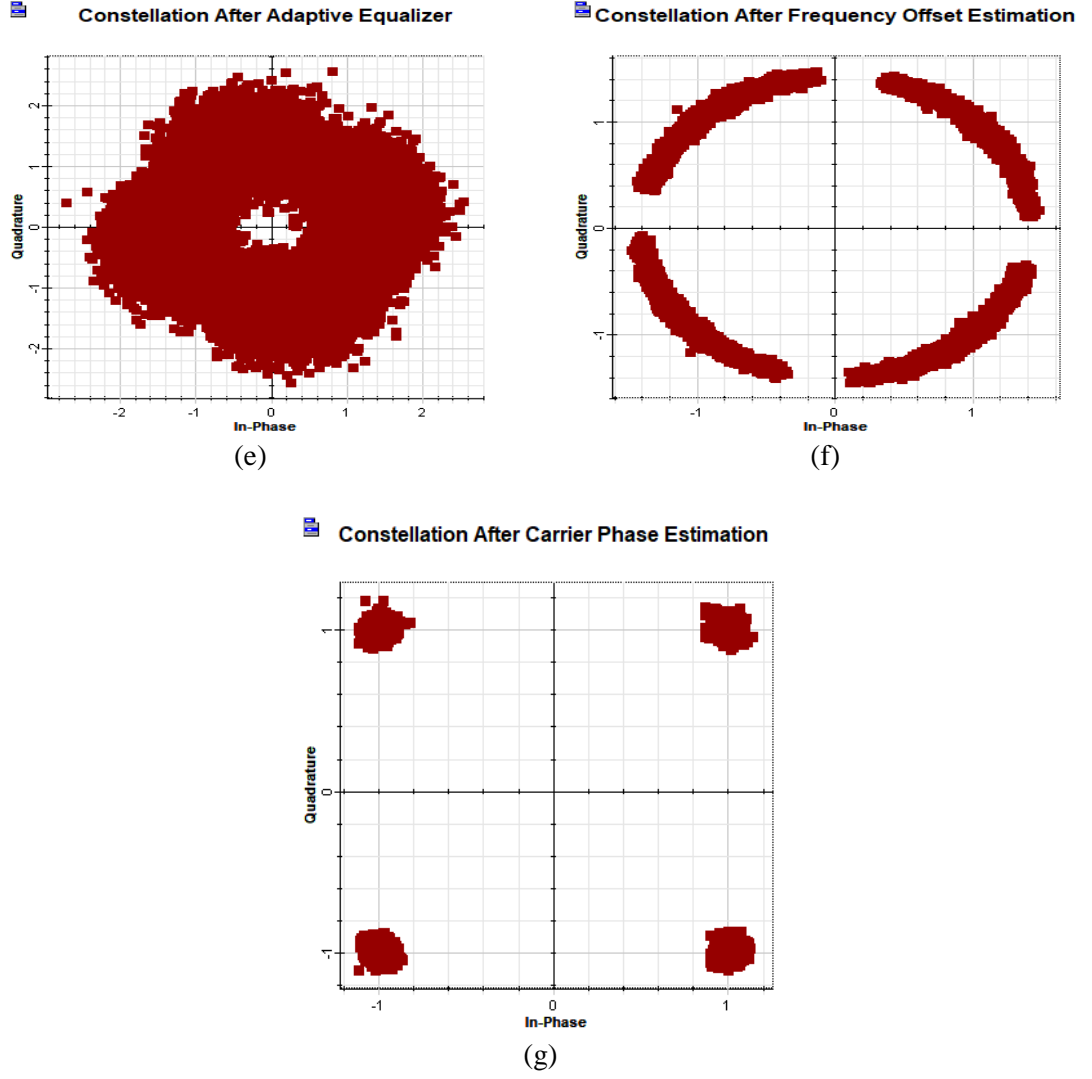
Fig. 5.6 Progress of the constellation diagrams down the DSP component after (a) BHD, (b) low pass filtering, (c) resampling, (d) QI compensation, (e) AE, (f) FOE, and (g) CPE for a 128 Gb/s-2.65 km DP-QPSK FSO transmission over fair climate.

then the new pair of orthonormal signals formed after the GSOP, denoted by $I_O(t)$ and $Q_O(t)$ are described as

$$I_O(t) = \frac{I_{NO}(t)}{\sqrt{P_I}} \tag{5.9}$$

$$Q'(t) = Q_{NO}(t) - \rho\left(\frac{I_{NO}(t)}{\sqrt{P_I}}\right) \tag{5.10}$$

$$Q_O(t) = \frac{Q'(t)}{\sqrt{P_Q}} \tag{5.11}$$

where $\rho = E[I_{NO}(t), Q_{NO}(t)]$ gives the correlation coefficient, $P_I = E[I_{NO}^2(t)]$, and $P_Q = E[Q'^2(t)]$, in which $E[...]$ represents the statistical expectation. Figure 5.6d shows the constellation diagram obtained after QI compensation. Next, AE eliminates polarization distortion in the event of DP-QPSK modulation and inter-symbol interference (ISI) by employing a double-phase constant modulus algorithm-radius directed (CMA-RD). For DP multiplexed system, the butterfly configuration is used for polarization de-multiplexing. The cost function of the CMA takes the form

$$J(k) = E\left[\left(|y(k)|^2 - R_p\right)^2\right] \tag{5.12}$$

where $y(k)$ denotes the AE output, R_p is the constant whose value depends only on the input data symbol $a(k)$. Figure 5.6e shows the constellation diagram after the AE. Following the AE stage, the data sequence is further resampled to 1 sample/symbol. But between the algorithm steps, the signals are up-sampled to their original rate, in this case, $2 \times$ samples per bit for a 4-PSK grid. Due to frequency and phase offsets caused by the mixing of transmitted and LO signals, overlapping and rotating constellations are generated. FOE[23] is employed to revoke this phase and frequency imbalance. Figure 5.6f shows the constellation diagram after the FOE. The received signal is described as

$$R(k) = D(k)e^{j(2\pi\Delta fkT+\phi_k)} + n(k) \tag{5.13}$$

where data symbols are represented by $\{D(k)\}$, carrier frequency offset is denoted by Δf, carrier phase (assumed constant) is signified by ϕ_k, symbol period is indicated by T, and zero-mean Gaussian random variable is given by $\{n(k)\}$. The fourth power of Eq. 5.13 takes the form

$$R^4(k) = A.e^{j4(2\pi\Delta fkT+\phi_k)} + e(k) \tag{5.14}$$

where $A = E[D_k^4]$ represents constant amplitude and $e(k)$ designates zero-mean noise process. The frequency offset based on the estimate of the spectral density of the information signal is expressed as

$$R^4(k) = \frac{1}{4} arg\{max[|Z(f)|]\} \tag{5.15}$$

where

$$Z(f) = \frac{1}{N} \sum_{k=0}^{N-1} R^4(k) e^{-j(2\pi f kT)} \tag{5.16}$$

where block length is represented by N, whose optimum value is based on the laser linewidth and symbol rate. Additionally, to recover and successively remove any residual phase misalliance amongst the LO and received signal, CPE using blind phase search (BPS) algorithm is employed that tries on to find one optimum phase among many different test phases. Figure 5.6g shows the information signal having clear and distinct constellation symbols obtained after CPE. After going through rotation of B test carrier phase angles (ϕ_b), the received information signal Z_k can be described as

$$\phi_b = \frac{b}{B} \cdot \frac{\pi}{2} - \frac{\pi}{4} \text{ where } b \in \{0.1,2,\dots,B-1\} \tag{5.17}$$

All the alternated symbols are directed into decision circuitry and required distance $|d_{k,b}|^2$ to the adjacent constellation point is estimated as follows

$$|d_{k,b}|^2 = |Z_k e^{j\phi_b} - \hat{X}_{k,b}|^2 \tag{5.18}$$

where $\hat{X}_{k,b}$ represents the decision of $Z_k e^{j\phi_b}$. Finally, the data stream is decoded by a PSK sequence decoder for distinct polarizations and led towards a P/S converter to get the final output.

Figure 5.7 outlines the BER performance of the proposed system with regard to rising link length. To obtain different values of BERs, the link range is varied from 0-4 km. As

follows from the graph, the BER of the information signal increases with increasing link distance. The result demonstrates a successful transmission of 128 Gb/s data-bearing DP-QPSK optical signal up to a distance of 2.65 km under acceptable performance criteria, that is, BER $\leq 2 \times 10^{-3}$ (FEC limit) under fair weather conditions. However, with the increase in the distance, distortion in the scattering diagram increases due to which information retrieval becomes harsh on the receiver terminal. This performance deterioration is triggered by free-space loss, laser phase noise, beating amongst optical sidebands, and OSNR degradation respectively.
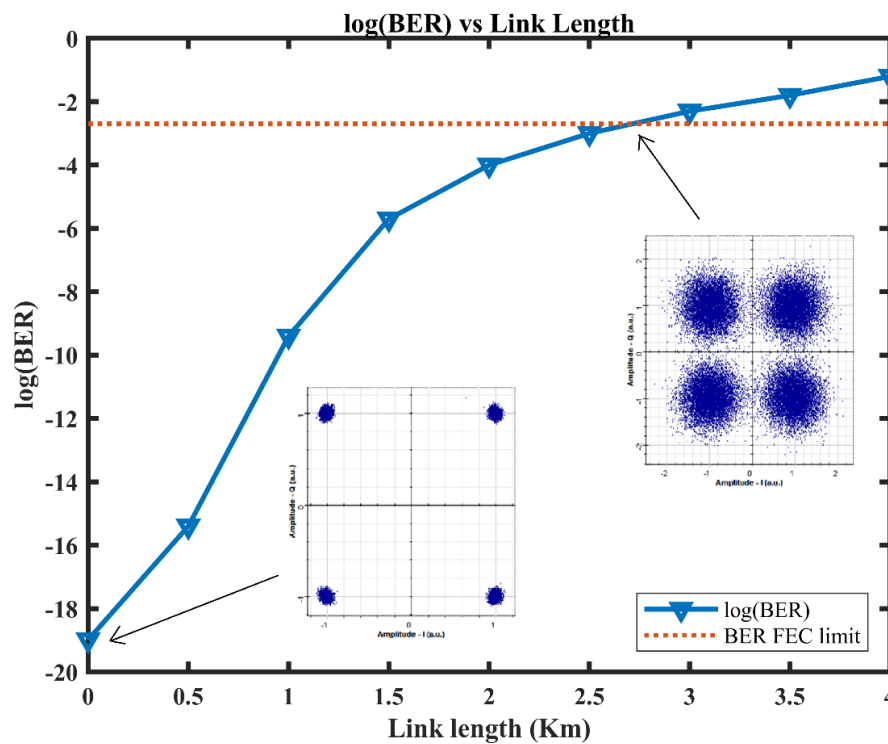

Fig. 5.7 log (BER) against link length graph under clear climate (insets: corresponding constellation plots).

The log (BER) and EVM (%) against launched laser power graph of the 128 Gb/s DP-QPSK FSO system at a link distance of 2.65 km can be found in Fig. 5.8. The BER and EVM (%) values are obtained while varying CW laser power. The result indicates that with rising optical launch power, both the BER and EVM (%) value drops. For eye and skin safety concerns, laser power not higher than 18 dBm is considered in the proposed link design.
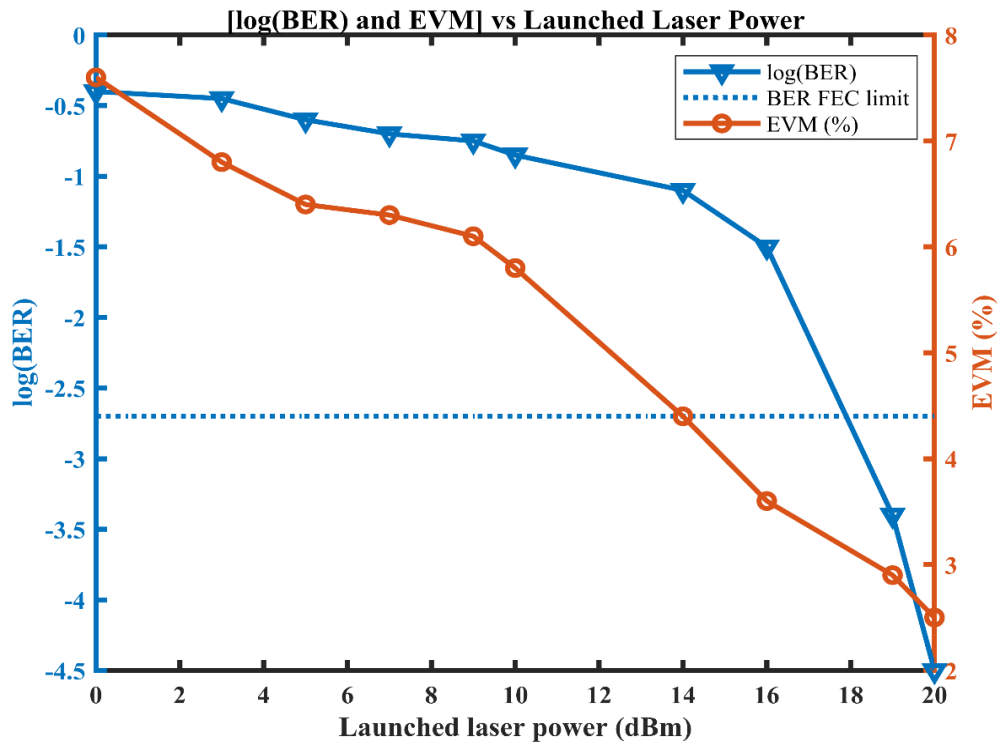
Fig. 5.8 log (BER) and EVM (%) against launched laser power at 2.65 km transmission distance.
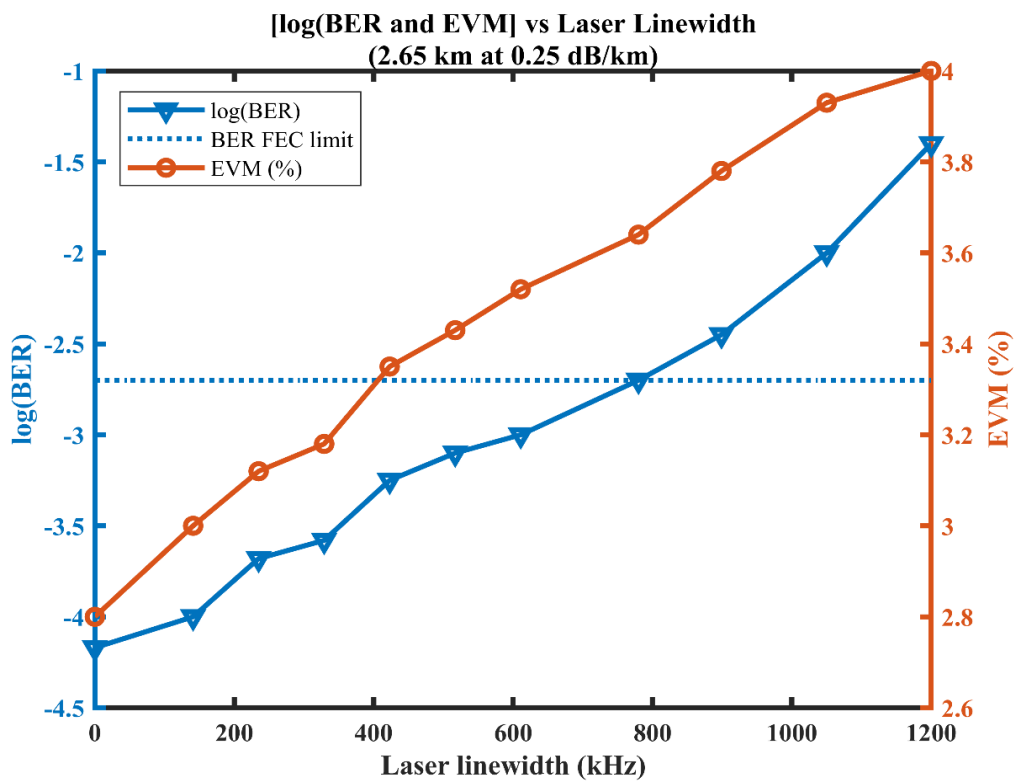

Fig. 5.9 log (BER) and EVM (%) against laser linewidth at 2.65 km transmission distance.

The log (BER) and EVM (%) against laser linewidth graph for proposed link design at 2.65 km transmission are illustrated in Fig. 5.9. Laser linewidth (Δf) dependence is followed as Eq. 2. From this figure, it can be seen that with growing laser linewidths, the BER and EVM (%) value decline. This trend is because higher laser linewidths cause optical spectrum broadening which contributes to the diffusion of the optical beam while transmission. Under linewidths $\leq$ 780 kHz, acceptable BER performance is obtained, nevertheless, all other analysis in this article was carried for laser linewidth of 100 kHz, since a narrow linewidth is a key to the high performance coherent optical receiver.
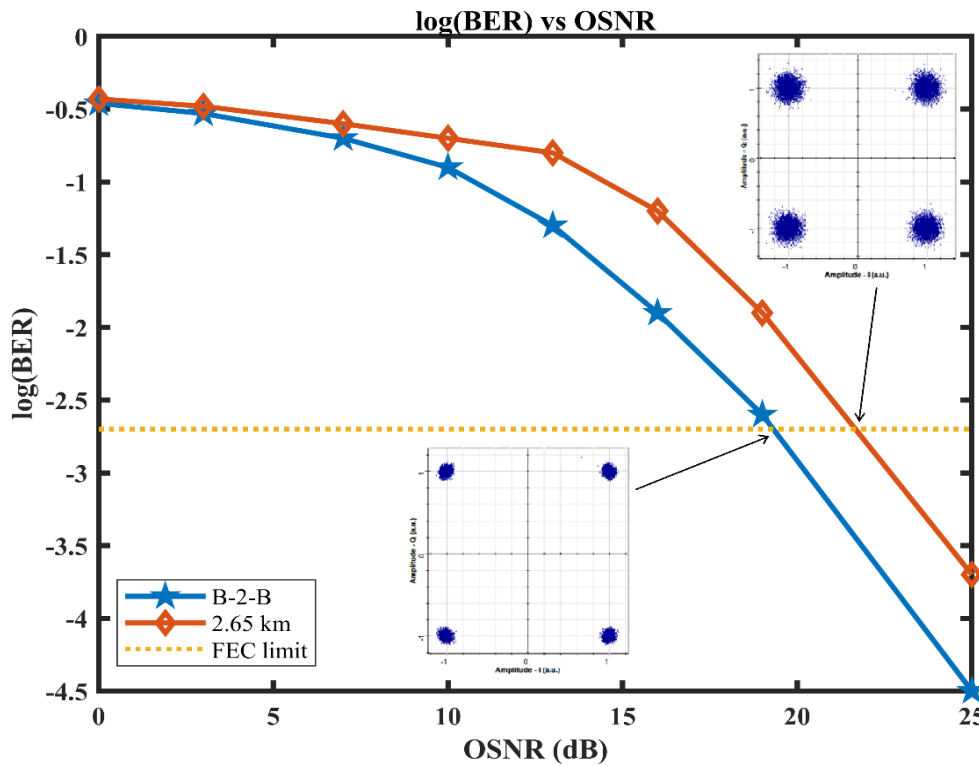
Fig. 5.10 log (BER) and OSNR plots for B-2-B case and 2.65 km distance (insets: corresponding constellation plots).

Figure 5.10 reports log (BER) against OSNR plot for B-2-B case and maximum link distance of 2.65 km over fair weather conditions. The results report clear progress in BER performance with the increase in OSNR, that is, the link is less susceptible to error. The OSNR requirement towards achieving realistic performance, BER $\leq 2 \times 10^{-3}$ (FEC limit) for B-2-B case is 19.5 dB which rises to 21.95 dB for a 2.65 km transmission distance.

Consequently, a 2.45 dB OSNR penalty appears for 2.65 km transmission as per comparison with the B-2-B scenario. As can be seen from the inserts of the figure, clear and distinct QPSK symbols demonstrate an acceptable link performance. Thus it can be said that the OSNR prerequisite to upholding the standard performance grows higher as the link distance increases. The OSNR sensitivity reflects noise tolerance of the modulation technique in a way that the lesser the mandatory OSNR to sustain an adequate BER performance, the better noise-tolerant the system would be.
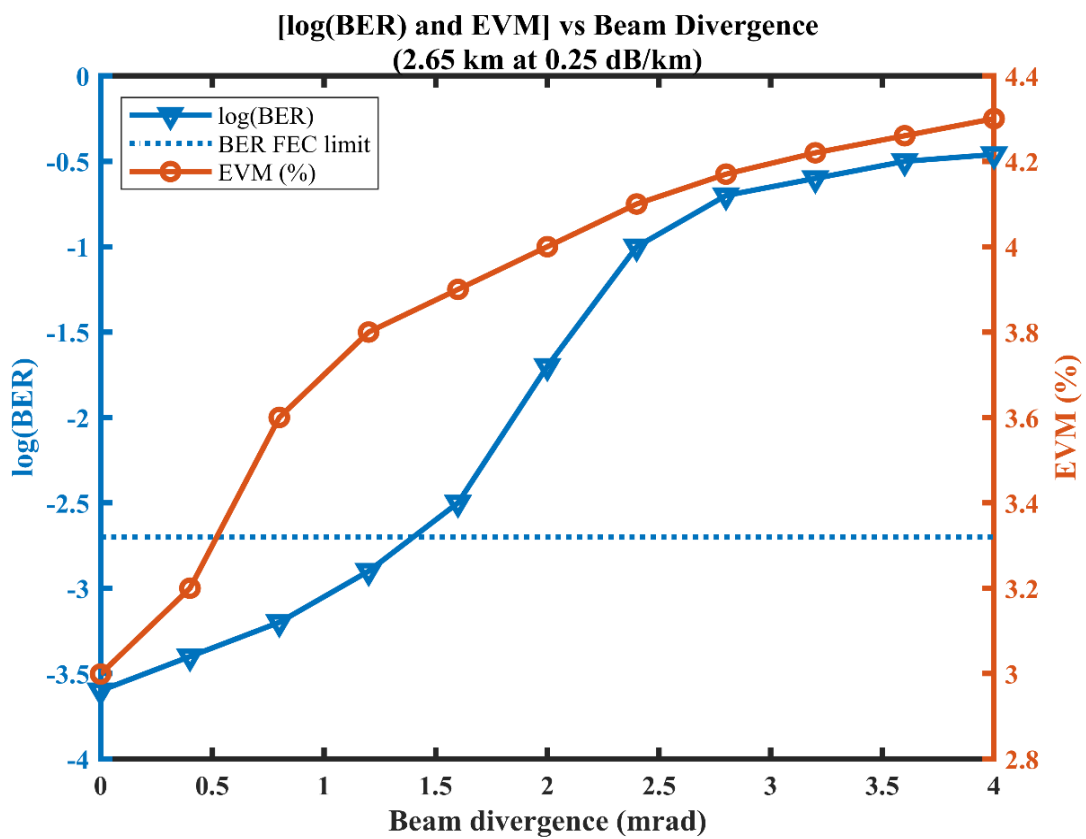
Fig. 5.11 log (BER) and EVM (%) against beam divergence at 2.65 km link distance.

The log (BER) and EVM (%) versus beam divergence graph using the proposed system at 2.65 km transmission under fair atmospheric conditions is illustrated in Fig. 5.11. The result reveals that the BER increases with increasing beam divergence. To be specific, log (BER) increases from -3.6 at 0 mrad beam divergence angle to -0.46 at 4 mrad beam divergence angle. The distortion generated in the received information signal with growing

laser beam diffusion makes it hard for the detector module to effectively catch the incoming signal.

5.4 Concluding remarks

In this work, we design a high-speed and long-haul single-channel coherent FSO communication system utilizing DP-QPSK and DSP techniques. From the outcomes of our investigation, it is possible to conclude that the joint implementation of BHD and DSP algorithms like Bessel filter, cubic interpolation, GSOP, CMA-RD, FOE, and BPS noticeably improved the link performance with a 3 dB increase in the receiver sensitivity and effective compensation of the free-space loss. The utilization of the hybrid DP-QPSK technique enhanced both the SE and information-carrying capacity of the proposed system. Besides, the single-channel scheme reduced the cost and complexity of the proposed transceiver design. With 32 GBaud symbol rate, the system achieved successful transportation of 128 Gb/s information signal over a transmission range of 2.65 km for an OSNR penalty below 2.5 dB compared to the optical B-2-B case measured at a BER of 2×10^{-3}. Furthermore, we demonstrated that a narrow laser linewidth and small beam divergence angle are crucial for acceptable link performance even under clear weather conditions. This work is a modest contribution to the development of near future high-performance coherent optical transmission systems.

CHAPTER 6: DESIGN AND ANALYSIS OF 400 GBPS DP-16-QAM FREE SPACE OPTICAL COHERENT TRANSCEIVER SYSTEM WITH DSP TECHNIQUES

6.1 Introduction

Multi-level quadrature amplitude modulation (QAM) encodes data on the amplitude as well as the phase of the laser beam and hence is the efficacious approach to achieve higher data rate and transmission coverage without increasing the bandwidth [46]. Advanced digital signal processors (DSPs) run digital domain impairment compensation algorithms to retrieve the original transmission signal precisely [109]. BER, constellation diagram, optical signal to noise ratio (OSNR) [110], and in recent times error vector magnitude (EVM), can be used as ultimate performance indicators to measure the transmission quality in optical wireless networks [111]. From time to time, researchers have been working to overcome the challenges in the FSO link and to enhance potential system capacity, spectral efficiency, and transmission distance using advanced optical modulation techniques [112]. A Higher-order QAM transceiver system provides higher data rates [113] but at the cost of noise margin however recently, it has been shown that employing diversity techniques in coherent FSO communication systems improves receiver SNR significantly [35]. Industries prefer a single-channel communication scheme since it offers the essential bit rate and vigorous communication link at a minor cost [36]. By employing DSP techniques including CMA, it is now possible to mitigate the multipath effect in a 400G optical wireless system combined with polarization division multiplexing (PDM) [37]. Even though the most decisive measure of quality for any communication system was considered to be BER [114] but newly, EVM is encouraged as a more fitting parameter to assess the worth of space vector-modulated signals [37]. The OSNR requirement of an optical wireless network is acute since it reduces the working budget and supplements the data transmission rate [38]. In this chapter, a DP-16-QAM terrestrial FSO transceiver system has been proposed for 400 Gb/s bit rate, single-channel, low power consumption, and higher spectral efficient wireless optical communication systems. To compensate for signal

transmission impairments, DSP algorithms have been implemented to recover incoming signal after coherent detection. All such techniques have made it possible to achieve a link range of 2 km for 400 Gb/s data signal under fair climatic conditions on simulation software.

6.2 Design schematic

The simulation setup of single-carrier coherent DP-16-QAM terrestrial FSO transceiver system is displayed in Fig. 6.1 consisting of optical DP-16-QAM transmitter, FSO channel, DP-16-QAM homodyne receiver, universal DSP, a decision component, QAM sequence decoders, and a parallel to serial (P/S) converter.
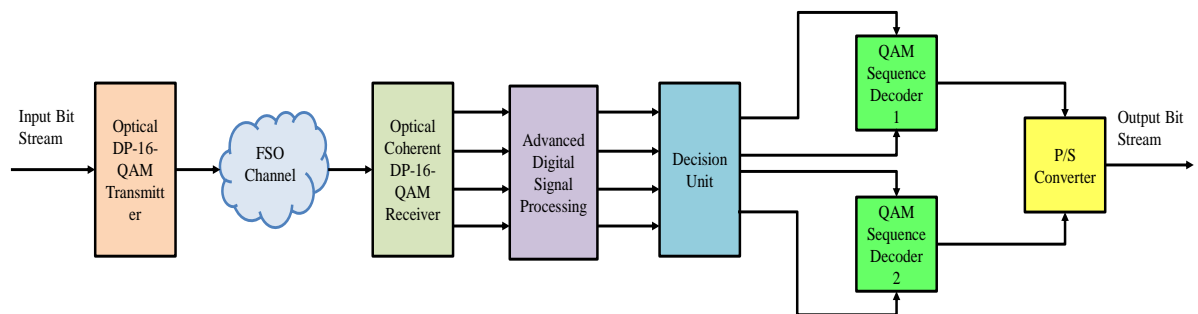

Fig. 6.1 Simulation setup of DP-16-QAM terrestrial FSO transceiver system.

The laser beam generated from the continuous wave (CW) laser, is bisected into two quadratic polarization components, X and Y by way of PBS, which are modulated and then passed into a polarization combiner [115]. FSO channel imitates the behavior of free space and hence lets for the modeling of FSO links. DP-16-QAM receiver is built over the homodyne receiver structure. It has a local oscillator (LO) polarized at 45° with respect to PBS. Each LO component separately demodulates the received signal with two 16-QAM demodulators. The universal DSP component carries out several impairment compensation algorithms to aid in recovering the incoming transmission signal after coherent detection. The decision unit normalizes the amplitudes of in-phase and quadrature-phase electrical signals and compares each received symbol based on normalized threshold settings. QAM sequence decoders decrypt the square 16-QAM constellation points and output is generated

56

from two parallel input I/Q subsequences. In QAM modulation, the amplitude of the modulated signal can be varied according to the binary symbols. The value of amplitude for each output signal is taken from the set of amplitudes given by [116]

$$a_{1=} (2k - 1 - M) \tag{6.1}$$

where k = 1, 2, - - -, M and M is the number of possible binary sequences, that is given by [117]

$$M = 2^{\frac{b}{2}} \tag{6.2}$$

where b represents bits for each symbol. The respective QAM set is given by the square of the term, M. This means, if b = 4 and M = 4, then it gives 16-QAM. To have only a single bit change between the successive symbols, Gray coding has been incorporated in the system. The output signal model is given by [118]

$$V_{out}(t) = \begin{cases} 0, & 0 \le t < t_1 \\ a_{s,} & t_1 \le t < t_1 + t_c \\ 0, & t_1 + t_c \le t < T \end{cases} \tag{6.3}$$

where a_s is the magnitude of the signal s, t_1 is the pulse position, t_c is the duty cycle and T is the bit period. The coherent 16-QAM receiver consists of PBS that splits the received optical signal into two output components [119], two back-to-back 90-degree optical hybrids that coherently demodulate the optical carrier signal, and balanced photodetectors (BDs) which translate optical intensities into I and Q electrical signals [120].

6.3 Results and analysis

The outcomes of the simulative investigation on the DP-16-QAM FSO transceiver system are discussed and the system performance is evaluated with regard to constellation diagram, BER, EVM, and OSNR. FSO channel is examined under clear climatic conditions with atmospheric attenuation of 0.25 dB/ km for 1550 nm optical window [121]

and low turbulence effect (index refraction structure, $c_n^2 = 5 \times 10^{-15} m^{-2/3}$) [122]. Simulation parameters considered for QAM/FSO transceiver design are listed in Table 6.1.

Figure 6.2 shows the variation of electrical constellation diagram with respect to varying transmission distance from 1-2 km From Fig. 6.2a-c, it can be seen that at a distance of 1 km, there are 16 distinct signaling points in the scattering diagram, however, with increasing link range from 1.5-2 km, the constellation points disperse and constellations get corrupted with noise.
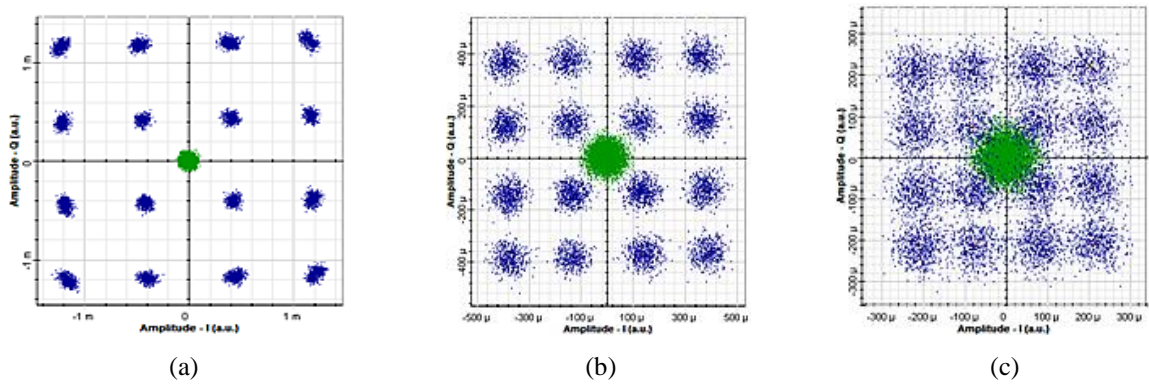

| (a) | (b) | (c) |

Fig. 6.2 Variation of electrical constellation diagrams for DP-16-QAM system with respect to link range at (a) 1 km, (b) 1.5 km, and (c) 2 km.

Figure 6.3 shows the variation of the electrical constellation diagram with respect to varying divergence angle from 0.25 mrad to 0.85 mad. From Fig. 6.3a-c, it can be seen that at a divergence angle of 0.25 mrad, there are 16 distinct signaling points in the scattering diagram, however, with an increase in beam divergence from 0.55 mrad to 0.85 mrad, the constellation points disperse, and constellations get corrupted with noise.

The DSP component performs digital domain impairment compensation to aid in recovering the incoming transmission signal after coherent detection of optical square 16-QAM modulated signal. It performs several important functions to recover the incoming transmission channel after coherent detection. It has been used with the optical coherent receiver that utilizes 16-QAM modulation. Figure 6.4 shows the constellation diagrams of the proposed 400 Gb/s DP-16-QAM transceiver system at various positions of the DSPU after 2 km transmission. Figure 6.4a shows constellation diagram just after coherent detection. LPF Bessel filter is used with $8 \times$ samples per bit and an optimal bandwidth of

Table 6.1 Simulation parameters.

Parameters	Values
Bit rate	400 Gbps
Frequency	193.414 THz
Power	20 dBm
Linewidth	0.1 MHz
Initial phase	0 degree
Baud rate	40 Gbaud
Range	2 Km
Beam divergence	0.25 mrad
OSNR	22 dB
Transmitter aperture diameter	5 cm
Receiver aperture diameter	20 cm
Receiver loss	1 dB
Responsivity	1 A/W
Dark current	10 nA

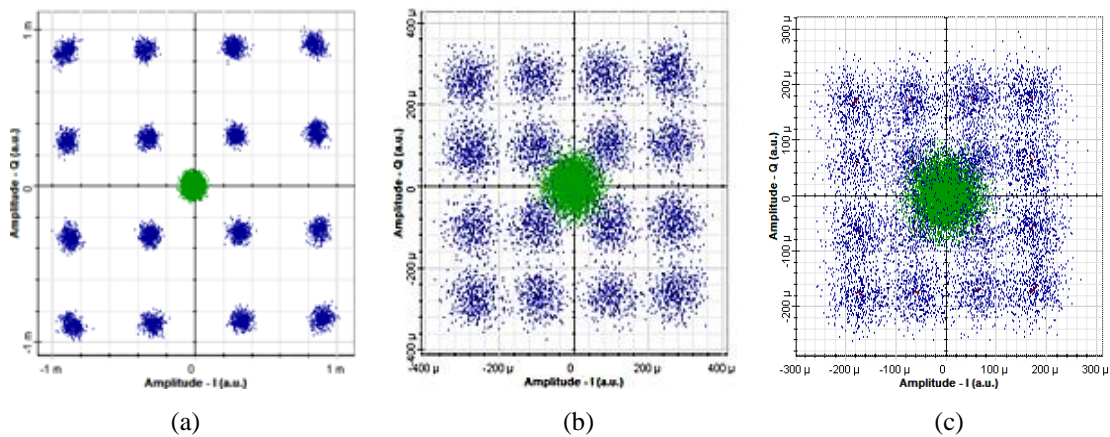(a)   (b)   (c)

Fig. 6.3 Variation of electrical constellation diagrams for DP-16-QAM system with respect to beam divergence at (a) 0.25 mrad, (b) 0.55 mrad and (c) 0.85 mrad.

$0.75 \times$ bit rate/8 with signal constellations as shown in Fig. 6.4b. Resampling is done at the rate of 4 samples/symbol. Cubic interpolation is used and the 1st and N/2+1 (where N = samples per symbol) sampled signals are used for resampling whose constellation diagram is shown in Fig. 6.4c. The amplitude and phase imbalances within the I and Q

59

signals are reduced with QI compensation as shown in Fig. 6.4d. The adaptive equalizer implements a butterfly structure [123][124] for de-multiplexing the X- and Y-polarizations of the signal as shown in Fig. 6.4e. FOE is used to cancel the frequency and phase mismatch between the transmitter and the LO as shown in Fig. 6.4f. After the CPE algorithm is implemented to eliminate the phase mismatch by attempting different test phases, the final constellation diagram looks as shown in Fig. 6.4g.
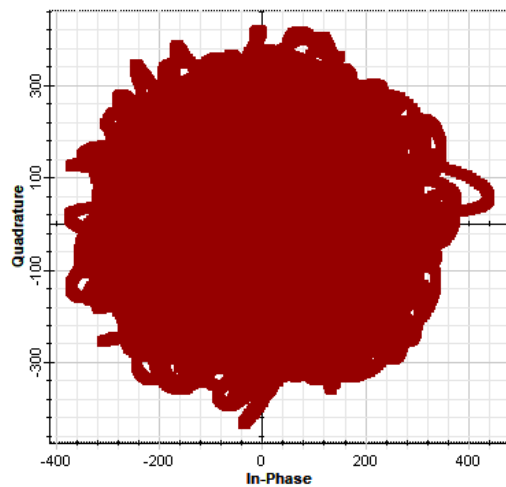
(a)

(b)

(c)

(d)

(e)   (f)

(g)
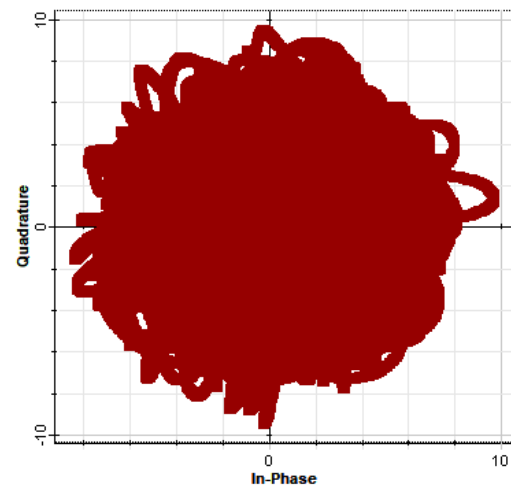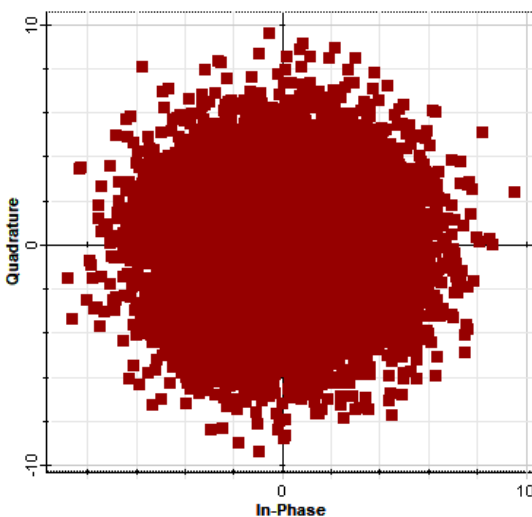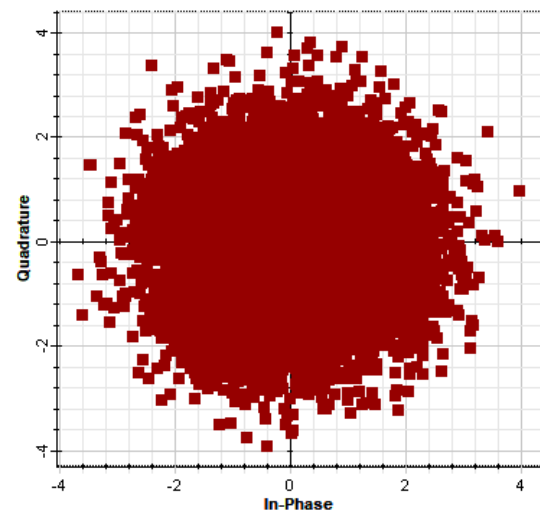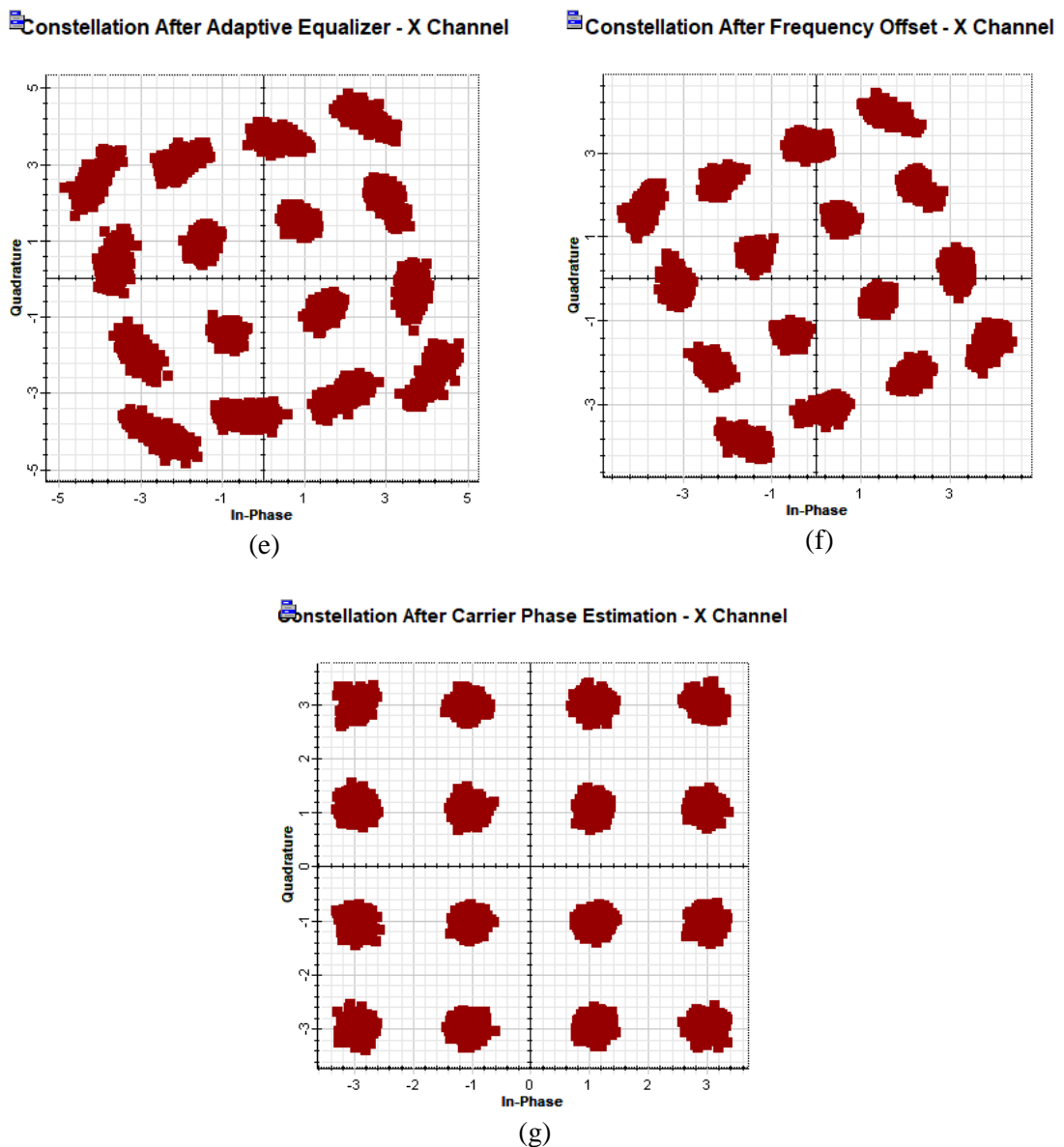
Fig. 6.4 Progress of the constellation diagrams down the DSP component after (a) BHD, (b) low pass filtering, (c) resampling, (d) QI compensation, (e) AE, (f) FOE, and (g) CPE for the fair climate.

Figure 6.5 illustrates the variation between BER and OSNR for the proposed system. With the increasing value of OSNR from 10-22 dB, initially, the BER value decreases but then remains constant. Hence, with greater values of OSNR, constellation points become more discrete. In communication systems, random noise causes erroneous bits, the occurrence of which is measured as BER. OSNR is a vital parameter since it quantifies the degree of impairment when the modulated laser signal is carried in free space. The OSNR

requirement of the optical wireless network is analytical since it reduces working expenditure and boosts the bit rate of the network. Following are the mathematical expressions used for the calculation of BER value and OSNR requirement:

BER for dual-polarization system is given by [125]

$$BER = \frac{X_{errors} + Y_{errors}}{sequence\ length - (2 \times guard\ bits)} \tag{6.4}$$

where only those errors add up which lie outside the portion of the sequence of the guard bits. BER for the X-polarization channel is given by

$$BER_x = \frac{X_{errors}}{(sequence\ length - 2 \times guard\ bits)/\ 2} \tag{6.5}$$

BER for the Y-polarization channel is given by

$$BER_y = \frac{Y_{errors}}{(sequence\ length - 2 \times guard\ bits)/\ 2} \tag{6.6}$$

In order to add a definite noise level to the transmitted optical signal, a set OSNR unit is used. The OSNR level is set based on the following equation [126]

$$OSNR(dB) = 10log_{10} \left[\frac{P_s\ (mW)}{P_{n0.1}\ (mW)} \right] = [dB(signal) - dB(noise)] \tag{6.7}$$

where P_s is the total signal power within the signal bandwidth and $P_{n0.1}$ is the noise power measured within a 0.1 nm bandwidth window. As the noise is added to the signal using a power combiner there is a 3 dB transmission loss applied to both the signal and noise source but the OSNR level is not affected. To achieve BER value under FEC limit [127] i.e. 2×10^{-3}, the minimum OSNR value denotes the noise acceptance of a modulation format finite bandwidth. The relation between BER and OSNR is given by [128]

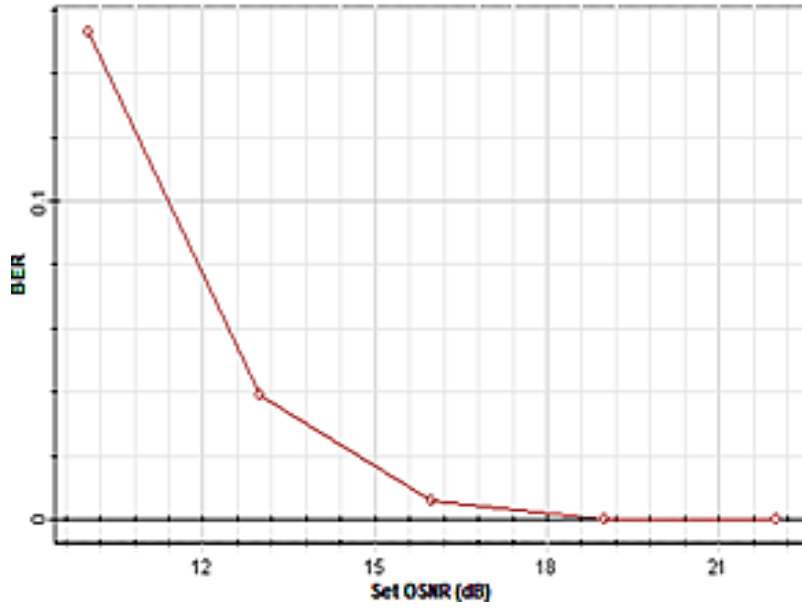$$BER = \frac{3}{8} erfc\left[\sqrt{OSNR_{NL}/2} \right] \tag{6.8}$$

Fig. 6.5 Variation of BER values with respect to OSNR.

Figure 6.6 depicts the relationship between BER and EVM for the system under consideration. The EVM and BER relation is of noteworthy importance for coherent optical systems [114] since EVM is well-matched than BER measurement for indefinite symbol sequences and to distinguish optical I/Q transmitters [129]. EVM is described as the root-mean-square (RMS) value of the deviation among calculated constellation points and ideal constellation points [130]. EVM is measured with vector signal analyzers directly from down-converted signals [131], as a result, additional computation is reduced that may be needed to figure out the BER. The EVM of the received signals is calculated as follows [132]

$$EVM = \frac{\sqrt{\overline{|S - \lfloor S \rfloor_u|^2}}}{\|\lfloor S \rfloor_u^2} \times 100\% \qquad (6.9)$$

where symbol sequence is denoted by S, mean value is written as $\overline{(|S - \lfloor S \rfloor_u|^2)}$ and $\lfloor S \rfloor_u$ represents the decision of S respectively. RMS value of EVM is given by [130]

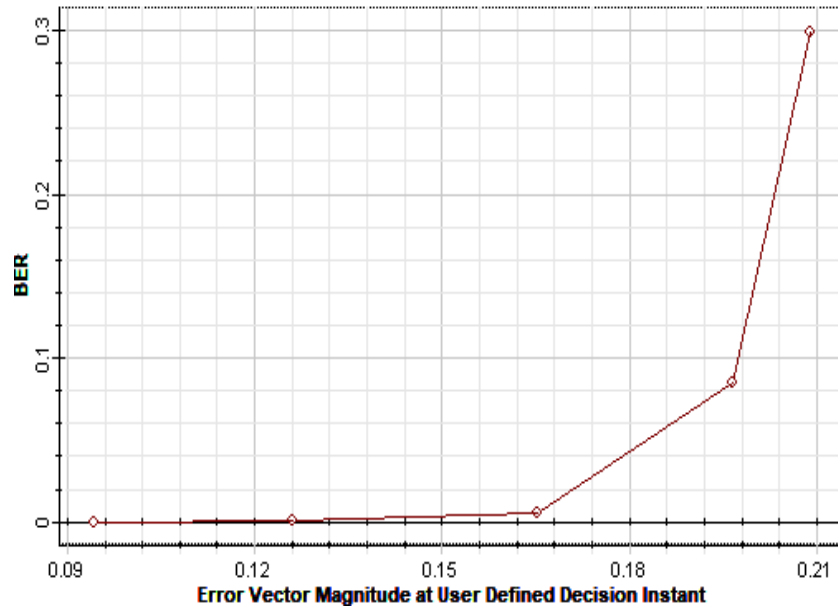$$EVM_{rms} = \sqrt{\frac{1/N \sum_{j=1}^{N} |E_{r,j} - E_{t,j}|^2}{P_a}} \qquad (6.10)$$

63

Fig. 6.6 Variation of BER with respect to EVM.

We can relate BER with EVM by [131]

$$BER = \frac{\left(1-M^{-1/2}\right)}{1/2 \, \log_2 M} \, erfc \sqrt{\frac{3/2}{(M-1)EV \, M_{rms}^2}} \tag{6.11}$$

6.4 Concluding remarks

In this work, the design and performance analysis of the coherent optical DP-16-QAM FSO system with homodyne detection has been carried out. DSP algorithms aid to compensate for various transmission impairments such as laser phase noise, QI, DC, NL, PMD, frequency, and phase gap between the received signal and LO optical carrier and provide better outcomes regarding data rates, transmission range, and signal constellations. As a result, the system supplies a data rate of 400 Gb/s up to a link distance of 2 km in simulation software. The system credibility has been tested at various link distances and divergence angles. It was observed that with increasing transmission distances and divergence angle, system performance deteriorated. The system presented fulfills the demands of next-generation ultra-high-speed wireless networks, with license-free spectrum operation at a modest cost and reliable network.

64

CHAPTER 7: DESIGN AND ANALYSIS OF 720 GBPS DP-256-QAM FSO SYSTEM WITH COHERENT DETECTION AND DSP ALGORITHMS

7.1 Introduction

The recent development of high-speed digital integrated circuits (ICs) has offered the possibility of treating the electrical signal in the DSP core and retrieving I/Q components of the complex amplitude of the optical carrier from the homodyne detected signal in a very stable manner. Since the carrier phase is recovered after homodyne detection through DSP, this type of receiver has now commonly been called the digital coherent receiver [133]. While an optical phase-locked loop (OPLL) that locks the LO phase to the signal phase is still difficult to achieve due to the loop delay problem, DSP circuits are becoming increasingly faster and provide us with simple and efficient means of estimating the carrier phase [134]. Very fast-tracking of the carrier phase improves system stability drastically as compared with the OPLL scheme. Any kind of multi-level modulation format like 256-QAM can be introduced by using the coherent receiver [135]. While the SE of binary modulation formats is limited to 1 bit/s/Hz/polarization, which is called the Nyquist limit [136], modulation formats with M bits of information per symbol can achieve up to the SE of M bit/s/Hz/polarization. 256-QAM modulation format can transmit 16 bits per symbol, each symbol is encoded by using the Gray code scheme. Also, since the phase information is preserved after detection, we can realize electrical post-processing functions such as compensation for CD and PMD in the digital domain. These advantages of the coherent receiver and DSP unit together have enormous potential for innovating existing optical communication systems.

7.2 Proposed system design

The overall block diagram of the proposed high-speed and long-haul FSO system consisting of DP-256-QAM transmitter, FSO link, dual-polarization coherent receiver, DSP unit, a decision unit, and a decoding unit is shown in Fig. 7.1. The PRBS generator

generates the input bit sequence with a sequence length of $2^{19} - 1$. The dual-polarization coherent receiver consists of PBS, (2×4) 90 degree optical hybrids, and balanced detectors in series which extracts the in-phase and quadrature-phase electrical signals. The DSP unit implements various signal processing algorithms to recover the transmitted symbols [137]. Finally, the symbols are decoded to obtain the output bit sequence. Gray coding is used so that there is only a one-bit change between the consecutive symbols. This results in lesser bandwidth of the modulated optical signal, and hence, we get a higher spectral efficiency of the system and small errors in baseband information.
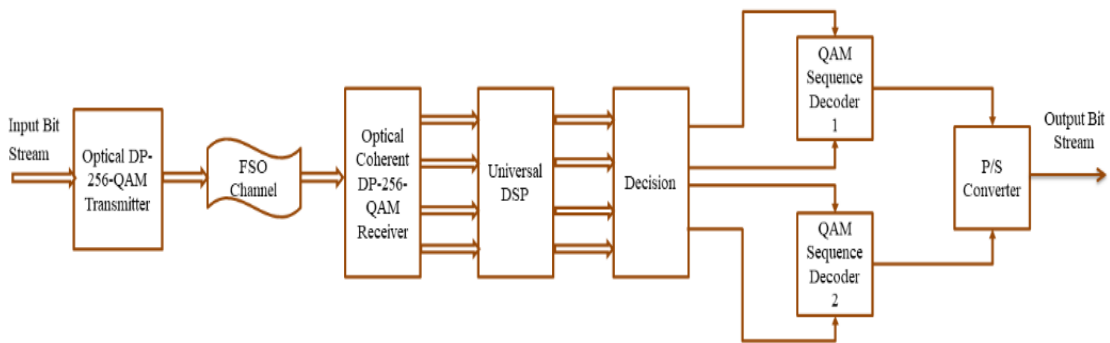
Fig. 7.1 Proposed system design for DP-256-QAM FSO communication system.

Figure 7.2 shows the internal design schematic of the DP-256-QAM transmitter. The polarization splitter splits the input optical carrier into X and Y orthogonal polarizations using a linear polarizer. X and Y polarized optical carriers are fed to the upper and lower branches of the IQM. A cross-coupler with a coupling coefficient of 0.5 is used to send the light-wave into the in-phase and quadrature-phase branches of the IQM. The input bit sequence (bit rate = R) is split into two parallel bit sequences (each has a bit rate R/2) and is sent to the upper and lower IQMs, respectively. The QAM sequence generator generates two parallel M-ary symbol sequences from the input binary sequence, and each sequence is transmitted in two parallel carriers while designing an optical QAM modulator. These multilevel raised cosine pulses are applied to the RF plates of the dual-drive LiNbO3 Mach–Zehnder modulator (MZM). Each modulator is set at its peak point of operation with an extinction ratio of 30 dB, switching bias voltage 3 V and bias voltages (V1 and V2) set to 0 V. A relative phase shift of is added to the quadrature-phase branch in both
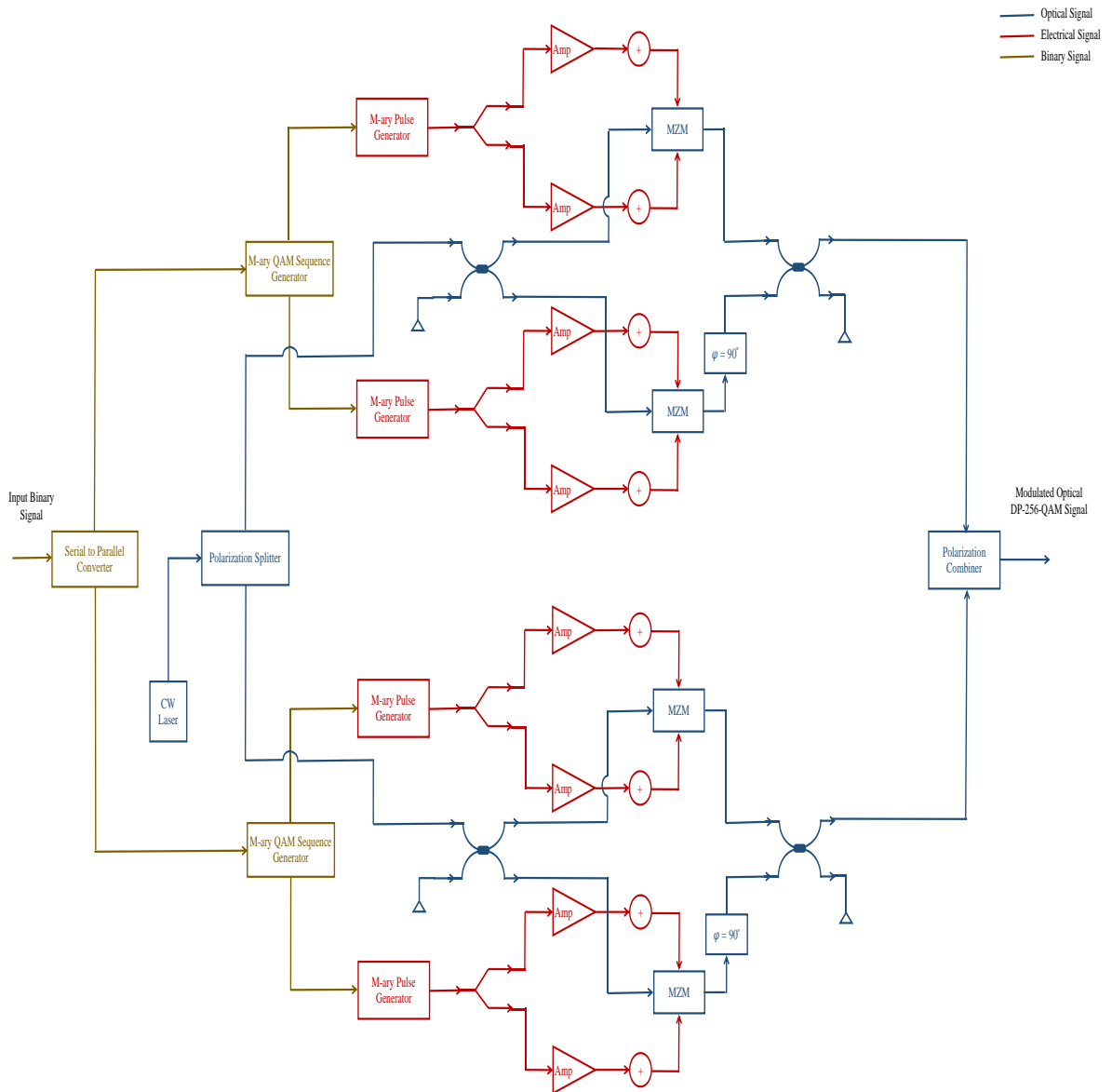
Fig. 7.2 Internal schematic design of optical DP-256-QAM transmitter.

the IQMs to generate the optical QAM signal. The data-bearing optical signals for the two polarizations are combined using the PBC. It selects the appropriate polarization component of each signal at the input ports and adds the chosen polarization component. At input port 2, an angle of 90° is attached to the device angle of the polarizer.

Figure 7.3 shows the dual-polarization homodyne receiver structure for the 256-QAM demodulation. It consists of PBS for extracting the X and Y polarization components, (2×4) 90 degree optical hybrid for converting the phase information into intensity equivalent,

and a balanced homodyne detector (BHD) converts the optical intensity into in-phase and quadrature-phase electrical signals [138]. The IQ demodulation by the digital coherent receiver is an entirely linear process; therefore, all the information on the complex amplitude of the transmitted optical signal is preserved even after detection [139], and signal-processing functions acting on the optical carrier, such as optical filtering and dispersion compensation, can be performed at the electrical stage after detection. The polarization alignment is also made possible after detection by introducing the polarization diversity scheme into the homodyne receiver. The complex amplitude of the horizontal polarization and that of the vertical polarization are simultaneously measured and processed by DSP. The combination of coherent detection and DSP is thus expected to become a part of the next generation of optical communication systems and provide new capabilities that were not possible without the detection of the phase of the optical signal.
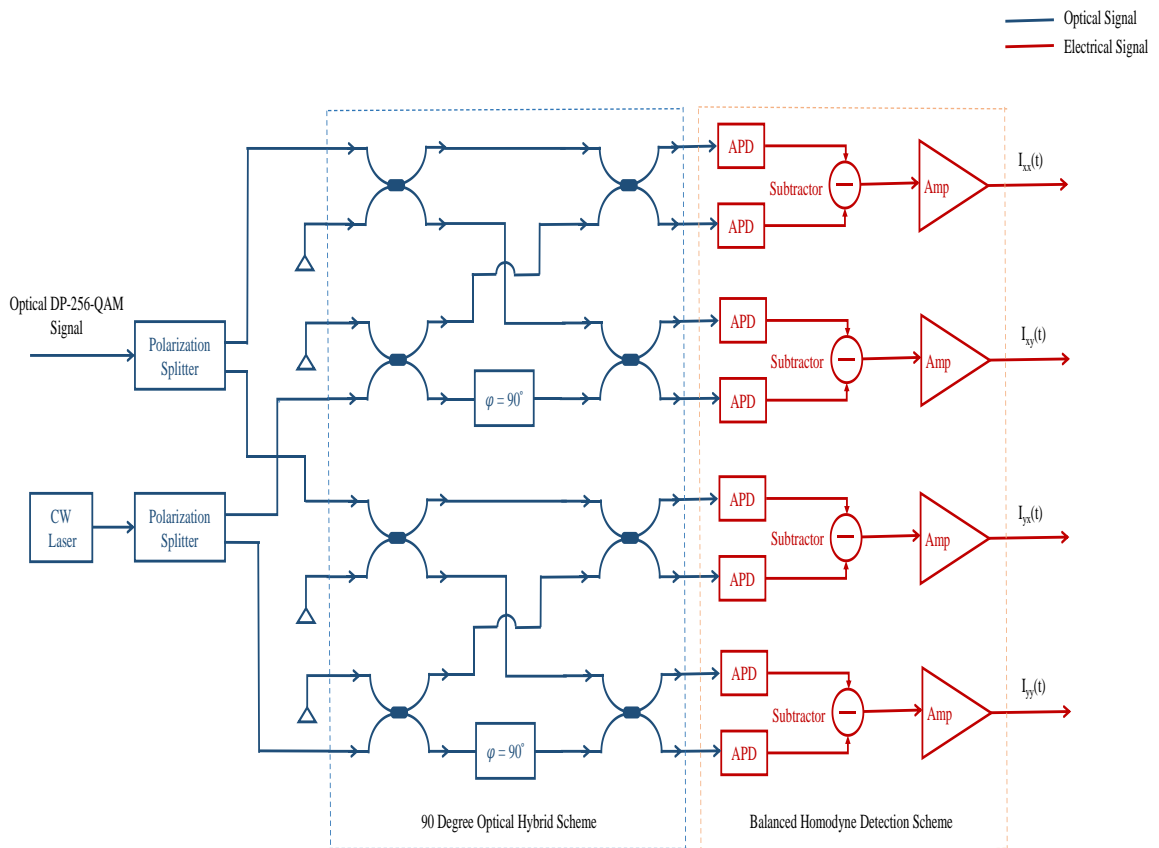

Fig. 7.3 Internal schematic design of optical coherent DP-256-QAM receiver.

7.3 Results and discussion

The proposed 720 Gb/s DP-256-QAM FSO transceiver system is designed in OptiSystem V.16 simulation software and the overall system performance is evaluated in terms of the impact of link length, launched optical power, laser linewidth, OSNR, and beam divergence over both the BER and EVM (%) in the MATLAB. Table 7.1 shows the simulation parameters and their values considered for the design of the proposed DP-256-QAM FSO communication link.

Table 7.1 Value of simulation parameters.

Parameters	Values
Bit rate	720 Gb/s
Launched optical power	20 dBm
Center frequency	193.414 THz
Atmospheric attenuation	0.25 dB/km
Baud rate	60 Gbaud
Laser linewidth	0.1 MHz
Beam divergence	0.25 mrad
Geometrical loss	Yes
Transmitter antenna aperture diameter	5 cm
Receiver antenna aperture diameter	20 cm
Photodetector responsivity	1 A/W
Photodetector dark current	10 nA
Receiver loss	1 dB

Figure 7.4 shows various steps associated with the 256-QAM DSP component. The DSP unit consists of various signal processing steps with various advanced algorithms to recover the transmitted symbols from the received electrical signals. It performs several essential functions recovering the incoming signals after coherent demodulation such as DC blocking, normalization, low pass filtering, resampling, QI compensation, timing recovery, AE, FOE, and CPE. It has been used with an optical coherent receiver that uses
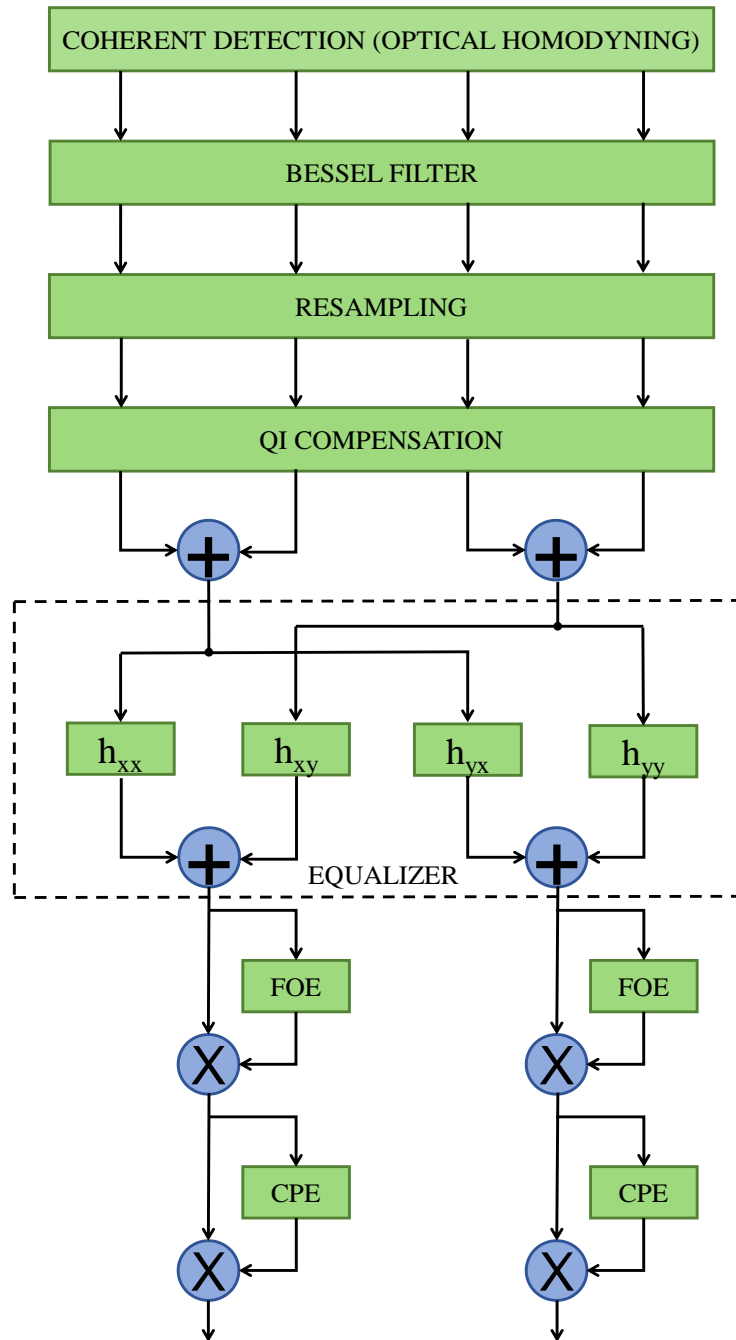
Fig. 7.4 Flowchart of 256-QAM high-level DSP algorithm design steps.

256-QAM modulation with dual polarization (X and Y channel) multiplexing. Figure 7.5
shows the constellation diagrams for both the X- and Y-polarization channels of the
proposed 720 Gb/s DP-256-QAM FSO transceiver system at various positions of the DSP
unit after a successful 1.31 km transmission. Figure 7.5a shows overlapping constellations
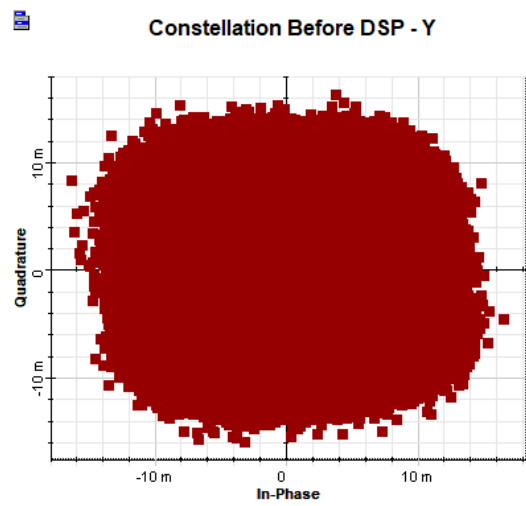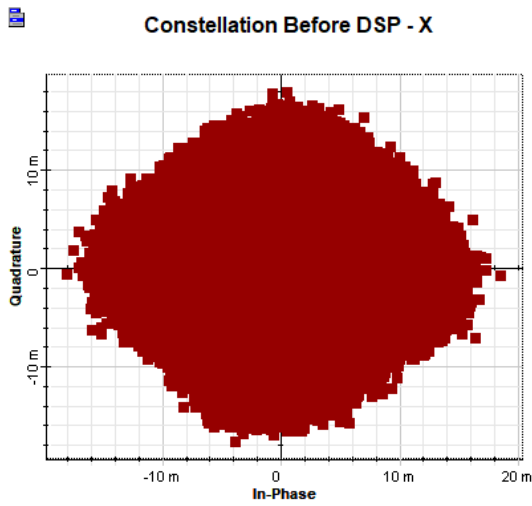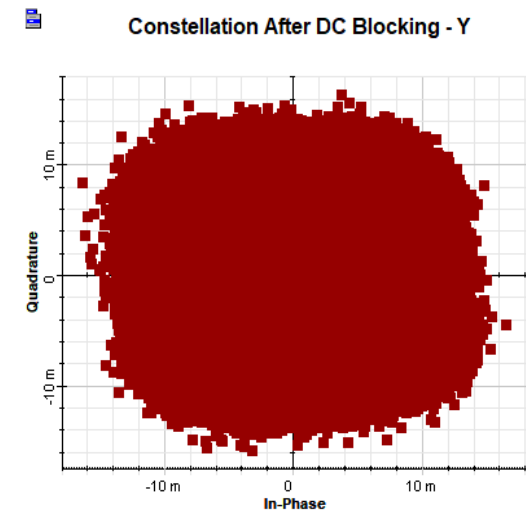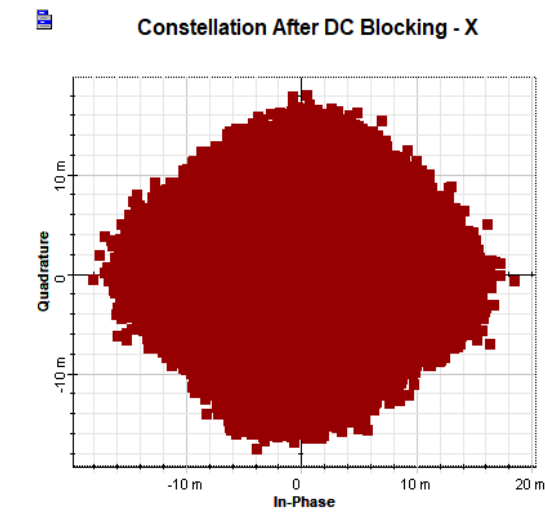
(a)

(b)
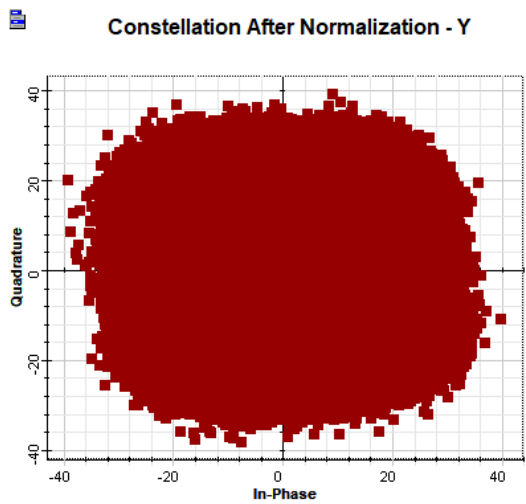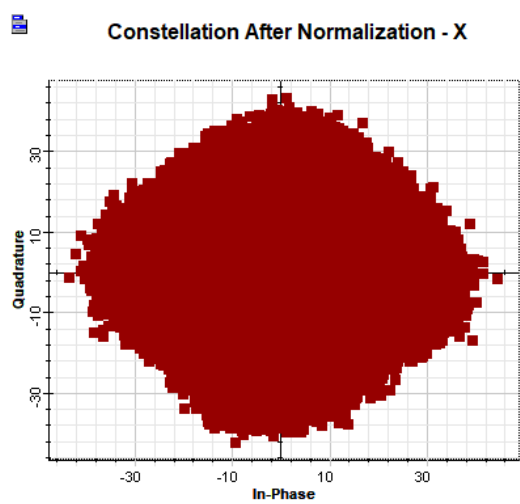
(c)
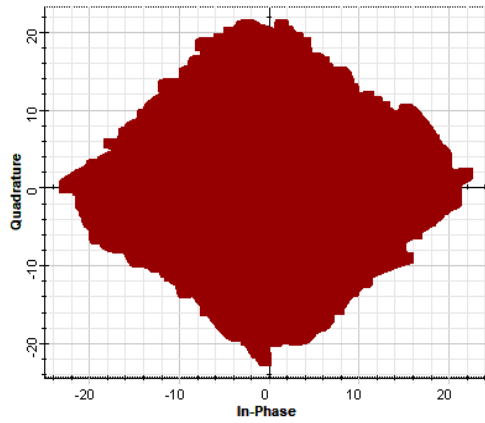
(d)

(e)

(f)

(g)

(h)

(i)

(j)
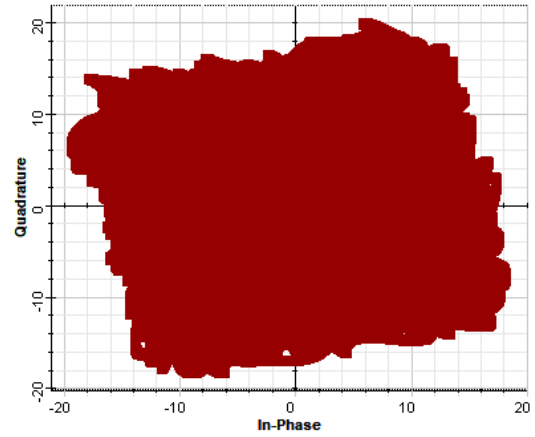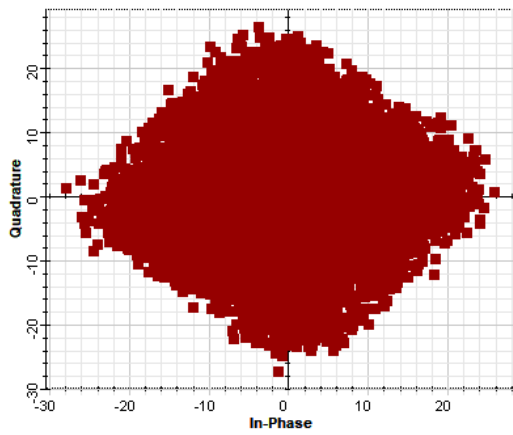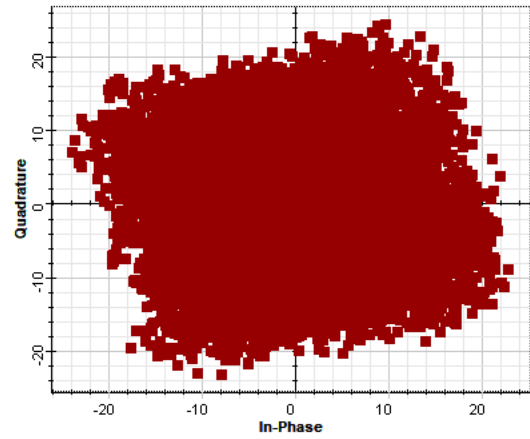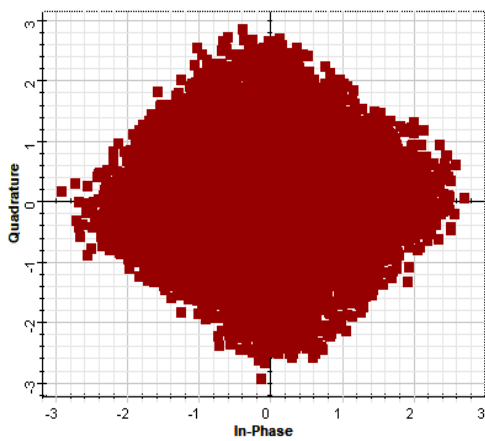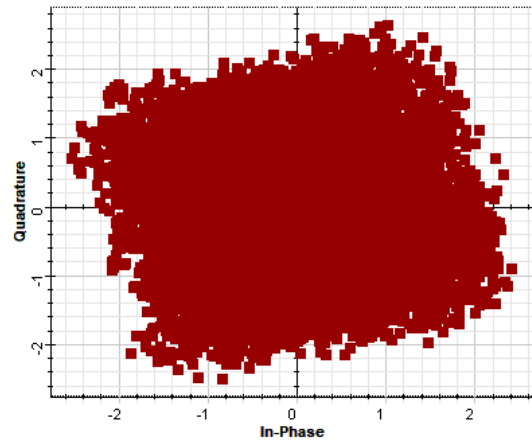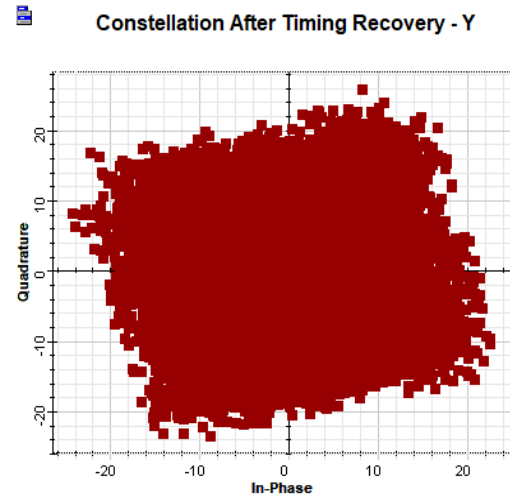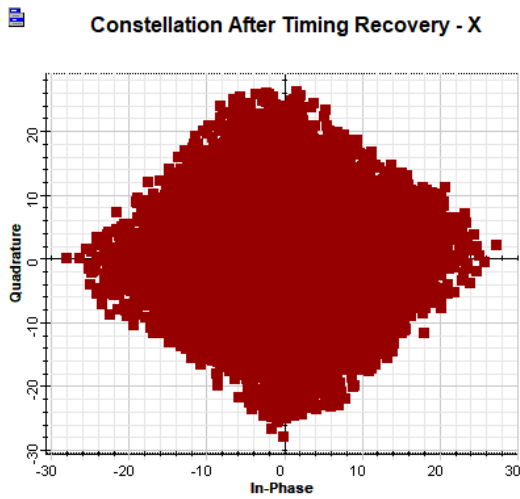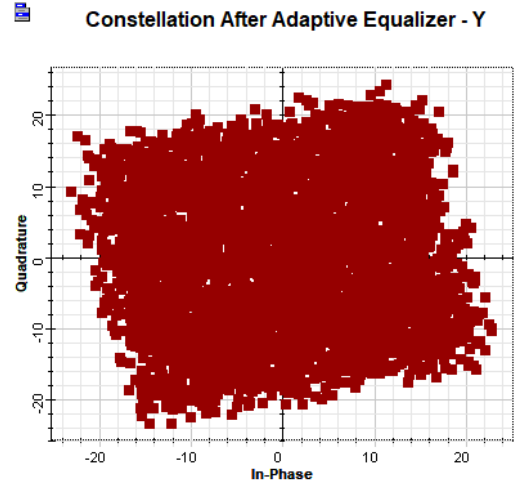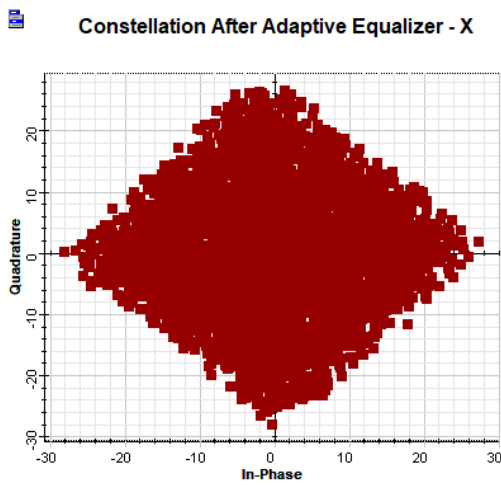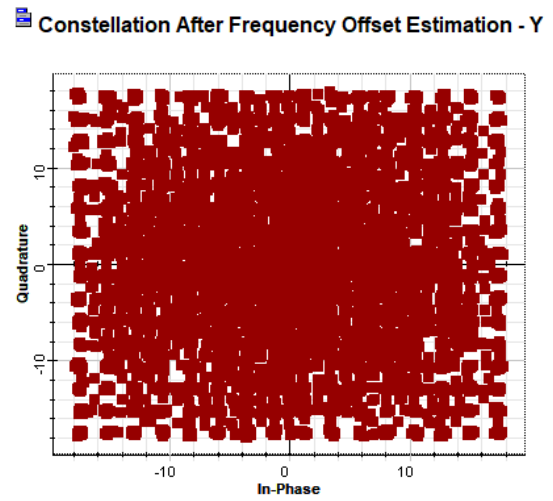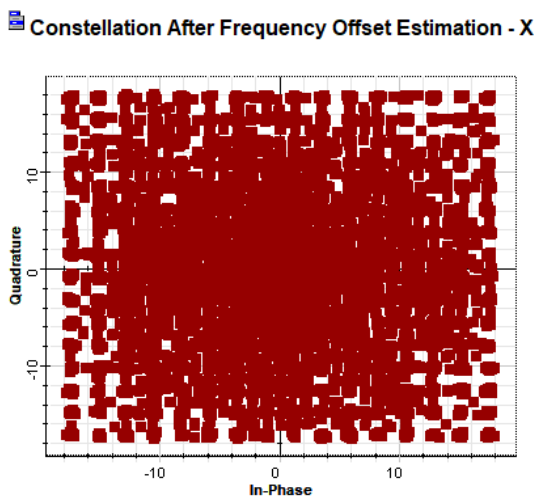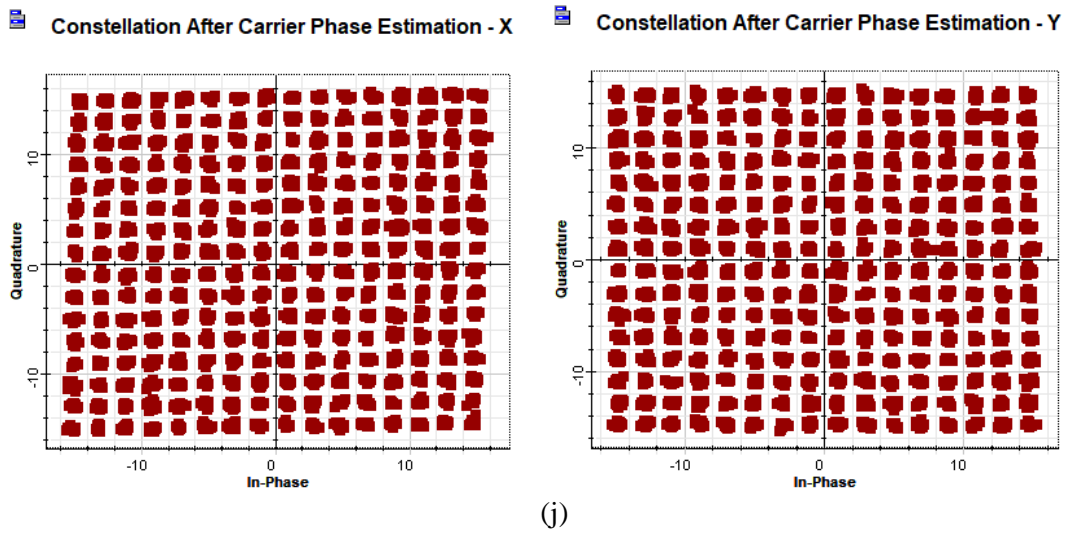
Fig. 7.5 X- and Y-polarization component signal constellation diagrams down the DSP unit for the 720 Gb/s-1.31 km DP-246-QAM FSO link after (a) BHD, (b) DC blocking, (c) normalization, (d) low pass filtering (e) resampling, (f) QI compensation, (g) timing recovery, (h) AE, (i) FOE, and (j) after CPE.

points of the X- and Y-polarization signals obtained from the demodulated in-phase and quadrature-phase electrical signals. This is due to the various transmission impairments like atmospheric attenuation, delay distortion, and noise. Figure 7.5b shows constellation points of the X- and Y-polarization channels obtained after DC blocking. The constellations are unclear due to imperfectly biased voltages of the MZMs and then normalized to the 256-QAM grid as shown in Fig. 7.5c. The band noise is filtered out using a third-order low pass Bessel filter with an optimal bandwidth of $0.75 \times$ bit rate/16 as shown in Fig. 7.5d. Resampling has been done at a rate of 16 samples/symbol with cubic interpolation with a constellation diagram as depicted in Fig. 7.5e. Figure 7.5f shows X- and Y-polarization constellations diagrams after QI compensation. Various system parameters such as modulator inappropriate bias voltages, PD responsivity mismatch, and imperfections in the 90∘ optical hybrids lead to amplitude and phase instability between the in-phase and quadrature-phase optical signals. Gram–Schmidt orthogonalization procedure (GSOP) is used to correct for non-orthogonalization [140] [132]. For the case of clock/timing recovery, the digital square filter (DSF) algorithm [125] is used to adaptively determine the correct time to sample and synchronize the symbols. Figure 7.5g shows the constellation diagram after timing recovery. Two-stage constant modulus

algorithm – radius directed-based (CMA-RD) AE is used to compensate for residual CD and PMD and to reduce inter-symbol interference (ISI). The cost function of the CMA takes the form [141]

$$J(k) = E[(|y(k)|^2 - R_p)^2]$$ (7.1)

where $E[.]$ Indicates the statistical expectation and $y(k)$ the equalizer output. R_p is the constant depending only on the input data symbol, $a(k)$, with dispersion order, p, set to 2 by default. It is defined as

$$R_p = \frac{E[|a(k)|^{2p}]}{E[|a(k)|^p]}$$ (7.2)

The equalizer output $y(k)$ is obtained from [142]

$$y(k) = W^H X(k)$$ (7.3)

$$W = [w_0(k), w_1(k), \dots, w_{N-1}(k)]^T$$ (7.4)

$$X_k = [x_0(k), x_1(k-1), \dots, x_{N-1}(k-N+1)]^T$$ (7.5)

where W is the equalizer tap weights vector, and $X(k)$ is the equalizer input data vector. N is the length of the equalizer tap weights, T stands for the transpose of a vector and H is the complex conjugate transpose. The tap weights vector is adapted using the stochastic gradient algorithm [143]

$$W(k+1) = W(k) + \mu X(k)e^*(k)$$ (7.6)

$$e(k) = y(k)(R_p - |y(k)|^2)$$ (7.7)

where μ is the step size parameter and e(k) is the error signal. The CMA algorithm minimizes the error power between the equalizer output and a constant. For a 256-QAM signal, the error $e(k)$ cannot reach zero and thus we use CMA for first-order convergence and the RD algorithm as the second stage to fine-tune the equalization. The RD optimization is based on the equalizer output and the nearest constellation radius. The error criterion for RD is defined as

$$e(k) = y(k)(\hat{R}_k^p - |y(k)|^p) \tag{7.8}$$

where R_k is the radius of the nearest constellation symbol for each equalizer output ($p=$ 2). The tap weights for the RD are then updated as follows

$$W(k + 1) = W(k) + \mu X(k)e^*(k) \tag{7.9}$$

$$e(k) = \hat{R}_k^p - |y(k)|^p \tag{7.10}$$

Figure 7.5h shows the constellation diagram after AE. Due to frequency and phase offsets caused by the mixing of transmitted and LO signals, overlapping and rotating constellations are generated. FOE [108] is employed to revoke this phase and frequency imbalance. Figure 7.5i shows the constellation diagram after the FOE [144]. The BPS algorithm is used to recover and subsequently remove the remaining phase mismatch between the local oscillator and the signal[145][146]. The idea of the BPS algorithm is to try different test phases and find the optimum one. Figure 7.5j shows the constellation diagram after the CPE. The decoded output symbol X_k can be selected from $X_{k,b}$ by a switch controlled by the index $m_{k,min}$ of the minimum distance sum. Unwrapping is used after calculating the phase noise to remove the 16-fold ambiguity in the squared 256-QAM constellation. Linear interpolation can also be used to improve the performance especially when the phase noise varies rapidly.

Figure 7.6 shows the BER and EVM versus launched optical power plots of the 720-Gb/s DP-256-QAM system. Both the BER and EVM decrease with increasing launch

power, but a maximum launch power of 20 dBm is considered for eye and skin safety considerations. CW laser power is varied to obtain various launched optical power values.
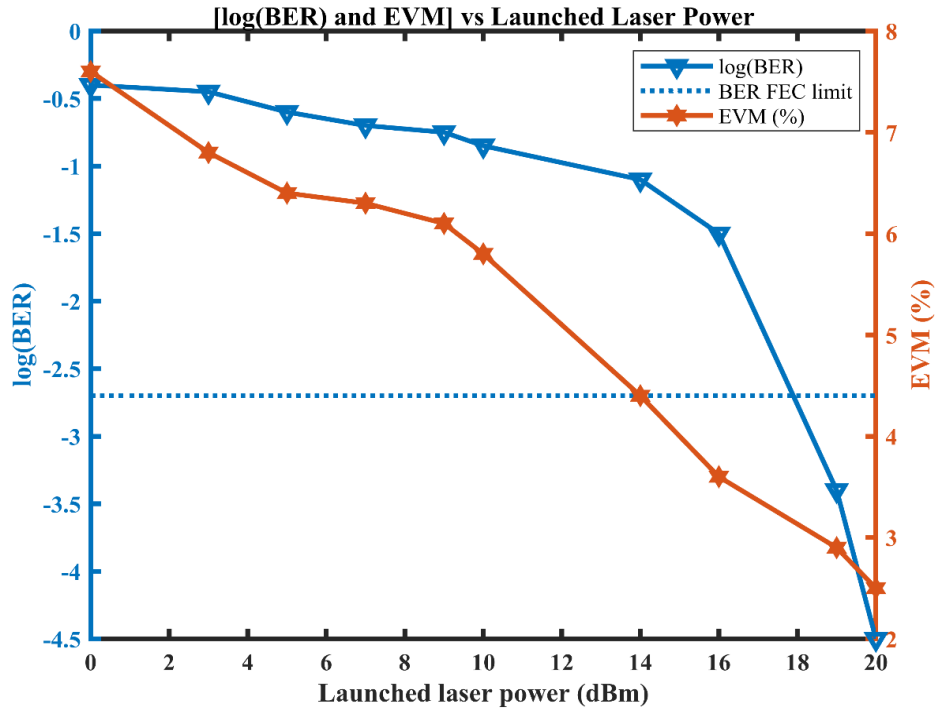
Fig. 7.6 BER and EVM (%) versus launched laser power plot of the proposed system.
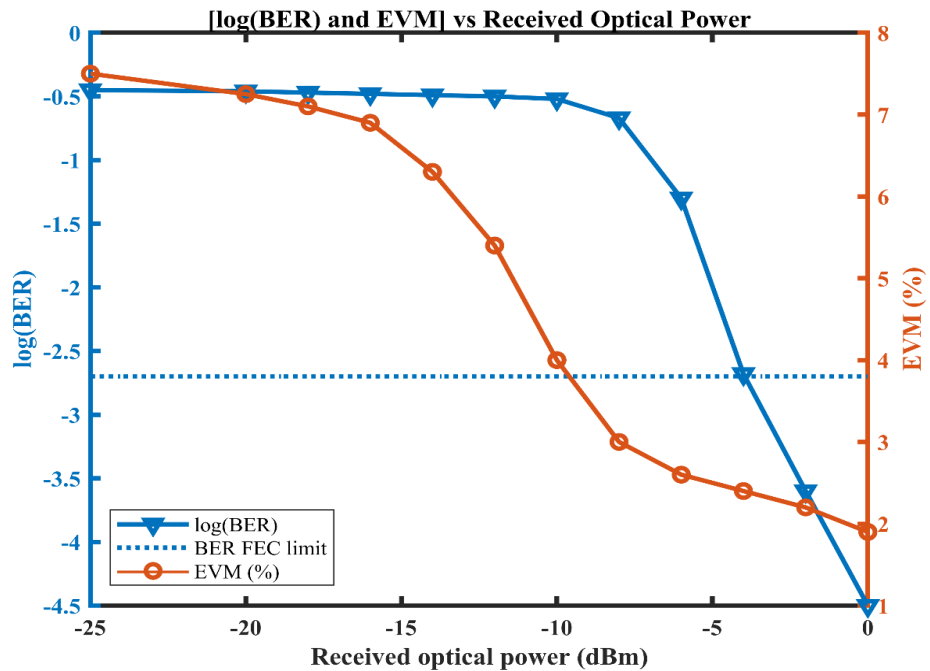
Fig. 7.7 BER and EVM (%) versus received optical power of the designed system.

Figure 7.7 shows the BER and EVM (%) versus received optical power graphs of the proposed FSO system. FSO system performance has been evaluated at maximum transmission distances of 1.31 km. The received optical power is varied with the help of an optical attenuator at the receiver input, and the corresponding EVM (%) and BER are found out.

Figure 7.8 shows the OSNR performance of the system at the maximum transmission distance of 1.31 km. OSNR is used to quantify the degree of optical noise to interference on the optical signal. It is observed that for a higher value of OSNR, the system is less prone to error. This graph reflects a warning of the BER and EVM deterioration and suggests the degree of impairments in an optical signal carried by an optical system. The OSNR required by the system to maintain a BER of $2 \times 10{-}3$ (i.e., the BER FEC limit) is found to be around 40 dB Moreover, the noise has a greater impact on OSNR tolerance in higher-order optical modulation format because of the increased number of bits per symbol and the lesser Euclidean distance between the constellation points.
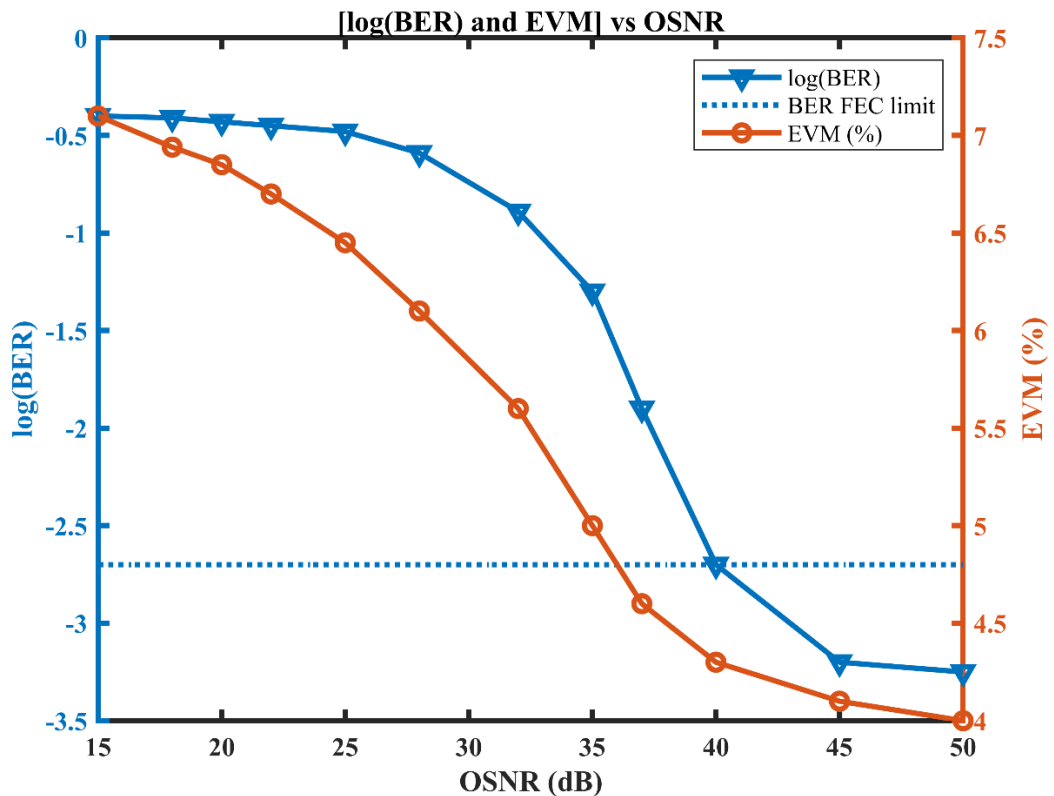
Fig. 7.8 BER and EVM (%) versus OSNR plot of the proposed system under fair weather conditions.
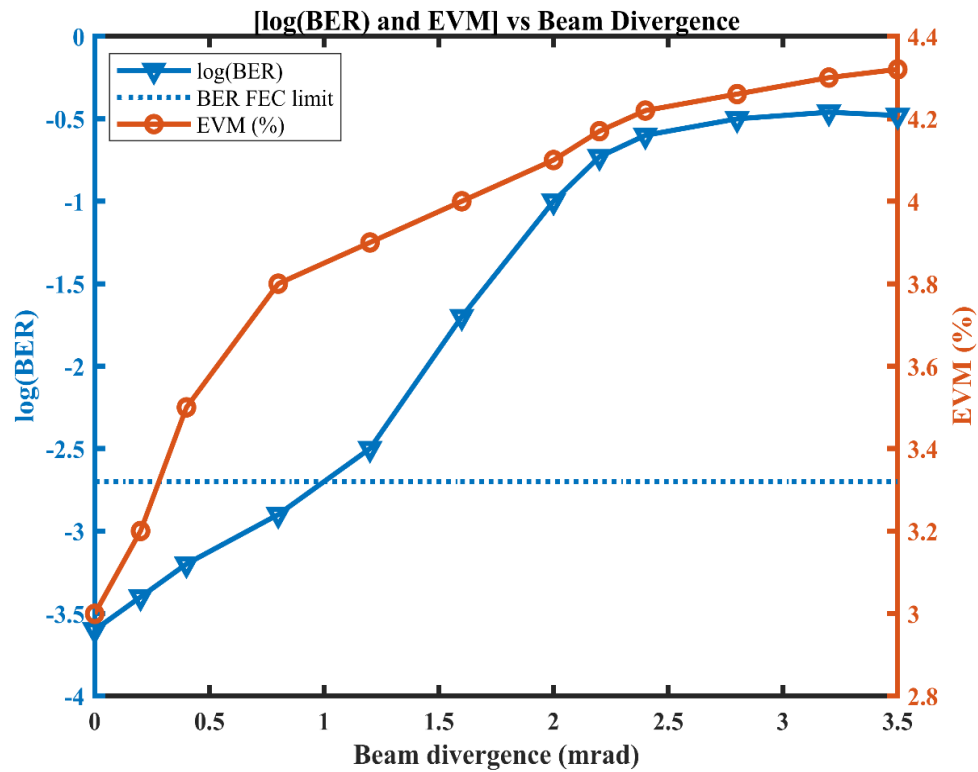
Fig. 7.9 BER and EVM (%) versus beam divergence plot of the designed system.

Figure 7.9 shows the BER and EVM (%) performance of the 720 Gb/s DP-256-QAM system for different beam divergence angles after 1.31 km FSO transmission. It is observed that both the EVM and BER degrade with increasing values of beam divergence angle because at greater divergence angle, the laser beam divergence gets wider and it contributes to dispersion in the optical signal while propagation.

7.4 Concluding remarks

A 720 Gb/s optical transceiver system has been proposed for next-generation optical wireless networks using single-channel optical DP-256-QAM. DSP algorithms help to compensate for various signal impairments such as laser amplitude and phase noise, PMD, frequency, and phase mismatch between the received signal and LO optical carrier, such that a maximum transmission distance of 1.31 km is achieved in the simulation platform. The optical DP-256-QAM system with the FSO channel demonstrates a higher data rate for the small cell. The system requires a laser linewidth of 100 kHz or lower, minimum OSNR of 40 dB, and a receiver sensitivity of − 14.2 dBm to maintain an acceptable BER.

CHAPTER 8: CONCLUSIONS AND RECOMMENDATIONS

8.1 Introduction

This thesis embodies findings from the research carried out for the design and analysis of ultra-high-speed and long-haul FSO communication systems using advanced digital modulation techniques with coherent detection and high-level DSP algorithms for the development of next-generation optical wireless networks. The major objectives of the research were – (I) to design M-ary modulation driven FSO communication system for high SE and better linearity, (II) to implement balanced homodyne detection and several DSP algorithms for digital compensation of the transmission impairments in demodulated in-phase and quadrature-phase electrical signals, and (III) to analyze the performance of all the proposed systems concerning BER, EVM, OSNR, transmission distance, launched optical power, received optical power, laser linewidth, and beam divergence and carry out the performance comparison between all the proposed FSO systems with various M-ary modulation formats as shown in Table 8.1.

Table 8.1 Performance comparison between all the proposed M-ary modulation based FSO communication systems.

Parameters	M-ary modulation format		
	QPSK	**16-QAM**	**256-QAM**
Bit rate (Gbps)	128	400	720
Baud rate (Gbaud)	32	40	60
Transmission range (km)	2.65	2	1.31
Launched laser power (dBm)	18	20	20
Photodetector type	PIN	PIN	APD
Required OSNR (dB)	20	22	40
Beam divergence (mrad)	0.25	0.25	0.25
Spectral efficiency (M bits/s/Hz/polarization)	2	4	16

The major novelty in the present research is the implementation of a 60 Gbaud DP-256-QAM FSO transceiver system with the utilization of high-level DSP algorithms that made the transmission of 720 Gb/s data-bearing optical signals up to a distance of 1.31 km possible. This approach will eventually lead to the successful implementation of 5G network having small cell size and optical IoT.

8.2 Research conclusions and contributions

In this work, we have proposed the design and analysis of a single-channel FSO transceiver system for multiple advanced digital modulation techniques like QPSK, 16-QAM, and 256-QAM using coherent detection and DSP algorithms at the receiver. The major research conclusions and contributions can be summarized as follows:

(i) The wireless optical communication system with two transmission channels, one being an FSO channel and another one an OWC channel was investigated. Both the systems have been analyzed using Q-factor and BER as performance metrics. The mathematical model for received optical power and Pointing error has been taken into account for system considerations. It was observed that superior Q-factor and minimum BER for long transmission distance (80 km) were achieved with the OWC channel while FSO did well only for short-range (800 m) communication.

(ii) The study of the FSO communication system for three optical transmission windows; 850 nm, 1310 nm, and 1550 nm utilizing the OOK digital modulation technique was carried out. The system analysis has been done taking BER, Q-factor, and received optical power as the performance metrics. Their variation pattern with respect to varying link parameters such as range, transmitted optical power, and beam divergence has been investigated.

(iii) The design and analysis of the DP-QPSK FSO coherent transceiver with DSP at the receiver was carried out for a high-speed data link. The overall performance of the proposed system was analyzed with respect to BER, OSNR, link distance, launched optical power, and constellation diagram. The system achieved successful transportation of 128 Gb/s DP-QPSK data over a maximum reach of 2.65 km.

(iv) The design and analysis of 400 Gb/s single-carrier coherent FSO transceiver system was made using IQM based DP-16-QAM with homodyne receiver design and DSP

techniques. The system performance was estimated using BER, OSNR requirement, and EVM as performance metrics. In addition, the impact of DSP algorithms was presented by comparing the before and after DSP stage constellation plots. A transmission distance of 2 km was achieved at an acceptable BER value.

(v) The design and analysis of the 720 Gb/s DP-256-QAM FSO system using coherent detection and DSP algorithms was carried out. The system performance was evaluated using OSNR, transmission distance, launched optical power, received optical power, laser linewidth, and beam divergence with regard to BER and EVM. A transmission distance of 1.31 km was achieved at a required OSNR of 40 dB.

8.3 Recommendations for future work

From the knowledge of researching the field of FSO communication, the author believes that the present research work can be further extended as follows:

(i) In this research, advanced digital modulation techniques such as QPSK, 16-QAM, and 256-QAM have been used. However, the presented performance analysis can be extended to even higher-order modulation formats such as 1024-QAM and 4096-QAM.

(ii) This work has implemented polarization division multiplexing with advanced M-ary modulation formats. However, it is also possible to use spatial division multiplexing with combining techniques at the receiver.

(iii) In the present analysis, fair weather conditions have been considered throughout. But, it is possible to employ log-normal distribution, Gamma-Gamma, and negative exponential distribution models for weak, moderate, and strong turbulence environments, respectively.

REFERENCES

[1] M. A. Khalighi and M. Uysal, "Survey on free-space optical communication: A communication theory perspective," *IEEE Commun. Surv. Tutorials*, vol. 16, no. 4, pp. 2231–2258, 2014, doi: 10.1109/COMST.2014.2329501.

[2] Z. Gu, J. Zhang, and Y. Ji, "Topology Optimizing in FSO-based UAVs Relay Networks for Resilience Enhancement," *Mob. Networks Appl.*, 2019, doi: 10.1007/s11036-019-01290-y.

[3] V. Dhasarathan and M. Singh, "Development of high-speed FSO transmission link for the implementation of 5G and Internet of Things," *Wirel. Networks*, vol. 5, 2020, doi: 10.1007/s11276-019-02166-5.

[4] D. R. Kolev, K. Wakamori, and M. Matsumoto, "Transmission analysis of OFDM-based services over line-of-sight indoor infrared laser wireless links," *J. Light. Technol.*, vol. 30, no. 23, pp. 3727–3735, 2012, doi: 10.1109/JLT.2012.2227456.

[5] A. K. Majumdar, "Fundamentals of free-space optical (FSO) communication system," *Springer Ser. Opt. Sci.*, vol. 186, pp. 1–20, 2015, doi: 10.1007/978-1-4939-0918-6_1.

[6] J. A. Akinwumi and J. O. Bandele, *Free Space Optical Communication : Review Paper*, vol. 7, no. 10. 2018.

[7] E. Pincemin *et al.*, "Optical Fiber Technology Challenges of 40 / 100 Gbps and higher-rate deployments over long-haul transport networks," *Opt. Fiber Technol.*, vol. 17, no. 5, pp. 335–362, 2011, doi: 10.1016/j.yofte.2011.07.011.

[8] S. Lath, R. Goyal, and R. S. Kaler, "A Review on Free Space Optics with Atmospheric and Geometrical Attenuation," *J. Opt. Commun.*, vol. 37, no. 4, pp. 331–336, 2016, doi: 10.1515/joc-2016-0009.

[9] G. Kaur and G. S. Bal, "Performance analysis of SAC-OCDMA in free space optical medium using DDW code," *Optik (Stuttg).*, vol. 133, no. December, pp. 36–42, 2017, doi: 10.1016/j.ijleo.2016.12.057.

[10] www.slideshare.net/XJM6Q/free-space-optical-communication.

[11] R. Martinek, L. Danys, and R. Jaros, "Visible light communication system based on software defined radio: Performance study of intelligent transportation and indoor applications," *Electron.*, vol. 8, no. 4, 2019, doi: 10.3390/electronics8040433.

[12] T. S. Rappaport, G. R. MacCartney, M. K. Samimi, and S. Sun, "Wideband millimeter-wave propagation measurements and channel models for future wireless communication system design," *IEEE Trans. Commun.*, vol. 63, no. 9, pp. 3029–3056, 2015, doi: 10.1109/TCOMM.2015.2434384.

[13] P. Deng, X. Yuan, Y. Zeng, M. Zhao, and H. Luo, "Influence of wind speed on free space optical communication performance for Gaussian beam propagation through non Kolmogorov strong turbulence," *J. Phys. Conf. Ser.*, vol. 276, no. 1, 2011, doi: 10.1088/1742-6596/276/1/012056.

[14] C. Yeh, B. Guo, Y. Chang, C. Chow, and C. Gu, "Bidirectional free space optical communication (FSO) in WDM access network with 1000-m supportable free space link," *Opt. Commun.*, vol. 435,

no. October 2018, pp. 394–398, 2019, doi: 10.1016/j.optcom.2018.11.060.

[15]   J. B. Padhy and B. Patnaik, "Optik Multiplexed free-space optical system design using Manchester coding," *Opt. - Int. J. Light Electron Opt.*, vol. 174, no. April 2017, pp. 266–273, 2018, doi: 10.1016/j.ijleo.2018.07.140.

[16]   S. Chaudhary and A. Amphawan, "The role and challenges of free-space optical systems," *J. Opt. Commun.*, vol. 35, no. 4, pp. 327–334, 2014, doi: 10.1515/joc-2014-0004.

[17]   M. A. A. Ali and S. A. Adnan, "Transporting 8×10 Gbps WDM Ro-FSO Under Various Weather Conditions," no. Mdm, pp. 6–12, 2017.

[18]   K. Balamurugan, K. Chitra, and A. Jawahar, "Reconfigurable routing protocol with optical sphere in FSO MANET," *Concurr. Comput.* , vol. 31, no. 14, 2019, doi: 10.1002/cpe.4874.

[19]   H. Nouri and M. Uysal, "Adaptif Çok Vericili Serbest Uzay Optik Haberle¸sme Sistemi Adaptive Free Space Optical Communication System with Multiple Apertures," pp. 2–5, 2016.

[20]   S. Zhalehpour, M. Uysal, O. A. Dobre, T. Ngatched, A. Science, and E. Engineering, "Multiuser FSO Systems," pp. 143–146, 2015.

[21]   M. A. Hasabelnaby, H. A. I. Selmy, and M. I. Dessouky, "Joint Optimal Transceiver Placement and Resource Allocation Schemes for Redirected Cooperative Hybrid FSO / mmW 5G Fronthaul Networks," *IEEE/OSA J. Opt. Commun. Netw.*, vol. 10, no. 12, pp. 975–990, 2018, doi: 10.1364/JOCN.10.000975.

[22]   V. Jain and H. Kaushal, "Free Space Optical Communication : Laser sources , Modulation Schemes and Detection," no. March 2018, 2013.

[23]   B. Kasprzak, J. Pękala, A. F. Stępień, and Z. Świerczyński, "Metrology and measurement systems," *Architecture*, vol. XVII, no. 4, pp. 537–547, 2010, doi: 10.2478/v10178-012-0001-3.Brought.

[24]   M. Rani, H. Singh, and V. Singh, "Performance analysis of free space optical communication system using homotopy perturbation method under different weather conditions," vol. 20, no. 1, pp. 33–37, 2018.

[25]   R. Miglani and J. Singh, "Investigation on R – S Coded Coherent OFDM Free Space Optical (CO - OFDM - FSO) Communication Link Over Gamma – Gamma Channel," *Wirel. Pers. Commun.*, no. 0123456789, 2019, doi: 10.1007/s11277-019-06571-z.

[26]   H. A. Fadhil *et al.*, "Optik Optimization of free space optics parameters : An optimum solution for bad weather conditions," *Opt. - Int. J. Light Electron Opt.*, vol. 124, no. 19, pp. 3969–3973, 2013, doi: 10.1016/j.ijleo.2012.11.059.

[27]   S. Singh and G. Soni, "Pointing error evaluation in FSO link," *IET Conf. Publ.*, vol. 2013, no. 645 CP, pp. 365–370, 2013, doi: 10.1049/cp.2013.2215.

[28]   www.slideshare.net/Rajanmishra1994/free-space-optics-communication-37202244

[29]   P. T. Dat *et al.*, "A study on transmission of RF signals over a turbulent free space optical link," *2008 IEEE Int. Meet. Microw. Photonics jointly held with 2008 Asia-Pacific Microw. Photonics Conf. MWP2008/APMP2008*, pp. 173–176, 2008, doi: 10.1109/MWP.2008.4666664.

[30]   T. H. Duyen and A. T. Pham, "Performance analysis of mimo/fso systems using SC-QAM signaling over atmospheric turbulence channels," *IEICE Trans. Fundam. Electron. Commun. Comput. Sci.*, vol. E97-A, no. 1, pp. 49–56, 2014, doi: 10.1587/transfun.E97.A.49.

[31]   A. Al-kinani, C. Wang, L. Zhou, and W. Zhang, "Optical Wireless Communication Channel Measurements and Models," vol. XX, no. X, pp. 1–24, 2018, doi: 10.1109/COMST.2018.2838096.

[32]   A. Mansour, R. Mesleh, and M. Abaza, "New challenges in wireless and free space optical communications," *Opt. Lasers Eng.*, vol. 89, pp. 95–108, 2016, doi: 10.1016/j.optlaseng.2016.03.027.

[33]   S. Al-Ahmadi, "The gamma-gamma signal fading model: A survey," *IEEE Antennas Propag. Mag.*, vol. 56, no. 5, pp. 245–260, 2014, doi: 10.1109/MAP.2014.6971962.

[34]   N. Varshney, A. K. Jagannatham, and L. Hanzo, "Asymptotic ser Analysis and Optimal Power Sharing for Dual-Phase and Multi-Phase Multiple-Relay Cooperative Systems," *IEEE Access*, vol. 6, pp. 50404–50423, 2018, doi: 10.1109/ACCESS.2018.2868853.

[35]   Z. Yu *et al.*, "Performance evaluation of direct-detection coherent receiver array for free-space communications with full-link simulation," *Opt. Commun.*, 2020, doi: 10.1016/j.optcom.2019.124520.

[36]   D. Kakati and S. C. Arya, "A full-duplex optical fiber/wireless coherent communication system with digital signal processing at the receiver," *Optik (Stuttg).*, 2018, doi: 10.1016/j.ijleo.2018.05.140.

[37]   J. Yu, X. Li, and N. Chi, "Faster than fiber: over 100-Gb/s signal delivery in fiber wireless integration system," *Opt. Express*, vol. 21, no. 19, p. 22885, 2013, doi: 10.1364/oe.21.022885.

[38]   M. Singh and J. Malhotra, "Performance comparison of M-QAM and DQPSK modulation schemes in a 2 × 20 Gbit/s–40 GHz hybrid MDM–OFDM-based radio over FSO transmission system," *Photonic Netw. Commun.*, vol. 38, no. 3, pp. 378–389, 2019, doi: 10.1007/s11107-019-00861-z.

[39]   V. Sacchieri *et al.*, "DWDM transparent FSO system for in/outdoor applications at high bit rates," *Proc. 2007 9th Int. Conf. Transparent Opt. Networks, Ict. 2007*, vol. 4, pp. 1–4, 2007, doi: 10.1109/ICTON.2007.4296326.

[40]   K. Kikuchi, *High Spectral Density Optical Communication Technologies*. 2010.

[41]   W. Wang *et al.*, "5 Gbaud QPSK coherent transmission in the mid-infrared," *Opt. Commun.*, vol. 466, no. January, p. 125681, 2020, doi: 10.1016/j.optcom.2020.125681.

[42]   M. Singh, J. Malhotra, M. S. Mani Rajan, V. Dhasarathan, and M. H. Aly, "Performance evaluation of 6.4 Tbps dual polarization quadrature phase shift keying Nyquist-WDM superchannel FSO transmission link: Impact of different weather conditions," *Alexandria Eng. J.*, vol. 59, no. 2, pp. 977–986, 2020, doi: 10.1016/j.aej.2020.03.031.

[43]   X. Feng *et al.*, "Experimental demonstration of bidirectional up to 40 Gbit/s QPSK coherent free-space optical communication link over ~1 km," *Opt. Commun.*, vol. 410, no. November 2017, pp. 674–679, 2018, doi: 10.1016/j.optcom.2017.11.024.

[44]   A. Chaman-Motlagh, V. Ahmadi, and Z. Ghassemlooy, "A modified model of the atmospheric effects on the performance of FSO links employing single and multiple receivers," *J. Mod. Opt.*, vol.

57, no. 1, pp. 37–42, 2010, doi: 10.1080/09500340903497465.

[45]   N. M. M. C, "2013 Third International Conference on Advances in Computing and Communications FREESPACE OPTICAL COMMUNICATION USING APERTURE AVERAGING AND SPATIAL DIVERSITY IN LOG NORMAL CHANNEL," no. 1, 2013, doi: 10.1109/ICACC.2013.25.

[46]   W. Jiao, H. Liu, J. Yin, Z. Wei, A. Luo, and D. Deng, "Performance of a QAM/FSO communication system employing spatial diversity in weak and saturation turbulence channels," *J. Mod. Opt.*, vol. 66, no. 9, pp. 965–975, 2019, doi: 10.1080/09500340.2019.1596321.

[47]   K. Prabu, S. Gupta, and S. Jaiswal, "Impact of pointing errors and turbulence effects on POLSK and coherent OWC-based FSO system over generalized turbulence channel model," *Photonic Netw. Commun.*, vol. 36, no. 1, pp. 96–105, 2018, doi: 10.1007/s11107-018-0759-7.

[48]   N. Dayal, P. Singh, and P. Kaur, "Long Range Cost-Effective WDM-FSO System Using Hybrid Optical Amplifiers," *Wirel. Pers. Commun.*, vol. 97, no. 4, pp. 6055–6067, 2017, doi: 10.1007/s11277-017-4826-7.

[49]   A. O. Aldhaibani, S. Yaakob, R. Q. Shaddad, S. M. Idrus, M. Z. A. Kadir, and A. B. Mohammad, "Optik 2 . 5 Gb / s hybrid WDM / TDM PON using radio over fiber technique," *Opt. - Int. J. Light Electron Opt.*, vol. 124, no. 18, pp. 3678–3681, 2013, doi: 10.1016/j.ijleo.2012.11.013.

[50]   N. Zdravkovic, M. I. Petkovic, G. T. Djordjevic, and K. Kansanen, "Outage analysis of mixed FSO/WiMAX link," *IEEE Photonics J.*, vol. 8, no. 1, pp. 1–14, 2016, doi: 10.1109/JPHOT.2016.2516250.

[51]   B. T. Vu, N. T. Dang, T. C. Thang, and A. T. Pham, "Bit error rate analysis of rectangular QAM/FSO systems using an APD receiver over atmospheric turbulence channels," *J. Opt. Commun. Netw.*, vol. 5, no. 5, pp. 437–446, 2013, doi: 10.1364/JOCN.5.000437.

[52]   N. Albakay, "Design and Analysis of Binary Driven Coherent M- ary Qam Transmitter for Next Generation Optical Networks," 2018.

[53]   R. Goyal and R. S. Kaler, "Optical Fiber Technology A novel architecture of hybrid (WDM / TDM) passive optical networks with suitable modulation format," *Opt. Fiber Technol.*, vol. 18, no. 6, pp. 518–522, 2012, doi: 10.1016/j.yofte.2012.08.006.

[54]   W. Ali *et al.*, "10 Gbit / s OWC System for Intra-Data Centers Links," *IEEE Photonics Technol. Lett.*, vol. 31, no. 11, pp. 805–808, 2019, doi: 10.1109/LPT.2019.2905647.

[55]   A. Israr, A. Israr, F. Khan, and F. Khan, "Optimal Modulation Technique for MIMO FSO Link," *Wirel. Pers. Commun.*, no. 0123456789, 2019, doi: 10.1007/s11277-019-06586-6.

[56]   G. Pandey and A. Goel, "100 Gbps long reach coherent PON downstream transmission using dual polarization-QPSK with digital signal processing," *Opt. Quantum Electron.*, vol. 47, no. 11, pp. 3445–3453, 2015, doi: 10.1007/s11082-015-0220-4.

[57]   J. Sun, P. Huang, Z. Yao, and J. Guo, "Adaptive digital combining for coherent free space optical communications with spatial diversity reception," *Opt. Commun.*, vol. 444, no. March, pp. 32–38, 2019, doi: 10.1016/j.optcom.2019.03.069.

[58]   S. Beppu, K. Kasai, M. Yoshida, and M. Nakazawa, "2048 QAM (66 Gbit / s) single-carrier coherent optical transmission over 150 km with a potential SE of 15 . 3 bit / s / Hz," vol. 23, no. 4, pp. 1024–1033, 2015, doi: 10.1364/OE.23.004960.

[59]   M. Mehra, H. Sadawarti, and M. L. Singh, "Performance analysis of coherent optical communication system for higher order dual polarization modulation formats," *Optik (Stuttg).*, vol. 135, pp. 174–179, 2017, doi: 10.1016/j.ijleo.2017.01.034.

[60]   P. M. Krummrich, G. D. Khoe, and H. De Waardt, "1 . 6-b / s / Hz Spectrally Efficient Transmission Over POLMUX-RZ-DQPSK," *Lightwave*, vol. 25, no. 1, pp. 222–232, 2007.

[61]   G. Raybon and P. J. Winzer, *100 Gb/s challenges and solutions*, no. February. 2008.

[62]   S. Ding, R. Li, Y. Luo, and A. Dang, "Polarization coherent optical communications with adaptive polarization control over atmospheric turbulence," *J. Opt. Soc. Am. A*, vol. 35, no. 7, p. 1204, 2018, doi: 10.1364/josaa.35.001204.

[63]   P. W. Berenguer *et al.*, "Nonlinear Digital Pre-distortion of Transmitter Components," *J. Light. Technol.*, vol. 34, no. 8, pp. 1739–1745, 2016, doi: 10.1109/JLT.2015.2510962.

[64]   F. I. El-Nahal, "Coherent quadrature phase shift keying optical communication systems," *Optoelectron. Lett.*, vol. 14, no. 5, pp. 372–375, 2018, doi: 10.1007/s11801-018-8032-y.

[65]   P. J. Winzer, "High-spectral-efficiency optical modulation formats," *J. Light. Technol.*, vol. 30, no. 24, pp. 3824–3835, 2012, doi: 10.1109/JLT.2012.2212180.

[66]   N. Sharma, S. Agrawal, and V. Kapoor, "Improved adaptive equalization with fixed step size CMA for DP-QPSK DWDM system," *Opt. Quantum Electron.*, vol. 52, no. 5, 2020, doi: 10.1007/s11082-020-02352-2.

[67]   G. Song, T. Wang, F. Dong, and Y. Zhang, "Transmission characteristics of 24 . 5 Gb / s atmospheric laser communication based on optical frequency comb," *Opt. Commun.*, vol. 465, no. February, p. 125602, 2020, doi: 10.1016/j.optcom.2020.125602.

[68]   K. Kikuchi, "Coherent optical modulation and demodulation," *Dig. 9th Int. Conf. Opt. Internet, COIN 2010*, pp. 3–5, 2010, doi: 10.1109/COIN.2010.5546589.

[69]   J. Yu, "Spectrally ef fi cient single carrier 400G optical signal transmission," vol. 12, no. 1, pp. 15–23, 2019.

[70]   B. Châtelain *et al.*, "SPM-tolerant pulse shaping for 40- and 100-Gb/s dual-polarization QPSK systems," *IEEE Photonics Technol. Lett.*, vol. 22, no. 22, pp. 1641–1643, 2010, doi: 10.1109/LPT.2010.2077624.

[71]   V. Janyani, M. Tiwari, G. Singh, and P. Minzioni, *Optical and Wireless Technologies: Proceedings of OWT 2017*, vol. 472. 2018.

[72]   X. Zhou and L. Nelson, "Advanced DSP for 400 Gb / s and Beyond Optical Networks," *J. Light. Technol.*, vol. 32, no. 16, pp. 2716–2725, 2014, doi: 10.1109/JLT.2014.2321135.

[73]   T. Sasai, F. Hamaoka, A. Matsushita, M. Nakamura, H. Kawakami, and Y. Kisaka, " Experimental Investigation of Laser Linewidth Tolerance of 32-GBaud DP-256QAM Optical Coherent System,"

2018 23rd Opto-Electronics Commun. Conf., no. c, pp. 1–2.

[74]   M. Kong *et al.*, "High Spectral Efficiency 400 Gb/s Transmission by Different Modulation Formats and Advanced DSP," *J. Light. Technol.*, vol. 37, no. 20, pp. 5317–5325, 2019, doi: 10.1109/JLT.2019.2932384.

[75]   A. Gupta, A. Singh, S. Bakshi, and S. Nagpal, "Digital Signal Processing of 400 Gbps CO-QPSK-WDM System Over Optical Wireless Channel for Carrier Phase Estimation," *Wirel. Pers. Commun.*, vol. 99, no. 1, pp. 111–120, 2018, doi: 10.1007/s11277-017-5042-1.

[76]   R. Miglani and J. S. Malhotra, "Performance enhancement of high-capacity coherent DWDM free-space optical communication link using digital signal processing," *Photonic Netw. Commun.*, vol. 38, no. 3, pp. 326–342, 2019, doi: 10.1007/s11107-019-00866-8.

[77]   W. U. Hui-jun, Z. H. U. Bo, L. I. U. Guo-qing, S. Jia-wei, and H. U. Fang-ren, "A novel chromatic dispersion monitoring method for 400 Gbit / s 256 QAM fiber-optic system based on asyn- chronous amplitude sampling ∗," vol. 11, no. 6, pp. 1–4, 2015, doi: 10.1007/s11801-015-5195-7.

[78]   X. Zhou and L. Nelson, "Advanced DSP for 400 Gb/s and beyond optical networks," *J. Light. Technol.*, vol. 32, no. 16, pp. 2716–2725, 2014, doi: 10.1109/JLT.2014.2321135.

[79]   J. Singh and N. Kumar, "Optik Performance analysis of different modulation format on free space optical communication system," *Opt. - Int. J. Light Electron Opt.*, vol. 124, no. 20, pp. 4651–4654, 2013, doi: 10.1016/j.ijleo.2013.02.014.

[80]   H. Kaushal and G. Kaddoum, "Optical Communication in Space: Challenges and Mitigation Techniques," *IEEE Commun. Surv. Tutorials*, vol. 19, no. 1, pp. 57–96, 2017, doi: 10.1109/COMST.2016.2603518.

[81]   M. Bilgi and M. Yuksel, "Ad Hoc Networks Capacity scaling in free-space-optical mobile ad hoc networks," *Ad Hoc Networks*, vol. 12, pp. 150–164, 2014, doi: 10.1016/j.adhoc.2011.12.003.

[82]   S. Kaur, "Analysis of inter-satellite free-space optical link performance considering different system parameters," *Opto-electronics Rev.*, vol. 27, no. 1, pp. 10–13, 2019, doi: 10.1016/j.opelre.2018.11.002.

[83]   S. Saini and A. Gupta, "Investigation to find optimal modulation format for low power inter-satellite optical wireless communication (LP-IsOWC)," *IFIP Int. Conf. Wirel. Opt. Commun. Networks, WOCN*, pp. 9–12, 2014, doi: 10.1109/WOCN.2014.6923094.

[84]   M. Najjar and H. Rezig, "Performance study of high bit rate indoor wireless optical networks," *ICTON-MW 2008 - Int. Conf. Transparent Opt. Networks "Mediterranean Winter" 2008 - Conf. Proc.*, no. Dl, pp. 1–5, 2008, doi: 10.1109/ICTONMW.2008.4773089.

[85]   A. Polishuk and S. Arnon, "Optimization of a laser satellite communication system with an optical preamplifier," *J. Opt. Soc. Am. A*, vol. 21, no. 7, p. 1307, 2004, doi: 10.1364/josaa.21.001307.

[86]   B. P. P. K. Sahu, "Inter-satellite optical wireless communication system design and simulation," no. June, pp. 2561–2567, 2012, doi: 10.1049/iet-com.2012.0044.

[87]   X. Liu, "Free-space optics optimization models for building sway and atmospheric interference using variable wavelength," *IEEE Trans. Commun.*, vol. 57, no. 2, pp. 492–498, 2009, doi:

10.1109/TCOMM.2009.02.070089.

[88] S. Arnon, "Performance of a laser μsatellite network with an optical preamplifier," *J. Opt. Soc. Am. A*, vol. 22, no. 4, p. 708, 2005, doi: 10.1364/josaa.22.000708.

[89] L. Gan, H. Zhang, J. Wang, and B. Liu, "Optik In fl uence of dynamic impact on optical properties of optical transmission window of laser measurement system," *Opt. - Int. J. Light Electron Opt.*, vol. 202, no. October 2019, p. 163643, 2020, doi: 10.1016/j.ijleo.2019.163643.

[90] A. Wason and R. S. Kaler, "Optik Investigation of four wave mixing effect with different number of input channels at various channel spacing," *Opt. - Int. J. Light Electron Opt.*, vol. 124, no. 20, pp. 4227–4230, 2013, doi: 10.1016/j.ijleo.2013.02.006.

[91] K. P. Swain, A. Nayyar, and G. Palai, "Optik Prediction of optical speci fi cations through ANN model to design a monochromatic optical fi lter for all three optical windows," *Opt. - Int. J. Light Electron Opt.*, vol. 198, no. May, p. 163314, 2019, doi: 10.1016/j.ijleo.2019.163314.

[92] S. P. Mohanty, S. K. Sahoo, A. Panda, and G. Palai, "FDTD method to photonic waveguides for application of optical demultiplexer at 3-communication windows," *Optik (Stuttg).*, vol. 185, no. January, pp. 146–150, 2019, doi: 10.1016/j.ijleo.2019.03.083.

[93] A. Jurado-Navas, A. Tatarczak, X. Lu, J. J. V. Olmos, J. M. Garrido-Balsells, and I. T. Monroy, "850-Nm Hybrid Fiber/Free-Space Optical Communications Using Orbital Angular Momentum Modes," *Opt. Express*, vol. 23, no. 26, p. 33721, 2015, doi: 10.1364/oe.23.033721.

[94] W. A. E. L. G. A. Lheadary *et al.*, "Free-space optical channel characterization and experimental validation in a coastal environment," vol. 26, no. 6, pp. 1–14, 2018.

[95] M. Glick, H. Rastegarfar, R. C. P. Jr, and L. C. Kimerling, "Transceiver Scaling and the IPSR-I Roadmap," *2018 20th Int. Conf. Transparent Opt. Networks*, pp. 1–4, 2020.

[96] G. P. Agrawal, *Fiber Optic Communication Systems*. New York: john wiley & sons, 1997.

[97] S. Bloom, E. Korevaar, J. Schuster, and H. Willebrand, "understanding the performance of free space optics," *J. Opt. Netw.*, vol. 2, no. 6, pp. 178–200, 2003.

[98] J. Yu and J. Zhang, "Recent progress on high-speed optical transmission," *Digit. Commun. Networks*, vol. 2, no. 2, pp. 65–76, 2016, doi: 10.1016/j.dcan.2016.03.002.

[99] M. Singh and J. Malhotra, "Performance Comparison of Different Modulation Schemes in High-Speed MDM Based Radio Over FSO Transmission Link Under the Effect of Atmospheric Turbulence Using Aperture Averaging," *Wirel. Pers. Commun.*, vol. 111, no. 2, pp. 825–842, 2020, doi: 10.1007/s11277-019-06886-x.

[100] M. Nakazawa, T. Hirooka, M. Yoshida, and K. Kasai, *Extremely Higher-Order Modulation Formats*, Sixth Edit. Elsevier Inc., 2013.

[101] H. Li, Y. Huang, Q. Wang, D. He, Z. Peng, and Q. Li, "Phase offset tracking for free space digital coherent optical communication system," *Appl. Sci.*, vol. 9, no. 5, 2019, doi: 10.3390/app9050836.

[102] J. Renaudier *et al.*, "8 Tb / s Long Haul Transmission Over Low Dispersion Fibers Using 100 Gb / s PDM-QPSK Channels Paired With Coherent Detection," vol. 14, no. 4, 2010, doi: 10.1002/bltj.

[103]   V. A. Vardanyan and Q. Sample, "Laser Diode Modulation under Multichannel Digital 64-QAM and 256-QAM TV Signals," vol. 51, no. 6, pp. 544–547, 2015.

[104]   M. Adel, H. Seleem, M. Nasr, and H. El-Khobby, "Transmission of 128 Gb/s Optical QPSK Signal over FSO Channel under Different Weather Conditions and Pointing Errors," *J. Phys. Conf. Ser.*, vol. 1447, no. 1, 2020, doi: 10.1088/1742-6596/1447/1/012055.

[105]   W. Count, T. Submitted, and P. Id, "By sahil," 2020.

[106]   A. J. Lowery, "Fiber nonlinearity mitigation in optical links that use OFDM for dispersion compensation," *IEEE Photonics Technol. Lett.*, vol. 19, no. 19, pp. 1556–1558, 2007, doi: 10.1109/LPT.2007.903962.

[107]   D. Kassegne, "Influence of nonlinear effects on 6 . 4 Tb / s dual polarization quadrature phase shift keying modulated dense wavelength division multiplexed system," no. April, pp. 1–12, 2019, doi: 10.1002/dac.4021.

[108]   M. Morelli and U. Mengali, "Feedforward Frequency Estimation for PSK: A Tutorial Review," *Eur. Trans. Telecommun.*, vol. 9, no. 2, pp. 103–116, 1998, doi: 10.1002/ett.4460090203.

[109]   M. S. Faruk, "Compensation of quadrature imbalance in an optical 16-QAM digital coherent receiver," *14th Int. Conf. Comput. Inf. Technol. ICCIT 2011*, vol. 20, no. 20, pp. 538–541, 2011, doi: 10.1109/ICCITechn.2011.6164847.

[110]   J. C. Cartledge, J. D. Downie, J. E. Hurley, A. S. Karar, Y. Jiang, and K. Roberts, "Pulse shaping for 112 Gbit/s polarization multiplexed 16-QAM signals using a 21 GSa/s DAC," *Opt. InfoBase Conf. Pap.*, vol. 19, no. 26, pp. 628–635, 2011, doi: 10.1364/oe.19.00b628.

[111]   I. Fatadin, "Estimation of BER from Error Vector Magnitude for Optical Coherent Systems," 2016, doi: 10.3390/photonics3020021.

[112]   D. Kakati and S. C. Arya, "A 640 - Gbps , 15 . 2344 - b / s / Hz full - duplex optical fiber / wireless single - channel coherent communication system using IQM - based DP - 256 - QAM and DSP techniques," *Photonic Netw. Commun.*, no. Ld, 2019, doi: 10.1007/s11107-019-00875-7.

[113]   L. A. Kadhim, "16 / 64QAM Modulation Technique for Free Space Optical Communication System," vol. 6, no. 6, pp. 1–13, 2014.

[114]   M. Hudlicka, C. Lundstrom, D. A. Humphreys, and I. Fatadin, "BER estimation from EVM for QPSK and 16-QAM coherent optical systems," *2016 IEEE 6th Int. Conf. Photonics, ICP 2016*, pp. 0–2, 2016, doi: 10.1109/ICP.2016.7510025.

[115]   D. Jain and R. Mehra, "Performance of 120 Gbps single and dual polarized 16-QAM coherent FSO systems under various turbulence regimes," *2017 Int. Conf. Comput. Commun. Technol. Smart Nation, IC3TSN 2017*, vol. 2017-Octob, pp. 89–94, 2018, doi: 10.1109/IC3TSN.2017.8284457.

[116]   S. Benedetto and E. Biglieri, *Digital transmission theory: With Wireless Applications*. New York: Prentice-Hall, 1999.

[117]   D. Kakati and S. C. Arya, "Performance of 120 Gbps single channel coherent DP-16-QAM in terrestrial FSO link under different weather conditions," *Optik (Stuttg).*, vol. 178, no. May 2018, pp. 1230–1239, 2019, doi: 10.1016/j.ijleo.2018.10.035.

[118]   R. Zhang *et al.*, "Full-duplex fiber-wireless link with 40 Gbit/s 16-QAM signals for alternative wired and wireless accesses based on homodyne/heterodyne coherent detection," *Opt. Fiber Technol.*, 2014, doi: 10.1016/j.yofte.2014.02.008.

[119]   D. Hillerkuss *et al.*, "Single-laser 32.5 Tbit/s Nyquist WDM transmission," *J. Opt. Commun. Netw.*, vol. 4, no. 10, pp. 715–723, 2012, doi: 10.1364/JOCN.4.000715.

[120]   D. Kakati and S. C. Arya, "A full-duplex optical fiber/wireless coherent communication system with digital signal processing at the receiver," *Optik (Stuttg).*, vol. 171, no. May, pp. 190–199, 2018, doi: 10.1016/j.ijleo.2018.05.140.

[121]   J. Yu, X. Li, and W. Zhou, "Tutorial: Broadband fiber-wireless integration for 5G+ communication," *APL Photonics*, vol. 3, no. 11, 2018, doi: 10.1063/1.5042364.

[122]   D. Kakati and S. C. Arya, "A full-duplex pilot-assisted DP-16-QAM CO-OFDM system for high-speed long-haul communication," *2019 2nd Int. Conf. Innov. Electron. Signal Process. Commun.*, no. 1, pp. 183–187, 2019.

[123]   R. C. Srinivasan and J. C. Cartledge, "On Using Fiber Transfer Functions to Characterize Laser Chirp and Fiber Dispersion," *IEEE Photonics Technol. Lett.*, vol. 7, no. 11, pp. 1327–1329, 1995, doi: 10.1109/68.473487.

[124]   L. B. Du and A. J. Lowery, "Improved single channel backpropagation for intra-channel fiber nonlinearity compensation in long-haul optical communication systems," *Opt. Express*, vol. 18, no. 16, p. 17075, 2010, doi: 10.1364/oe.18.017075.

[125]   M. Oerder and H. Meyr, "Digital Filter and Square Timing Recovery," *IEEE Trans. Commun.*, vol. 36, no. 5, pp. 605–612, 1988, doi: 10.1109/26.1476.

[126]   K. Kikuchi, M. Fukase, and S. Y. Kim, "Electronic post-compensation for nonlinear phase noise in a 1000-km 20-Gbit/s optical QPSK transmission system using the homodyne receiver with digital signal processing," *Opt. InfoBase Conf. Pap.*, no. 3, pp. 6–8, 2007.

[127]   J. Karaki *et al.*, "Dual-polarization multi-band OFDM versus single-carrier DP-QPSK for 100 Gbps long-haul WDM transmission over legacy infrastructure," *Eur. Conf. Opt. Commun. ECOC*, vol. 21, no. 14, pp. 16982–16991, 2012, doi: 10.1364/oe.21.016982.

[128]   J. Hwang, Y. Chiu, and C. Liao, "Angle differential-QAM scheme for resolving phase ambiguity in continuous transmission system," no. December 2007, pp. 631–641, 2008, doi: 10.1002/dac.

[129]   R. A. Shafik, M. S. Rahman, A. H. M. R. Islam, and N. S. Ashraf, "On the error vector magnitude as a performance metric and comparative analysis," *Proc. - 2nd Int. Conf. Emerg. Technol. 2006, ICET 2006*, no. November, pp. 27–31, 2006, doi: 10.1109/ICET.2006.335992.

[130]   H. A. Mahmoud and H. Arslan, "Error vector magnitude to SNR conversion for nondata-aided receivers," *IEEE Trans. Wirel. Commun.*, vol. 8, no. 5, pp. 2694–2704, 2009, doi: 10.1109/TWC.2009.080862.

[131]   R. Schmogrow *et al.*, "Erratum: Corrections to error vector magnitude as a performance measure for advanced modulation formats (IEEE Photonics Technology Letters (2012) 24:1 (61-63))," *IEEE Photonics Technol. Lett.*, vol. 24, no. 23, p. 2198, 2012, doi: 10.1109/LPT.2012.2219471.

[132] S. J. Savory, "Digital filters for coherent optical receivers," vol. 16, no. 2, pp. 804–817, 2008.

[133] N. Shibata *et al.*, "256-QAM 8 wireless signal transmission with DSP-assisted analog RoF for mobile front-haul in LTE-B," *2014 Optoelectron. Commun. Conf. OECC 2014 Aust. Conf. Opt. Fibre Technol. ACOFT 2014*, no. July, pp. 129–131, 2014.

[134] K. Toyoda, Y. Koizumi, T. Omiya, M. Yoshida, T. Hirooka, and M. Nakazawa, "Marked performance improvement of 256 QAM transmission using a digital back-propagation method," *Opt. Express*, vol. 20, no. 18, p. 19815, 2012, doi: 10.1364/oe.20.019815.

[135] T. D. Memon, W. Ghangro, B. S. Chowdhry, and A. A. Shaikh, "Quadrature phase shift keying modulator & demodulator for wireless modem," *2009 2nd Int. Conf. Comput. Control Commun. IC4 2009*, no. March, 2009, doi: 10.1109/IC4.2009.4909180.

[136] Y. Wang, K. Kasai, M. Yoshida, and M. Nakazawa, "320 Gbit/s, 20 Gsymbol/s 256 QAM coherent transmission over 160 km by using injection-locked local oscillator," *Opt. Express*, vol. 24, no. 19, p. 22088, 2016, doi: 10.1364/oe.24.022088.

[137] A. Matsushita, M. Nakamura, F. Hamaoka, S. Okamoto, and Y. Kisaka, "High-spectral-efficiency 600-Gbps/carrier transmission using PDM-256QAM format," *J. Light. Technol.*, vol. 37, no. 2, pp. 470–4760, 2019, doi: 10.1109/JLT.2018.2890124.

[138] K. Kasai, Y. Wang, S. Beppu, M. Yoshida, and M. Nakazawa, "80 Gbit / s , 256 QAM coherent transmission over 150 km with an injection-locked homodyne receiver," vol. 23, no. 22, pp. 29174–29183, 2015, doi: 10.1364/OE.23.029174.

[139] T. Omiya, M. Yoshida, and M. Nakazawa, "400 Gbit / s 256 QAM-OFDM transmission over 720 km with a 14 bit / s / Hz spectral efficiency by using high-resolution FDE," vol. 21, no. 3, pp. 2632–2641, 2013.

[140] B. Zlatkovic, D. Stojanovic, I. Multilevel, and E. Engineering, "256-QAM in," vol. 77, no. 6, pp. 863–867, 1994.

[141] W. A. Sethares, G. A. Rey, and C. R. Johnson, "Approaches to blind equalization of signals with multiple modulus," *ICASSP, IEEE Int. Conf. Acoust. Speech Signal Process. - Proc.*, vol. 2, no. June 1989, pp. 972–975, 1989, doi: 10.1109/icassp.1989.266592.

[142] D. N. Godard, "Self-Recovering Equalization and Carrier Tracking," vol. C, pp. 1867–1875, 1980.

[143] X. Xu *et al.*, "A nonlinearity-tolerant frequency domain root M-shaped pulse for coherent optical communication systems," vol. 21, no. 26, pp. 12879–12884, 2013, doi: 10.1364/OE.21.031966.

[144] P. Ciblat and L. Vandendorpe, "Blind carrier frequency offset estimation for noncircular constellation-based transmissions," *IEEE Trans. Signal Process.*, vol. 51, no. 5, pp. 1378–1389, 2003

[145] J. A. Armstrong, "Theory of Interferometric Analysis of Laser Phase Noise*," *J. Opt. Soc. Am.*, vol. 56, no. 8, p. 1024, 1966, doi: 10.1364/josa.56.001024.

[146] X. Zhou *et al.*, "Modulation-format-independent blind phase search algorithm for coherent optical square M - QAM systems," vol. 22, no. 20, pp. 1051–1053, 2014, doi: 10.1364/OE.22.024044.